A Chemical Biology Approach Towards Targeting Understudied Lipid Kinases in Cancer and Ebola

A Chemical Biology Approach Towards Targeting Understudied Lipid Kinases in Cancer and Ebola

A dissertation presented

by

Sindhu Carmen Sivakumaren

to

The Division of Medical Sciences

in partial fulfillment of the requirements

for the degree of

Doctor of Philosophy

in the subject of

Biological Chemistry and Molecular Pharmacology

Harvard University

Cambridge, Massachusetts

May 2019

Dissertation Advisor: Nathanael S. Gray Sindhu Carmen Sivakumaren

A Chemical Biology Approach Towards Targeting Understudied Lipid Kinases in Cancer and Ebola

Abstract

Cellular processes are orchestrated in an intricate and highly coordinated fashion in order to facilitate proper metabolism, cell cycle progression, gene expression, and ultimately survival. Phosphoinositides, lipid moieties which exist in tiny proportions within the cell, are examples of important messengers whose complex signaling is controlled in a temporal and spatial manner by kinases and phosphatases, deregulation of which leads to disease.

The phosphatidylinositol 5-phosphate 4-kinases (PI5P4Ks) have been demonstrated to be important for cancer cell proliferation and other diseases. However, the therapeutic potential of targeting these kinases is understudied due to a lack of potent, specific small molecules available. Here we present the discovery and characterization of a novel pan-PI5P4K inhibitor, THZ-P1-2, that covalently targets cysteines on a disordered loop in PI5P4K$\alpha/\beta/\gamma$. THZ-P1-2 demonstrates cellular on-target engagement with limited off-targets across the kinome. AML/ALL cell lines were sensitive to THZ-P1-2, consistent with PI5P4K's reported role in leukemogenesis. THZ-P1-2 causes autophagosome clearance defects and upregulation in TFEB nuclear

localization and target genes, disrupting autophagy in a covalent-dependent manner and phenocopying the effects of PI5P4K genetic deletion.

PIKfyve, a related understudied lipid kinase, has also been validated as a target in Non-Hodgkin lymphoma and Ebola viral infection. We observed that THZ-P1-2 was also capable of covalently binding to PIKfyve, albeit at a much lower preference than PI5P4K. We reengineered compound selectivity towards PIKfyve and identified a class of compounds from the THZ-P1-2 scaffold exhibiting picomolar-to-nanomolar IC_{50}s. These inhibitors exhibit cellular on-target engagement and vacuolar enlargement, a well-established PIKfyve inhibitory phenotype. Docking/modeling studies and mass spectrometry revealed a similar distant cysteine, Cys1970, to be covalently labeled by these compounds. Lastly, this THZ-family of inhibitors, particularly two top compounds MFH-5-3 and MFH-5-4, exhibit potent antiproliferative activity in lymphoma cell lines and inhibition of Ebola viral infectivity.

Taken together, our studies demonstrate that the PI5P4Ks and PIKfyve are tractable targets, with inhibitors serving as useful tools to further interrogate the therapeutic potential of these noncanonical lipid kinases and inform drug discovery campaigns in the context of cancer, Ebola, and potentially other autophagy-dependent diseases.

Table of Contents

Acknowledgments

First of all, I am deeply indebted and grateful to my advisor, Dr. Nathanael S. Gray. I met Nathanael when I was interviewing for Harvard's BBS program 6 years ago. As an undergraduate, I was already deeply fascinated with the Gray lab's research. I kept in touch and ended up rotating in the lab and eventually joining. Nathanael's expertise and keen intellect as a scientist at the chemistry-biology interface is unparalleled and well-known, but what struck me over the years was his genuine caring as an advisor and guidance stemming from a deep desire to see his trainees succeed. Nathanael has delivered so much as a an advisor and mentor despite his incredibly busy schedule, allowing and encouraging me to pursue ideas and development opportunities outside the lab, and for that I am forever grateful.

I thank my dissertation advisory committee – Dr. Thomas M. Roberts, Dr. Alex Toker, and Dr. Sara Buhrlage – for the invaluable feedback, comments and advice over the years. Thank you for always making me feel like I was making progress, even when it didn't feel like it. A heartfelt thank you also to my thesis committee – Dr. Alex Toker, Dr. Eranthie Weerapana, Dr. Michael Eck, and Dr. Hao Wu – for making the time to read and evaluate my thesis and defense.

I thank my two undergraduate advisors who are a huge reason for me being on the path that I am – Dr. Marc M. Greenberg and Dr. Phil A. Cole, and my graduate student mentors in their respective labs, John Bajacan and Dr. David M. Bolduc, who were patient and encouraging with this blundering, low-confidence, but extremely passionate undergraduate.

I thank members of the Gray lab for providing a stimulating and supportive environment to pursue graduate research in. Huge thanks in particular to my lipid kinase partner-in-crime Theresa D. Manz, and my upper level mentors Dr. Fleur M. Ferguson, Dr. Tinghu Zhang, and Dr. Nick P. Kwiatkowski. I thank the best graduate student cohort, past and present, for all the hysterical laughs and also support when there were tears – Chelsea Powell, Benika Pinch, Liv Johanessen, Hubert Huang, Dennis Dobrovolsky, Inchul You, Anthony Ayala, Lara Gechijian, Zainab Doctor – and technician Katie Mowris. I thank Dr. Scott Ficarro and Dr. Chris Browne of the Marto lab for mass spectrometry expertise. I thank the structural biology core, led by Dr. Sirano Dhe-Paganon, as well as Dr. Hyuk-Soo Seo, for protein purification and crystallography magic. I thank members of the Cantley lab, especially Dr. Lewis C. Cantley, for being a walking encyclopedia of all things lipid kinase, and for always making the time even to meet for 15 min when I visited NYC. Thank you especially to my co-first author Dr. Hyeseok Shim for all her previous work on PI5P4K, and Dr. Marcia Paddock, Dr. Mark Lundquist, and Dr. Diana Wang for assay and experimental expertise. I thank Dr. Jim Cunningham and Dr. May Wang for the EBOV collaboration and expertise, and Jim especially for the advice on PI5P4K. I thank the NCATS group at NIH for providing PI5P4K biochemical assay development guidance and running assays for us.

I thank my BBS office (Kate Hodgins, Maria Bollinger, Danny Gonzalez, Anne O'Shea, Susan Dymecki, Thomas Bernhardt) and DMS administration (David Cardozo and others), as well as BCMP and DFCI Cancer Biology/Chemical Biology administration members, especially Program Director Milka Kostic, for making me feel supported throughout graduate school – and for the amazing retreats.

I thank all my friends throughout graduate school across graduate programs and student groups who have made this experience so enriching and rewarding, especially my best friend Michka Sharpe. I thank my family in Ohana New England and the Boston dragon boat community (especially Sizun, Candy, Helen, Keerthana, Matt) for making my life outside of the lab so rewarding. I thank my friends from Johns Hopkins University and INTI University College in Malaysia, especially my best friends – Brittany, Tiffany, Jiayi, Rose, Carolyn, and the Young Villains – David, Ava, Peter – for bonds that have lasted years and continued to keep me going even when I'm far away here in Boston. I thank my roommates for being a family I could come home to – Wei Yiing, Lu Quan, Richard Baarsvik, Matthew Whinihan.

Finally, I thank the most important people in my life – my family, nuclear and extended. I am the most grateful to my parents, my brother and sister-in-law, and my beautiful niece Naomi and nephew Noah, to whom this dissertation is dedicated. Thank you for always believing in me.

List of Tables

List of Figures

List of schemes

Chapter 1. Introduction

Kinases are one of the most highly pursued classes of proteins as drug targets (second to G-protein coupled receptors), with currently 38 FDA-approved inhibitors and several more in various stages of clinical trials. These enzymes function by transferring a phosphate group onto a substrate, often leading to activation or deactivation of a particular biological pathway. With 518 kinases encoded by the human genome, kinases are responsible for the phosphorylation of approximately one-third of the proteome as well as a variety of non-protein targets. Because almost all key signal transduction pathways proceed via a phosphotransfer cascade, kinases present themselves as targetable points within these biological processes, with misregulation of kinase activity leading to disorders and appropriate therapeutic modulation of aberrant kinases leading to correction of disease pathology (Ferguson & Gray, 2018; J. Zhang, Yang, & Gray, 2008).

As cancer therapy modalities have changed over the decades, an overwhelming majority of kinase targets continue to be investigated for cancer (Fig 1.1). About 30% of the current targeted therapies for cancer are kinase inhibitors, mostly targeted towards receptor tyrosine kinases (RTKs) with antibodies or small-molecules. There are multiple reasons for the popularity of kinase targeting in cancer. Firstly, kinases are often at the center of tumor growth and survival, given that many kinase-mediated phosphorylation cascades signal towards cell proliferation. Many kinases have the ability to be “transforming”, leading cancer cells to be dependent on the constitutive activity of the kinase for their proliferation and survival. This concept of “oncogene addiction” makes cancer cells much more sensitive to kinase-targeted therapies than normal cells, allowing for a therapeutic window to be achieved. Secondly, a deeper understanding of

what constitutes normal versus malignant cell states has enabled targeting of kinases in a manner that elicits real physiological responses. Indeed, recent advances have expanded beyond classical oncogene addiction and included basal cellular processes that cancers exhibit abnormal dependency on, such as transcription, immune signaling, and as extended upon later in this thesis, autophagy. Thirdly, the existence of an ATP-binding pockets in kinases renders them druggable, with the first kinase inhibitors developed as simple ATP mimetics. The misconception that the high degree of homology between kinase domains and millimolar cellular ATP concentrations makes it impossible to develop selective and potent compounds has been largely disproven by the designability of various kinase scaffolds.

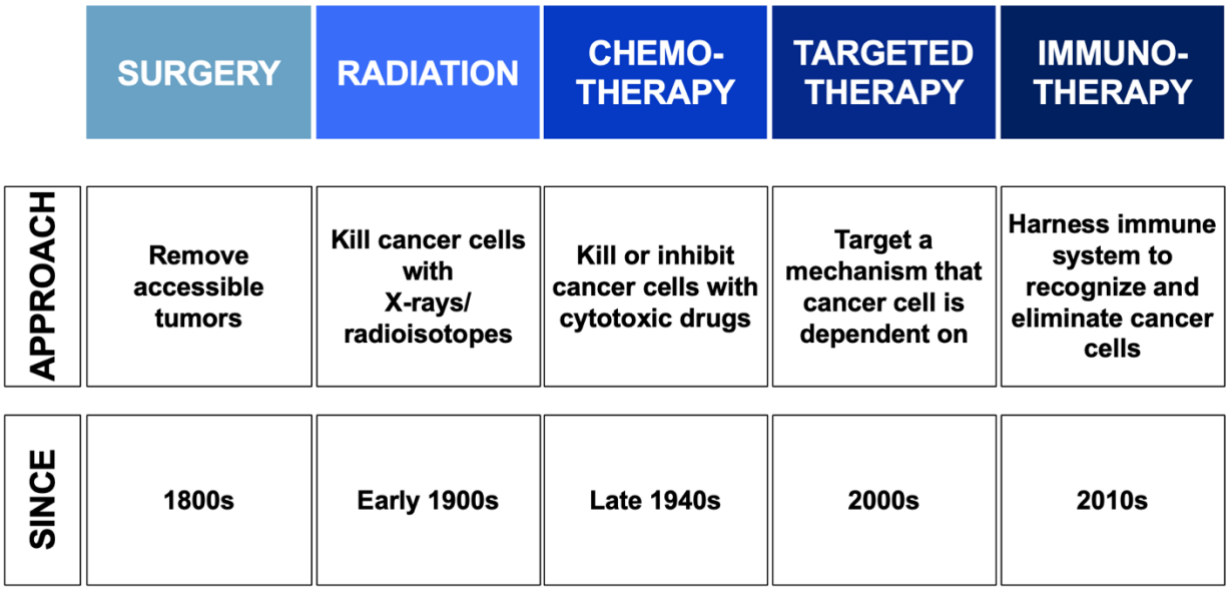

Figure 1.1 Cancer therapy modalities throughout the years. Kinase inhibitors represent about 30% of targeted therapies. As new therapeutic advances such as immunotherapy take the stage, there is a misconception that kinase inhibitors are fading out, as discussed later on in this introduction.

Lastly, the high-profile success of kinase inhibitors in the clinic, especially by drugs such as imatinib (Gleevec) for chronic myelogenous leukemia have continued to make kinases an attractive target despite existing challenges in target identification, drug development, and emerging resistance. These have all contributed to the rapid development of kinase drug discovery beyond oncology especially into autoimmune and inflammatory disease, infectious disease, as well as degenerative disorders (Fig. 1.2) (Ferguson & Gray, 2018; J. Zhang et al., 2008).

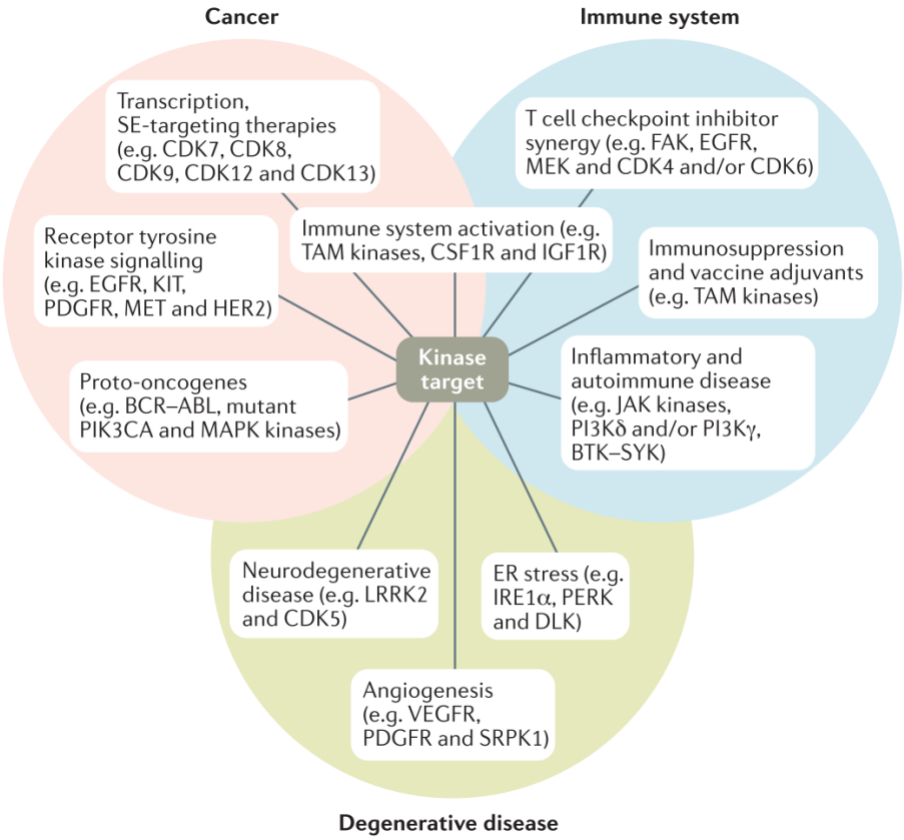

Figure 1.2 Kinase targets relevant for inhibition across therapeutic areas (Ferguson & Gray, 2018)**.**

For small-molecule kinase inhibitors, which are the focus of this thesis, there are four main types which are categorized by binding mode. The first protein kinase

inhibitors, or Type I inhibitors, that were developed in the 1980s were ATP competitive, mainly because these inhibitors were discovered in enzymatic assays where the kinase was present in its active conformation and because they were synthesized to mimic kinases' natural ligand, ATP (Fedorov, Müller, & Knapp, 2010). In contrast, Type II inhibitors recognize the inactive or "DFG-out" conformation of kinases, taking advantage of an additional exposed hydrophobic pocket due to the movement of the DFG motif. The third class of kinase-targeting compounds are allosteric inhibitors which bind outside of the kinase active site, usually demonstrating the highest degree of selectivity because they bind to unique sites allowing for differentiation between kinases. The last category of kinase inhibitors are covalent inhibitors which form an irreversible bond between an electrophilic warhead appended onto the compound and a nucleophilic amino acid residue, usually a cysteine. These targetable residues have since been expanded to include lysine, tyrosine, histidine and methionine. Covalent inhibitors offer some potential advantages, including superior potency due to prolonged inhibition, increased selectivity due to the combination of covalent and non-covalent binding modes, and pharmacological specificity validation through mutation of the targeted residue; thus, covalent inhibitors will be the focus of the majority of this thesis, although non-covalent inhibitors are also explored in our high-throughput screening approach in the search of novel scaffold starting points. Taken together, these binding modes demonstrate the high flexibility and mobility of kinase active sites in accommodating a variety of inhibitors, and offer a myriad of opportunities for compound design strategies, especially in modulating on-target potency and selectivity across the kinome (Liu et al., 2013; J. Zhang et al., 2008).

Given the relevance of kinases across a variety of diseases, we continue to focus on finding new strategies to study their underlying biology and target them. With the advent of other therapies especially for cancer such as immunotherapy, there is a misconception that the age of kinase-targeting is slowing down and all the “low-hanging fruits” in terms of targets have been harvested. In fact, the majority of the kinome, for cancer or other diseases, remains undiscovered and untargeted. A relatively small set of kinases are the major focus on most publications, citations and patents, while many kinases essential in disease pathology are unexplored (Fedorov et al., 2010; Isserlin et al., 2011). The “Harlow-Knapp” effect describes this propensity of biopharma and research communities to focus on a small fraction of the kinome (Fig. 1.3). The citation pattern due to this effect was found to be broadly observed in other druggable gene families as well, such as nuclear hormone receptors, methyltransferases and bromodomain-containing proteins (Isserlin et al., 2011). Clinical proof of concept has been touted as a motivating factor for the narrow scope of focus in targeting kinases, with more than 50% of approved clinical inhibitors targeting kinases that already have approved drugs available. Most kinase inhibitors were also derived from quinazolines, quinolines or the staurosporine scaffold, suggesting that scaffold diversifying is also sorely needed. With the current limitations of chemotherapy, antibodies, and immunotherapy in cancer, there is value in expanding the current arsenal of cancer therapeutics by mining the database of understudied kinases and developing probes and therapeutics for them. The largely ignored “dark” kinome can continue to be “deorphanized” by intentionally seeking out less annotated kinases and further

exploiting this expansion of the druggable genome to discover and validate novel targets (Fedorov et al., 2010).

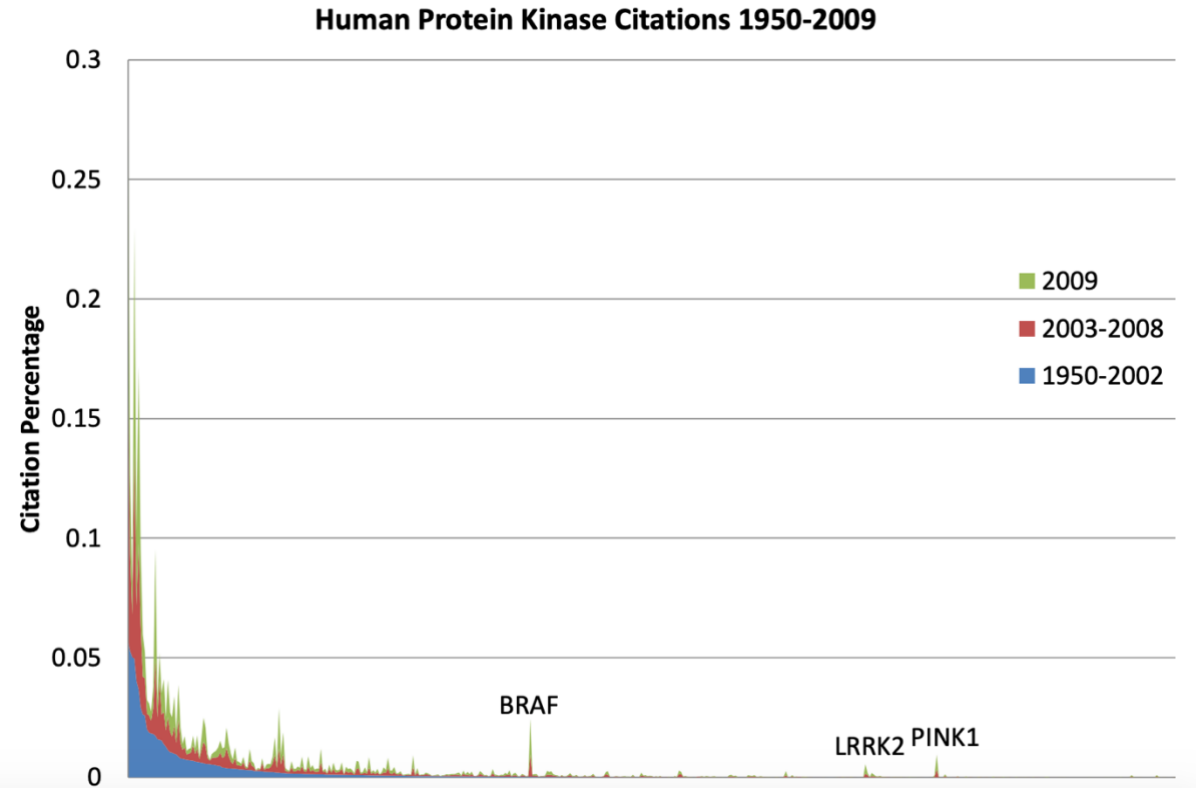

Figure 1.3 The Harlow-Knapp effect. The highest cited kinases represent about 50 targets within the kinome. BRAF, LRRK2 and PINK1 are exceptions that have emerged in 2009. This thesis aims to add PI5P4K and PIKfyve to the list of exceptions as well by garnering more interest in their druggability. Image from Fedorov et al. (2010).

kinases in developing small molecule inhibitors of the lipid kinases PI5P4K and PIKfyve, in an effort to further validate these in the context of disease and provide new starting points for therapeutic candidates. My dissertation work is centered mostly on the covalent inhibitors with the THZ inspired by imatinib, but includes the use of high-throughput screening in search of novel scaffolds (in this case, an interesting class of noncovalent thiazolidinediones or five-membered multiheterocyclic compounds) with which to diversify our targeting approach.

Phosphoinositide signaling presents itself as an opportunity for unearthing new amenable drug targets. Biological processes occur in a highly controlled manner due to the complex and intricate coordination of events and signaling agents in a temporal and spatial manner. Phosphoinositides – phosphorylated lipid moieities – represent a large number of these extremely regulated signaling pathways. Phosphoinositides are made up of two fatty acid chains linked to a glycerol moiety and a water-soluble inositol head group. The hydroxyl groups at the 3, 4, and 5 positions of the inositol ring can be differentially phosphorylated, giving rise to seven distinct phosphoinositide species: PI-3-P, PI-4-P, PI-5-P, PI-(3,4)-P_2, PI-(3,5)-P_2, PI-(4,5)-P_2, and PI-(3,4,5)-P_3. These lipids account for less than 1-5% of the total phospholipid content in mammalian cells, yet have an enormous impact on cell regulation (Tamas Balla, 2013; Thapa et al., 2016).

The composition and ratio of the various phosphoinositides is controlled and determined by phosphoinositide kinases and phosphatases that are expressed in the cell (Fig. 1.4). This “phosphoinositide profile” or “phosphoinositide code” of the cell, a result of the complex crosstalk between phosphoinositides, the enzymes modifying them and the effectors which recognize unique phosphate arrangements around the inositol ring, is crucial for the function of cellular processes, and slight changes in the overall proportions of various phosphoinositides can lead to very different consequences in signal transduction, gene expression, membrane trafficking, and cellular homeostasis (Craene, Bertazzi, Bär, & Friant, 2017; Hamann & Blind, 2017; Kutateladze, 2010; Stijf-Bultsma et al., 2015; Vicinanza, D ’angelo, Campli, & De Matteis, 2008). Thus, these kinases present a reasonable opportunity for modulating the

phosphoinositide profile of the cell, by directly inhibiting their catalyzing of different phosphoinositide species formation.

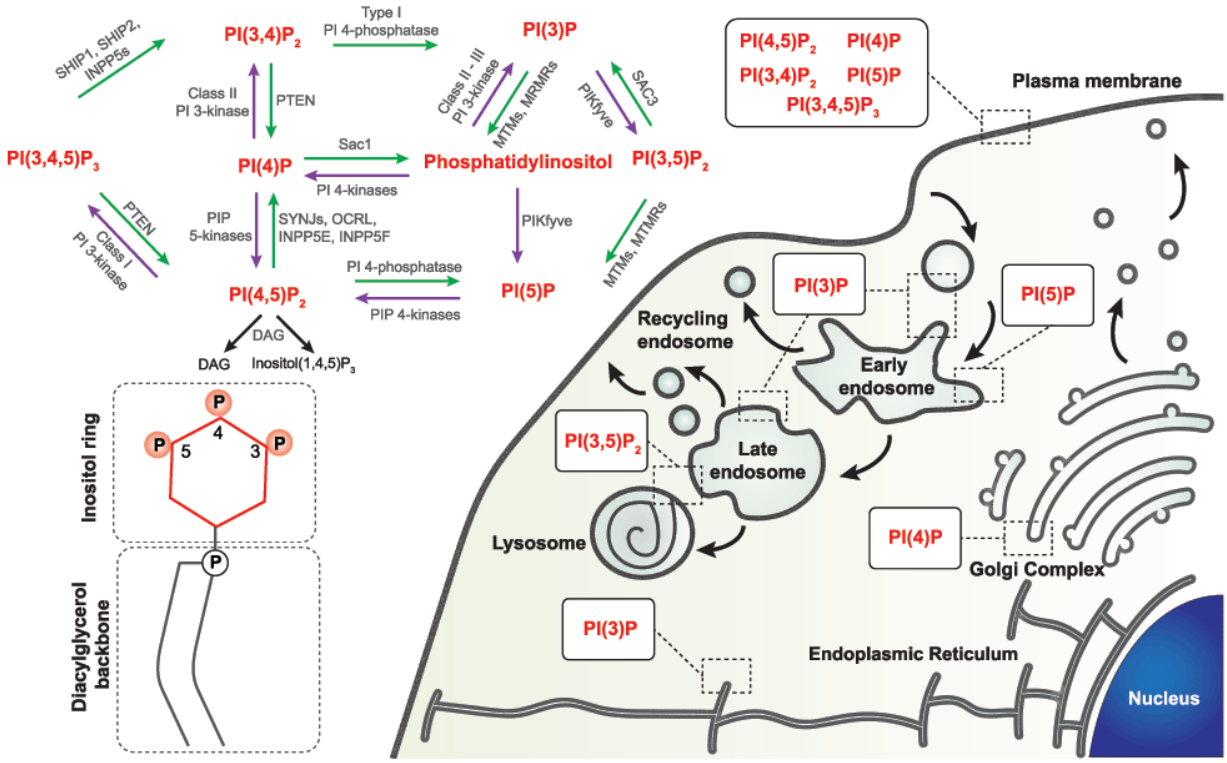

Figure 1.4 Phosphoinositide signaling network and cellular compartmentalization. Image from Picas et al. (2016).

The phosphoinositide-3-kinse (PI3K) is by far the most well-studied of this family of phosphoinositide regulators. It was identified in the 1980s as a novel phosphoinositide kinase associated with oncogenic activity, building upon several breakthrough studies elucidating the field of phospholipid signaling, phosphoinositide turnover, and discovery of second messengers diacylglycerol (DAG) and inositol-1,4,5-trisphosphate (IP_3) (Toker, 2012). Decades of intensive research has demonstrated that the PI3K pathway is central to almost all aspects of cellular physiology, with mutations

or aberrations in various components of the PI3K and AKT/mTOR downstream signaing cascade leading to disease (Cantley & Ph, 2018). PI3K has dominated the landscape of phosphoinositide signaling, but the landscape has widened tremendously in recent years, facilitating the coming of other noncanonical phosphoinositide kinases outside of PI3K into the limelight. In this thesis, we focus on two relatively understudied lipid kinase families – PI5P4K and PIKfyve – and how they function and can be targeted with small molecules in the context of disease.

Our journey with PI5P4K began with collaborators in the Cantley lab approaching us after their observation of potential synthetic lethality between the PI5P4Ks and p53 (Emerling et al., 2013). PI5P4K has also been implicated in other disease settings, as elaborated upon in Chapter 2, but there was a need for superior compounds both as tools to further validate them as druggable target, but also to serve as starting points for eventual therapeutic candidate development. Upon the fortuitous observation that a previously developed compound by our lab, JNK-IN-7, had off-target activity on PI5P4Kγ (T. Zhang et al., 2012), we embarked on a drug discovery campaign to design small molecule covalent inhibitors of the PI5P4K family. We obtained the compound THZ-P1-2, that covalently targets cysteines on a disordered loop in all three isoforms of PI5P4K. THZ-P1-2 demonstrates cellular on-target engagement with limited off-targets across the kinome. AML/ALL cell lines were sensitive to THZ-P1-2, consistent with PI5P4K's reported role in leukemogenesis (Fiume et al., 2015; Jude et al., 2014). THZ-P1-2 causes autophagosome clearance defects and upregulation in TFEB nuclear localization and target genes, disrupting autophagy in a covalent-dependent manner and phenocopying the effects of PI5P4K genetic deletion (Lundquist et al., 2018). Our

development of a covalent tool compound for PI5P4K allowed us to delve deeper into autophagy dysfunction as a phenotype of PI5P4K kinase inhibition. We also pursued alternative routes for compound generation with structure-guided rational design of THZ-P1-2 analogs and high-throughput screening to identify novel scaffolds as starting points. We are also currently pursuing a targeted protein degradation approach to investigate if acute depletion of the kinase family leads to different consequences than genetic deletion or enzymatic inhibition.

Our development of THZ-P1-2 unexpectedly led us to pursue development of inhibitors of a completely different but related lipid kinase PIKfyve. PIKfyve has also been validated as a target in Non-Hodgkin lymphoma and Ebola viral infection. We observed that THZ-P1-2 had some off-target activity on PIKfyve, albeit at a much lower level than PI5P4K. We sought to reengineer compound selectivity towards PIKfyve and identified a class of compounds from the original THZ-P1-2 scaffold exhibiting picomolar-to-nanomolar IC_{50}s in fixed time-point biochemical assays and nanomolar cellular IC_{50}s. Using our already-established multipronged approach with PI5P4K, we obtained inhibitors exhibiting cellular on-target engagement and vacuolar enlargement, a well-established PIKfyve inhibitory phenotype. Docking/modeling studies and mass spectrometry revealed a similar distant cysteine, Cys1970, to be covalently labeled by these compounds. Lastly, we discovered that this THZ-family of inhibitors, particularly two top compounds MFH-5-3 and MFH-5-4, exhibit potent antiproliferative activity in lymphoma cell lines and inhibition of Ebola viral infectivity.

This thesis aims to highlight how phosphoinositide kinases outside of PI3K can be targeted using a well-delineated logical chemical biology approach, and that their

interesting biology, which can be misregulated in disease, serves as a proximal node within the phosphoinositide signaling axis. Our studies demonstrate that the PI5P4Ks and PIKfyve are tractable targets, with our developed inhibitors serving as useful tools to further interrogate the therapeutic potential of these noncanonical lipid kinases and inform drug discovery campaigns in the context of cancer, Ebola, and potentially other autophagy-dependent diseases. We hope that the compound development approach outlined in this thesis proves that there is immense value in looking beyond the “low-hanging fruit” and continuing to expand the arsenal of therapeutics in cancer and beyond, by developing tools and agents to target, study, and validate understudied kinases.

Chapter 2. Targeting the PI5P4K lipid kinase family using small molecules

Development of novel covalent PI5P4K inhibitors in cancer

Abstract

The PI5P4Ks have been demonstrated to be important for cancer cell proliferation and other diseases. However, the therapeutic potential of targeting these kinases is understudied due to a lack of potent, specific small molecules available. Here we present the discovery and characterization of a novel pan-PI5P4K inhibitor, THZ-P1-2, that covalently targets cysteines on a disordered loop in PI5P4K$\alpha/\beta/\gamma$. THZ-P1-2 demonstrates cellular on-target engagement with limited off-targets across the kinome. AML/ALL cell lines were sensitive to THZ-P1-2, consistent with PI5P4K's reported role in leukemogenesis. THZ-P1-2 causes autophagosome clearance defects and upregulation in TFEB nuclear localization and target genes, disrupting autophagy in a covalent-dependent manner and phenocopying the effects of PI5P4K genetic deletion. We continued to pursue orthogonal approaches, including a structure-guided rational design strategy to produce improved analogs, a high-throughput screen which identified a novel thiazolidinedione scaffold which potently inhibits PI5P4K, and a degrader approach. Our studies demonstrate that PI5P4Ks are tractable targets, with THZ-P1-2 and next-generation compounds as a useful tool to further interrogate the therapeutic potential of PI5P4K inhibition or degradation, and inform drug discovery campaigns for these lipid kinases in cancer metabolism and other autophagy-dependent disorders.

Introduction

Phosphatidylinositol 5-phosphate (PI-5-P) is one of the seven phosphosinositides that regulate a wide range of cellular functions (T. Balla, Szentpetery, & Kim, 2009; Bulley, Clarke, Droubi, Giudici, & Irvine, 2015). Known to localize in the nucleus, Golgi, endoplasmic reticulum and at the plasma membrane, PI-5-P is an oxidative stress-induced regulator of AKT activation and is also regulated by proline isomerase Pin1 through Pin1's interactions with the phosphatidylinositol 5-phosphate 4-kinases (PI5P4K) in times of cellular stress (Keune et al., 2012; Keune, Jones, & Divecha, 2013). The phosphorylation of the low abundance phosphoinositide PI-5-P at the 4-position, yielding the product phosphatidylinositol-4,5-bisphosphate (PI-4,5-P_2), is catalyzed by PI5P4Kα, β and γ (encoded by genes *PIP4K2A*, *PIP4K2B* and *PIP4K2C*) (Rameh, & Cantley, 1999; Rameh, Tolias, Duckworth, & Cantley, 1997). PI-4,5-P_2 is an important precursor for second messengers inositol-1,4,5-triphosphate (IP3), diacylgycerol (DAG) and phosphatidylinositol-3,4,5-trisphosphate (PI-3,4,5-P_3) (Martelli et al., 1992; Divecha et al., 1993; Fiume et al., 2012; Fiume et al., 2015).

While the majority of PI-4,5-P_2 is generated by phosphorylation of phosphatidylinositol 4-phosphate (PI-4-P) on the 5-position by the Type I PI4P5K kinases, a PI5P4K-driven alternate route was discovered in 1997, hence the designation Type II (Rameh et al., 1997). The PI5P4Ks were traditionally thought to mainly be crucial direct regulators of PI-5-P levels (Bulley et al., 2015; Hasegawa, Strunk, & Weisman, 2017; Stijf-Bultsma et al., 2015). However, PI5P4Kα was found to synthesize a pool of PI-4,5-P_2 that is specifically important in mTORC2 regulation (Bulley et al., 2016) and to play a critical role in intracellular cholesterol transport by

modulating PI-4,5-P_2 homeostasis on peroxisome membranes (Hu et al., 2018). The low-activity isoform PI5P4Kγ was demonstrated to positively regulate Notch1 signaling by facilitating receptor recycling, suggesting that endosome-localized production of PI(4,5)P_2 is involved Notch transport (Zheng & Conner, 2018). PI5P4Kα/β were also shown to be required for autophagosome-lysosome fusion during times of metabolic stress, suggesting that they were evolved by multicellular organisms to produce sufficient PI-4,5-P_2 in nutrient-deficient conditions (Lundquist et al., 2018). These findings have dispelled the notion of PI5P4K as simply being functionally redundant in PI-4,5-P_2 production.

PI5P4K has been suggested to be important in several diseases. *PIP4K2B*-null mice were found to have increased insulin sensitivity and reduced adiposity (Lamia et al., 2004). *PIP4K2A* was found to be a dependency in AML and ALL (Jude et al., 2015; Rosales-Rodríguez, et al., 2016; Urayama et al., 2018) and *PIP4K2A*$^{-/-}$, *PIP4K2B*$^{+/-}$, *TP53*$^{-/-}$ mice had a dramatic tumor-free life extension compared to *TP53*$^{-/-}$ mice, uncovering a potential synthetic lethality of PI5P4K with p53 (Emerling et al., 2013). Knockdown of *PIP4K2A/B* in human retinal pigment epithelial cells and rabbit models abrogated the pathogenesis of proliferative vitreoretinopathy (Ma et al., 2016). Deletion of *PIP4K2C* in mice resulted in an increase of proinflammatory cytokines and T-helper-cells, as well as a decrease in regulatory T-cells via hyperactivation of mTORC1 signaling (Shim et al., 2016). Pharmacological inhibition or knockdown of PI5P4Kγ reduced mutant huntingtin protein in human patient fibroblasts and aggregates in neurons, and relieved neuronal degeneration in *Drosophila* models of Huntington's disease (Al-ramahi et al., 2017). The critical role of the PI5P4Ks in mediating autophagy

may explain their induced essentiality in various disease pathologies (Emerling et al., 2013; Vicinanza et al., 2015; Al-Ramahi et al., 2017; Lundquist et al., 2018). Collectively, these studies suggest that the PI5P4Ks represent a novel lipid kinase family whose underlying biology is important to numerous cellular processes and warrants further investigation of their therapeutic potential across a range of disease states.

The relevance of PI5P4K in a wide range of diseases has motivated efforts to develop PI5P4K inhibitors. Reported pan-PI5P4K inhibitors (Kitagawa et al., 2017) and isoform-specific inhibitors of PI5P4Kα (Davis et al., 2013), PI5P4Kβ (Voss et al., 2014) and PI5P4Kγ (Clarke et al., 2015; Al-Ramahi et al., 2017) have laid the foundation for evidence of PI5P4K druggability and motivated a need for inhibitors with further improved pharmacological properties. Here we present the identification of a novel potent, covalent PI5P4K inhibitor, THZ-P1-2, and characterize its cellular pharmacology in the contexts of autophagy and cancer. Using a multipronged approach combining biochemical and cellular assays, mass spectrometry, and crystallography, we discovered that THZ-P1-2 inhibits the PI5P4K family at sub-micromolar concentrations by reacting covalently with cysteine residues in a flexible loop outside the kinase domain of all three kinase isoforms. We show that THZ-P1-2 exhibits a reasonable selectivity profile across the kinome, with an S-score $S_{(10)}$ of 0.02 (Karaman et al., 2008, Davis et al., 2011) and inhibits cell proliferation at micromolar concentrations in a panel of leukemia cell lines in a manner dependent on covalent targeting. Finally, further investigation of the mechanism of action of THZ-P1-2 led us to the observation that THZ-P1-2 causes lysosomal disruption and defects in the clearance of

autophagosomes, halting autophagy and phenocopying the effects of genetic deletion of PI5P4Kα/β/γ (Al-Ramahi et al., 2017; Lundquist et al., 2018). These studies provide evidence that irreversible inhibition of PI5P4K by THZ-P1-2 compromises autophagy, an essential alternative energy source during periods of metabolic stress which cancer cells depend on to maintain cellular homeostasis and prolonged cell viability, further suggesting PI5P4K as a potentially important target in cancer metabolism and other autophagy-dependent diseases. We also pursued orthogonal approaches, including a structure-guided rational design strategy to study the structure-activity relationships of the THZ-P1-2 scaffold to PI5P4K, a high-throughput screen which identified a novel thiazolidinedione scaffold which potently inhibits PI5P4K, and a degrader approach which we are continuing to optimize to achieve PI5P4K degradation and investigate its cellular consequences.

Results

Chemoproteomic profiling and synthetic chemistry approaches reveal novel lead PI5P4K inhibitor THZ-P1-2

A previously developed acrylamide-based covalent JNK inhibitor, JNK-IN-7, was serendipitously discovered to also have activity on PI5P4Kγ through KiNativ cellular selectivity profiling (Fig. 2.1A, Fig. S1A) (T. Zhang et al., 2012). JNK-IN-7 was found to inhibit the kinase activity of PI5P4Kα/β/γ in a radiometric thin-layer chromatography (TLC) assay (Fig. S1B-C) and mass spectrometry revealed labeling of cysteine residues located on a disordered loop that is not observed in the available PI5P4K crystal

structures (Fig. S1D-E). We pursued a focused medicinal chemistry campaign guided by biochemical kinase assays and cellular pulldowns to optimize the potency and selectivity of phenylamino-pyrimidine which resulted in the development of THZ-P1-2 (Fig. 2.1A). THZ-P1-2 demonstrated inhibition of PI5P4Kα kinase activity (Fig. 2.1B), with an IC_{50} of 190 nM using an ADP-Glo (Promega) bioluminescence assay. THZ-P1-2 exhibited approximately 75% inhibition of PI-4,5-P_2 formation by PI5P4Kα and PI5P4K γ and 50% inhibition by PI5P4Kβ at a concentration of 0.7 μM monitored using a thin-layer chromatography (TLC) assay (Fig. 2.1C-D).

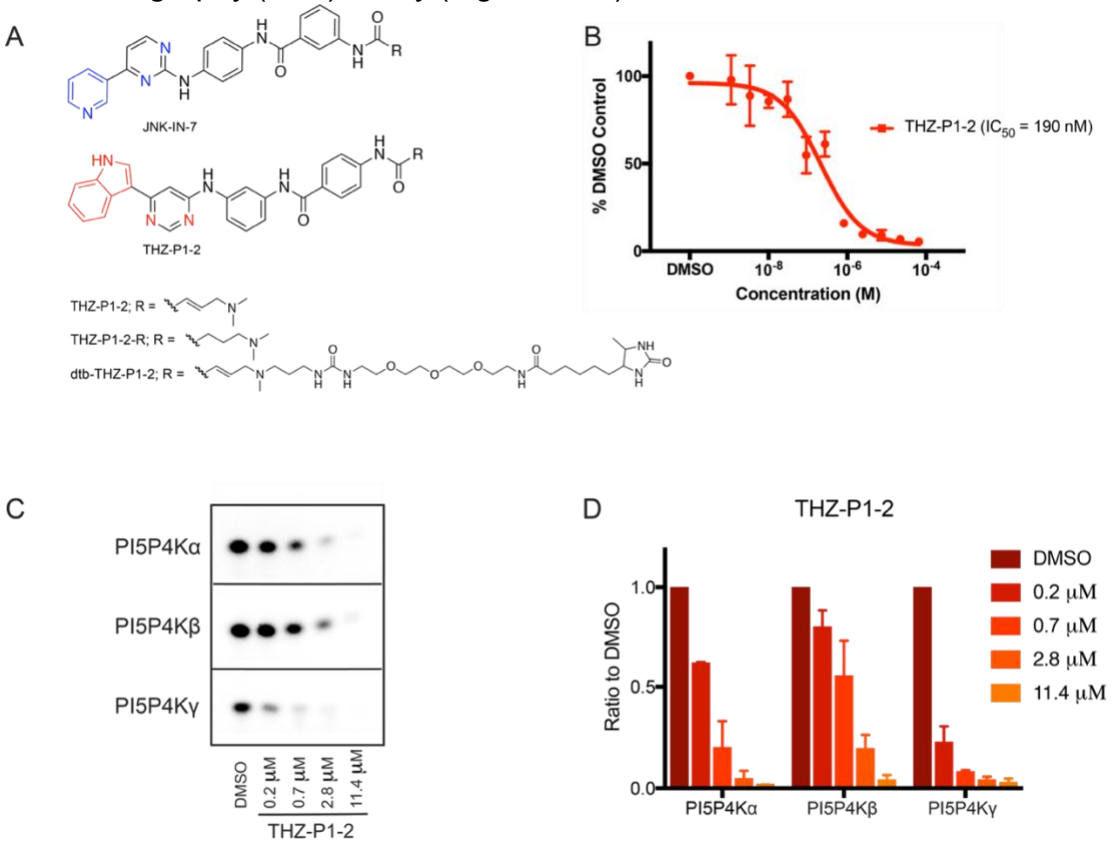

Figure 2.1. Chemoproteomic profiling and synthetic chemistry approaches reveal PI5P4K inhibitor THZ-P1-2. (A) Chemical structures of compound JNK-IN-7 as previously reported in Zhang et al (2012) and novel compound THZ-P1-2 with its reversible and desthiobiotinylated counterparts. (B) THZ-P1-2 potently inhibits PI5P4Kα kinase activity in the ADP-Glo luminescence assay. (C) THZ-P1-2 shows potent inhibition of kinase activity of all three PI5P4K isoforms in a radiometric TLC assay measuring radiolabeled PI-4,5-P_2. TLC image shown is representative of two independent experiments. (D) Quantification of (C). Radiolabeled PI-4,5-P_2 spots were imaged by autoradiography and quantified by densitometry.

THZ-P1-2 Binds in the Active Site and Covalently Modifies Cysteine Residues of the PI5P4K Kinases

Based on the initial evidence of ATP-competitive inhibition and the covalent binding of JNK-IN-7 to PI5P4Kγ, we sought to confirm covalent binding of THZ-P1-2 to each PI5P4K isoform. Upon incubating THZ-P1-2 with recombinant PI5P4Kα/β/γ protein and analyzing each sample by electrospray mass spectrometry, we discovered that the compound covalently labeled each isoform, as evidenced by the mass shift corresponding to the labeled protein, more efficiently than observed with JNK-IN-7 (Fig. 2.2A). Notably, THZ-P1-2 achieved 100% labeling of PI5P4Kα/β within 2 h, and PI5P4Kγ in 30 min, corroborating earlier observations in the TLC assay. This observed labeling is dependent on the compound possessing the cysteine-reactive acrylamide moiety, and we confirmed this using a non-cysteine-reactive analog of THZ-P1-2, containing a 4-(dimethylamino)butanamide warhead (Fig. 2.1A). The reversible counterpart, denoted by THZ-P1-2-R, did not label the recombinant PI5P4K protein (Fig. S2B).

To ascertain the specific residues covalently modified by THZ-P1-2, we performed protease digestion and tandem mass spectrometry. Here, we identified peptides containing previously unannotated cysteine residues on a conserved disordered loop residing outside of the PI5P4K isoforms kinase ATP-binding sites – Cys293 on PI5P4Kα, Cys307 and Cys318 on PI5P4Kβ, and Cys313 on PI5P4Kγ – that were covalently modified by THZ-P1-2 (Fig. 2.2B, Fig. S2A). We hypothesize that this interaction is possible as the disordered loop region is brought into close proximity of

the ATP-binding pocket through tertiary structure. These observations add PI5P4K to the list of kinases that possess targetable cysteines distant from the ATP-site in sequence yet accessible proximal to the ATP-site due to the overall kinase conformation (Zhang et al., 2016; Kwiatkowski et al., 2014; Browne et al., 2018).

Elucidation of the crystal structure of THZ-P1-2 bound to PI5P4Kα

To elucidate the detailed molecular interactions involved with the covalent and non-covalent interactions of THZ-P1-2 with the PI5P4Ks, we determined a crystal structure of PI5P4Kα in complex with THZ-P1-2 to 2.21 Å resolution (Fig. 2.2C, Fig. S2C). The crystal structure showed crucial non-covalent interactions within the ATP-binding pocket. Asn198 forms hydrogen-bonding interactions between the carbonyl of the benzamide and the amine linker connecting the phenylenediamine with the pyrimidine moiety of THZ-P1-2. Furthermore, aromatic π-stacking interactions between the phenylenediamine and Phe200, as well as hydrophobic interactions between the indole head group and linker regions of THZ-P1-2 and several residues in the active site were detected (Fig. 2.2C-D). Unfortunately, as has been observed in previously published crystal structures, there was insufficient electron density to resolve the disordered loop containing the reactive Cys293 (Fig. S2D). However, it is clear from the co-structure that the cysteine-containing loop could easily traverse the region adjacent to where the acrylamide warhead of THZ-P1-2 is situated. Alignment of crystal structures of PI5P4Kβ (1BO1) and γ (2GK9) deposited in the Protein Data Bank to our resolved co-crystal structure in PyMOL allowed for a more direct comparison between

the three isoforms, showing that THZ-P1-2 likely binds to the other two isoforms in a similar manner given the high degree of homology in the active sites and cysteine-containing loops (Fig. 2.2E).

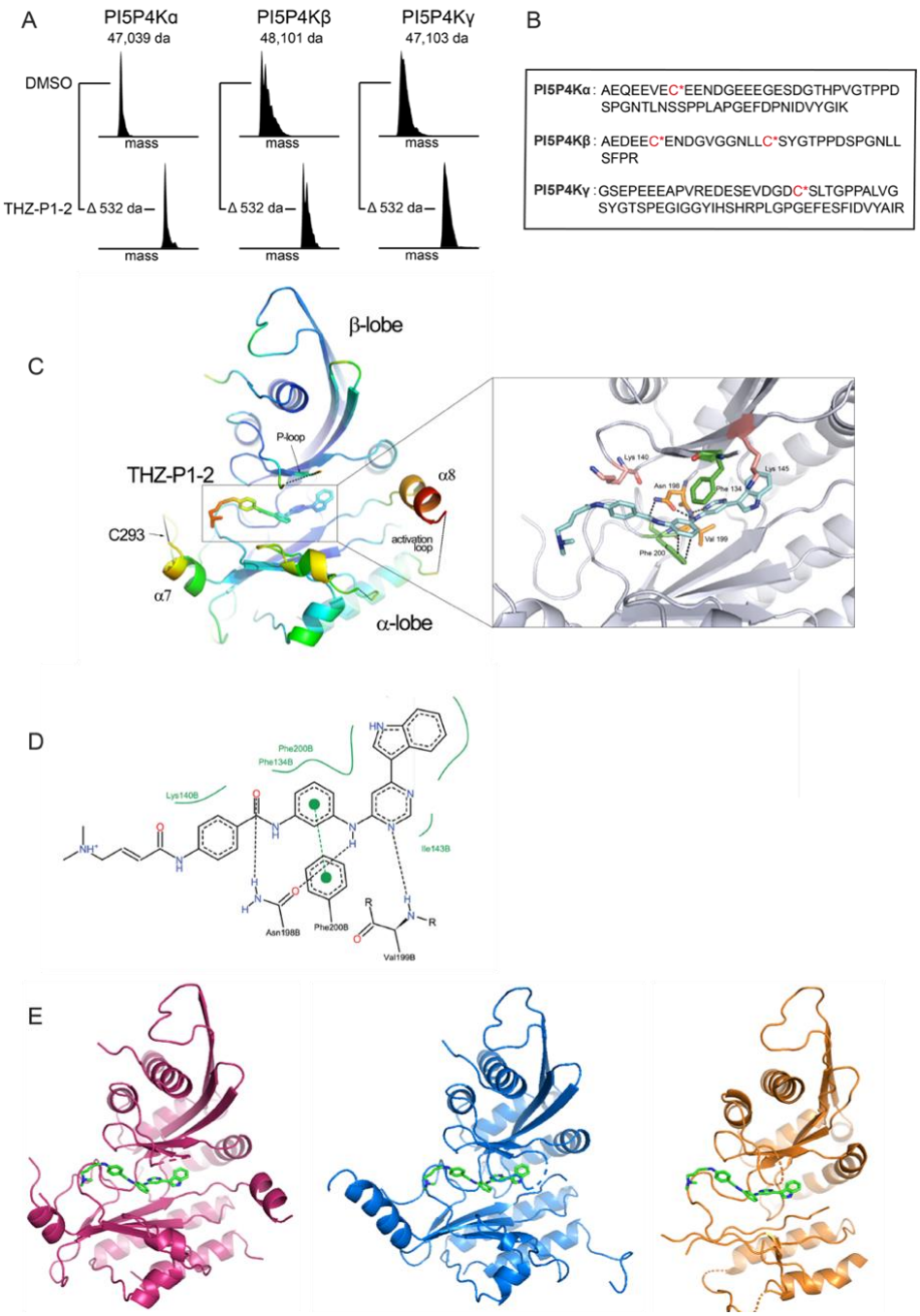

Figure 2.2. THZ-P1-2 binds covalently to all isoforms of the PI5P4K family on unique cysteine residues located on a disordered loop outside the kinase domain. (A) Electrospray mass spectrometry of recombinant PI5P4Kα/β/γ incubated with THZ-P1-2 demonstrates covalent labeling of PI5P4K isoforms. (B) Subsequent protease digestion and tandem mass spectrometry confirms that THZ-P1-2 covalently labels cysteine residues. (C) Crystal structure of PI5P4Kα in complex with THZ-P1-2, colored according to B factor and shown with covalent warhead extended out towards the covalently-targeted cysteine, C293 (labeled; not resolved in crystal structure). (D) Ligand interaction map of THZ-P1-2 with residues in the ATP-binding pocket of PI5P4Kα. (E) Modeled THZ-P1-2 binding showed for PI5P4Kβ (blue) and PI5P4Kγ (orange) based on alignment of published PI5P4Kβ and γ structures with obtained PI5P4Kα structure (magenta).

Kinase selectivity and cellular target engagement by THZ-P1-2

To confirm that the covalent binding observed *in vitro* is also observed in a cellular context, we synthesized a desthiobiotinylated derivative, dtb-THZ-P1-2, which maintained the biochemical potency of the parental compound (Fig. S3A). A streptavidin pulldown assay in HEK293T cell lysate confirmed that dtb-THZ-P1-2 could capture PI5P4K$\alpha/\beta/\gamma$ at a concentration of 1 μM (Fig. 2.3A). We further demonstrated cell permeability and cellular on-target engagement of THZ-P1-2 by performing the streptavidin pulldown assay in a competitive fashion, first pre-treating HEK293T cells with the parent compound, followed by pulldown in cell lysate with the desthiobiotinylated derivative. THZ-P1-2 demonstrated the ability to compete and block pulldown of PI5P4K with dtb-THZ-P1-2 in a dose-dependent manner (Fig. 2.3B). We observed that engagement measured by the streptavidin pulldown assay also determined covalent binding, as pre-treatment with THZ-P1-2-R was not able to block pulldown by dtb-THZ-P1-2 (Fig. 2.3B). We validated THZ-P1-2's continuous on-target engagement typical of covalent inhibitors by performing an additional pulldown with a washout at 2 hours and 4 hours, observing engagement as early as 2 hours with 1 μM compound treatment (Fig. S3B).

To broadly evaluate the kinome-wide selectivity of THZ-P1-2 we utilized the commercially available DiscoverX KINOMEScan profiling platform which revealed appreciable selectivity across the kinome with a selectivity score at a 10% DMSO control cutoff, $S_{(10)}$, of 0.02 (indicating THZ-P1-2 bound to 2% of queried kinases at the specified cutoff) (Fig. 2.3C) (Karaman et al., 2008, Davis et al., 2011). We found the related lipid kinase PIKfyve to be an off-target (6.4% DMSO control). Since PIKfyve and

PI4P5Kα/β/γ could reasonably be off-targets due to overall similar lipid kinase structure, we first tested THZ-P1-2 inhibitory activity on these kinases. We observed low micromolar IC_{50}s against PI4P5Kα/β/γ and an IC_{50} of 40 nM on PIKfyve in a fixed time-point ADP-Glo assay (Carna) (Fig. S3C). To further assess if THZ-P1-2 biochemical inhibition of these closely related lipid kinases was maintained in cells, we evaluated dtb-THZ-P1-2 binding of these targets by streptavidin pulldown. We observed no engagement of PI4P5Kα/β/γ and PIKfyve, establishing cellular selectivity of THZ-P1-2 against these related Type 1 and Type 3 lipid kinases (Fig. 2.3D). Because of THZ-P1-2's high potency on PIKfyve in the biochemical context, we took a step further to investigate its cellular activity on PIKfyve in a vacuolar enlargement assay. THZ-P1-2 produced the established PIKfyve-inhibitory phenotype in Vero cells only at a high concentration of 10 μM, 1000 x that of positive control apilimod (Cai et al., 2013; Choy & Saffi et al., 2018; Sharma & Guardia et al., 2018) which causes substantial vacuolar enlargement at 10 nM (Fig. S3D), but failed to show inhibition of PIKfyve at 1 μM. THZ-P1-2 was also unable to impair the ability of PIKfyve inhibitor apilimod to induce vacuolar enlargement when cells were either pre-incubated with THZ-P1-2 followed by apilimod, or co-incubated with both compounds (Fig. S3E).

The additional potential off-targets identified through KINOMEScan were further evaluated using the Adapta binding assay (Invitrogen). All top off-targets except for BRK and ABL1 were found to have IC_{50}s in the micromolar range (Fig. S4A). Engagement of both BRK and ABL1, both of which lack cysteines in or near the vicinity of the ATP-site, were assessed in the cellular pulldown assay with dtb-THZ-P1-2 and found to have little

to no pulldown, suggesting that the potency observed in the Adapta assay may have been due to tight noncovalent binding which was not perpetuated in the cellular context (Fig. S4B). THZ-P1-2 was markedly less potent than the ABL inhibitors imatinib, nilotinib and dasatinib, at killing BCR-ABL translocation containing cell lines (K562 and KU812F) indicating that THZ-P1-2 does not effectively inhibit BCR-ABL in cells (Fig. S4C). Interestingly, even with retention of the indole head group of THZ1 and THZ531, the switch in 2,4- to 4,6-pyrimidine from JNK-IN-7 to THZ-P1-2 was sufficient to alleviate engagement of kinases targeted by related phenylaminopyrimidine acrylamides including JNK, IRAK1, PKN3, CDK7 and CDK12 when probed in a streptavidin pulldown with their respective biotinylated or desthiobiotinylated compounds (Zhang et al., 2012; Kwiatkowski et al., 2014; Browne et al., 2018) (Fig. S4D).

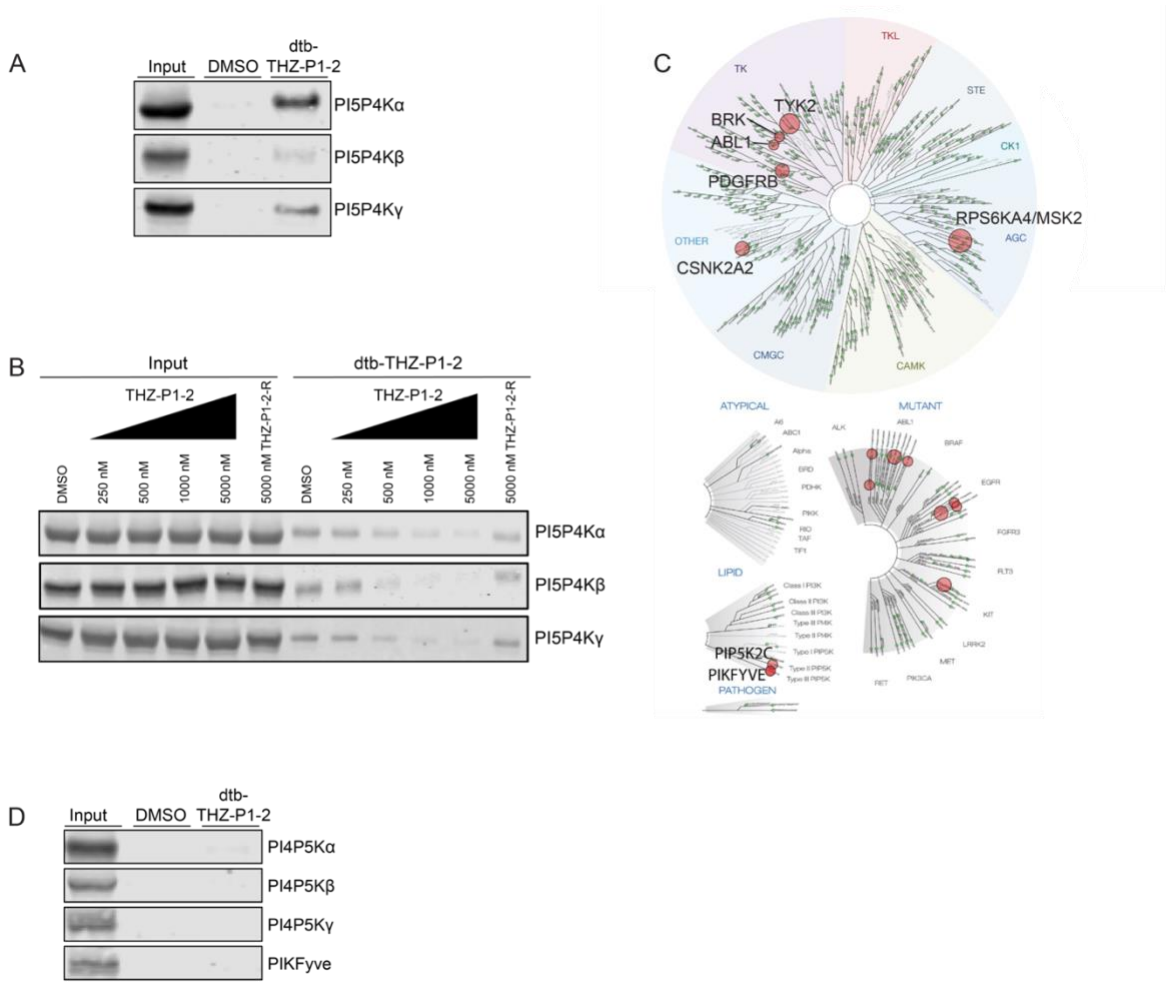

Figure 2.3. Cellular On-target Engagement and Selectivity Profile of THZ-P1-2. (A) A desthiobiotinylated analog of THZ-P1-2 irreversibly engages all PI5P4K isoforms in a streptavidin pulldown in HEK293T lysate. (B) THZ-P1-2, but not its reversible analog, exhibits dose-dependent on-target engagement of PI5P4K isoforms in a competitive streptavidin pulldown with 1 μM desthiobiotinylated-THZ-P1-2. (C) Kinome selectivity profile of THZ-P1-2. Full data to be submitted as ETD. (D) THZ-P1-2 does not engage the PI4P5Ks or PIKfyve in a streptavidin pulldown.

THZ-P1-2 as a probe for potential PI5P4K dependencies in cancer

PIP4K2A was found to be essential for cell survival in AML (Jude et al., 2015) and several variant SNPs in the *PIP4K2A* locus have been associated with ALL susceptibility and leukemogenesis (Rosales-Rodríguez, et al., 2016; Urayama et al., 2018). We evaluated the sensitivity of a small panel of leukemia cell lines to THZ-P1-2,

using a 72 h Cell-Titer Glo assay. We used THZ-P1-2-R as a negative compound to control for effects of THZ-P1-2 that are mediated solely by reversible binding. THZ-P1-2 demonstrated modest anti-proliferative activity in all six AML/ALL cell lines with IC_{50}s in the low micromolar range. We observed approximately 10-fold IC_{50} shifts between THZ-P1-2 to THZ-P1-2-R (Fig. 2.4), indicating that the presence of the PI5P4K cysteine-targeting acrylamide partially contributes to the anti-proliferative activity. ABL1 fusion genes are also heavily involved in hematological malignancies (Braekeleer et al., 2011), but the weak engagement of ABL1 in the cellular context (Fig. S4B-C), together with the covalent dependency, gave confidence that the anti-proliferative activity observed is not solely due to ABL1 inhibition.

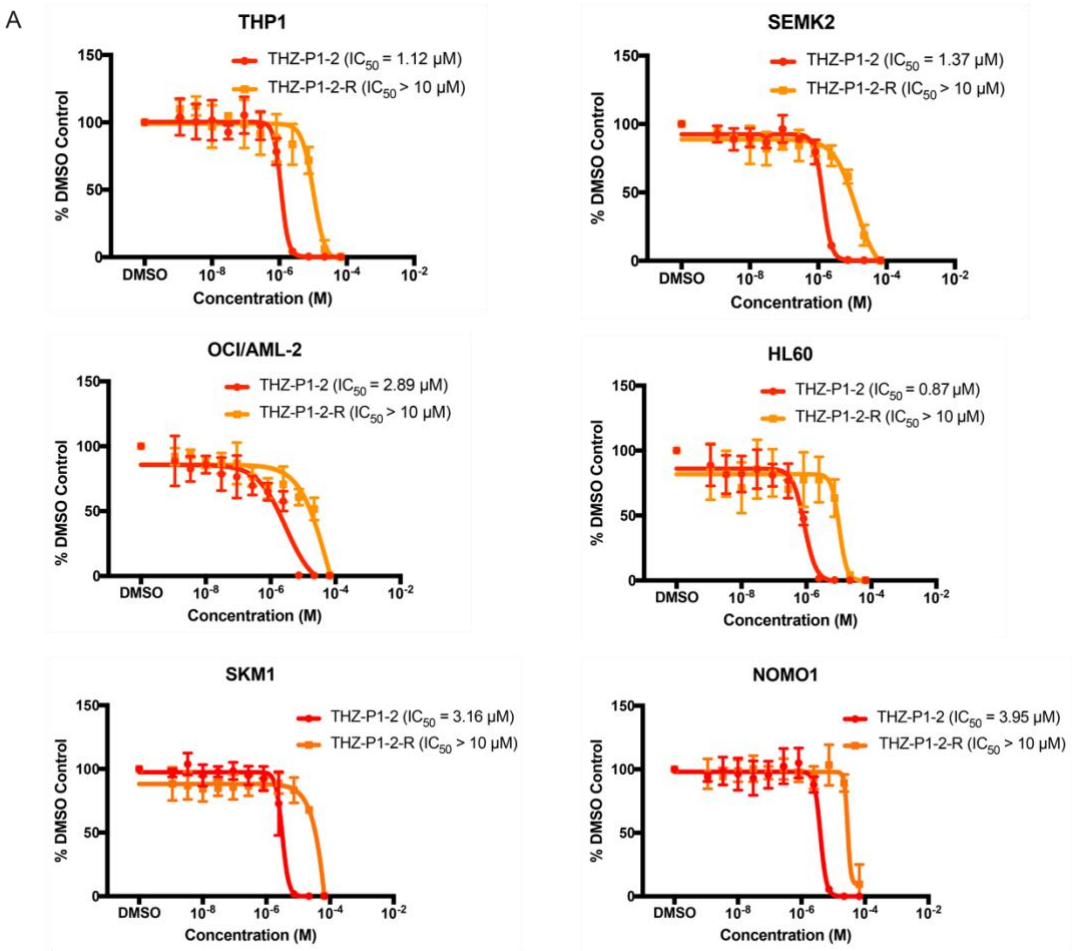

Figure 2.4. Preliminary cancer cell line profiling with THZ-P1-2 to identify potential PI5P4K dependencies. A panel of AML and ALL cell lines were treated with THZ-P1-2 and THZ-P1-2-R for 72h and cell proliferation was measured with a Cell-Titer Glo luminescence assay.

Inhibition of PI5P4K by THZ-P1-2 results in autophagy defects

Recently, PI5P4K was demonstrated to be necessary for the proper completion of autophagy in mouse models (Lundquist et al., 2018). Loss of *PIP4K2A* and *PIP4K2B* in mouse embryonic fibroblasts (MEFs) and mouse liver leads to accumulation of lysosomes and autophagosomes. Lysosomes are enlarged, fused to multiple

autophagosomes, and clustered at the nuclear membrane, indicating a defect in the autophagy process. The nuclear localization of the master autophagy transcription factor TFEB was also increased and downstream transcriptional targets were upregulated, indicating an activation of the autophagy gene program (Settembre et al., 2011). However, it has yet to be demonstrated whether these defects were caused by the loss of the full-length protein or the enzymatic activity.

To validate that PI5P4K enzymatic activity is necessary for completion of autophagy, we sought to demonstrate that THZ-P1-2 phenocopies the genetic loss of PI5P4Kα and PI5P4Kβ. We first treated HeLa cells with either DMSO or THZ-P1-2 for 18 hours and stained for the lysosomal and autophagosomal markers LAMP1 and LC3B, respectively. Similar to the genetic knockouts of PI5P4K, treatment with THZ-P1-2 at concentrations as low as 250 nM results in the formation of numerous, enlarged LAMP1 puncta with fusion defects to LC3B-stained autophagosomes (Fig. 2.5A). This upregulation in autophagosomal/autolysosomal puncta was accompanied by a slight increase in LAMP1 protein levels with 1 μM THZ-P1-2 treatment for 24 hours, and an increase in LC3B-II in serum starvation conditions (HeLa cells cultured in media supplemented with 0.3% FBS) (Fig. S4E). We also observed an increase in nuclear TFEB accumulation (Fig. 2.5B-C) and the upregulation of downstream TFEB targets with THZ-P1-2 treatment (Fig. 2.5F).

We next investigated whether the effects of THZ-P1-2 are specific to PI5P4K by rescuing the autophagy defects with the expression of PI5P4Kα/β Cys-Ser mutant isoforms, which are unable to bind the inhibitor covalently. We infected HeLa cell lines

to stably express a GFP-only vector, GFP-tagged PI5P4Kα/β, and GFP-tagged PI5P4K Cys-Ser mutants (α: C293S; β: C307,318S;). We treated the cells for 18 hours with either DMSO or THZ-P1-2. As observed with uninfected cells, cell lines expressing GFP alone saw an increase in lysosome/autophagosome dysfunction with THZ-P1-2 treatment (Fig. 2.5D-E). These effects were partially ameliorated by expression of the PI5P4K constructs and even more so by the cysteine to serine mutants (Fig. 2.5D-E). The PI5P4K Cys-Ser mutants also partially rescued the nuclear localization of TFEB.

Figure 2.5 Inhibition of PI5P4K with THZ-P1-2 leads to lysosomal-autophagosomal **defects and increased TFEB activation**

(A) Similar to genetic loss of *PIP4K2A/B*, inhibition of PI5P4K activity with THZ-P1-2 increases LAMP1-positive lysosomal size, number and contact with LC3B-positive autophagosomes. HeLa cells were cultured overnight with either DMSO, 0.25 μM, 0.5 μM or 1.0 μM THZ-P1-2 and stained for LC3B (magenta) or LAMP1 (green) with nuclei in blue. Scale bars, 10 μM. (B) Inhibition of PI5P4K activity with THZ-P1-2 increases TFEB nuclear localization. HeLa cells were cultured overnight with either DMSO, 0.25 μM, 0.5 μM or 1.0 μM THZ-P1-2 and stained for TFEB (green) with nuclei in blue. Scale bars, 10 μM. (C) Quantification of results in (B). The intensity of TFEB immunofluorescence was quantified in the nucleus and the cytoplasm, and used to calculate the ratio. Statistical significance determined by ANOVA (***$p < 0.0005$) with Dunnett multiple comparison post-test. Each group was compared to control control HeLa cells treated with DMSO, ($n \geq 30$). (D) Expression of PI5P4K cysteine to serine mutants alleviates lysosomal dysfunction induced by THZ-P1-2 treatment. HeLa cells were infected with viruses expressing GFP, GFP-PI5P4Kα, GFP- PI5P4Kα C293S, GFP-PI5P4Kβ, or GFP-PI5P4Kβ C307S C318S and treated with either DMSO or 250 nM THZ-P1-2 overnight. Expression of both the PI5P4Kα and PI5P4Kβ cysteine to serine mutants alleviated dysfunctional lysosomes (green) with nuclei in blue. Scale bars, 10 μM. (E) Quantification of results in (D). The number of lysosomes was quantified per cell. Statistical significance determined by ANOVA (***$p < 0.0005$) with Dunnett multiple comparison post-test. Each group was compared to control HeLa cells expressing GFP and treated with DMSO, ($n \geq 30$). (F) HeLa cells expressing GFP, GFP-PI5P4Kα, GFP- PI5P4Kα C293S, GFP-PI5P4Kβ, or GFP-PI5P4Kβ C307S C318S were treated with either DMSO or 250 nM THZ-P1-2 overnight for 16 hours and subsequently harvested for qPCR of TFEB targets. Fold change is calculated by comparison to HeLa cells expressing GFP treated with DMSO. *$p < 0.05$, Student's t-test, ($n \geq 8$).

Figure 2.5 (Continued)

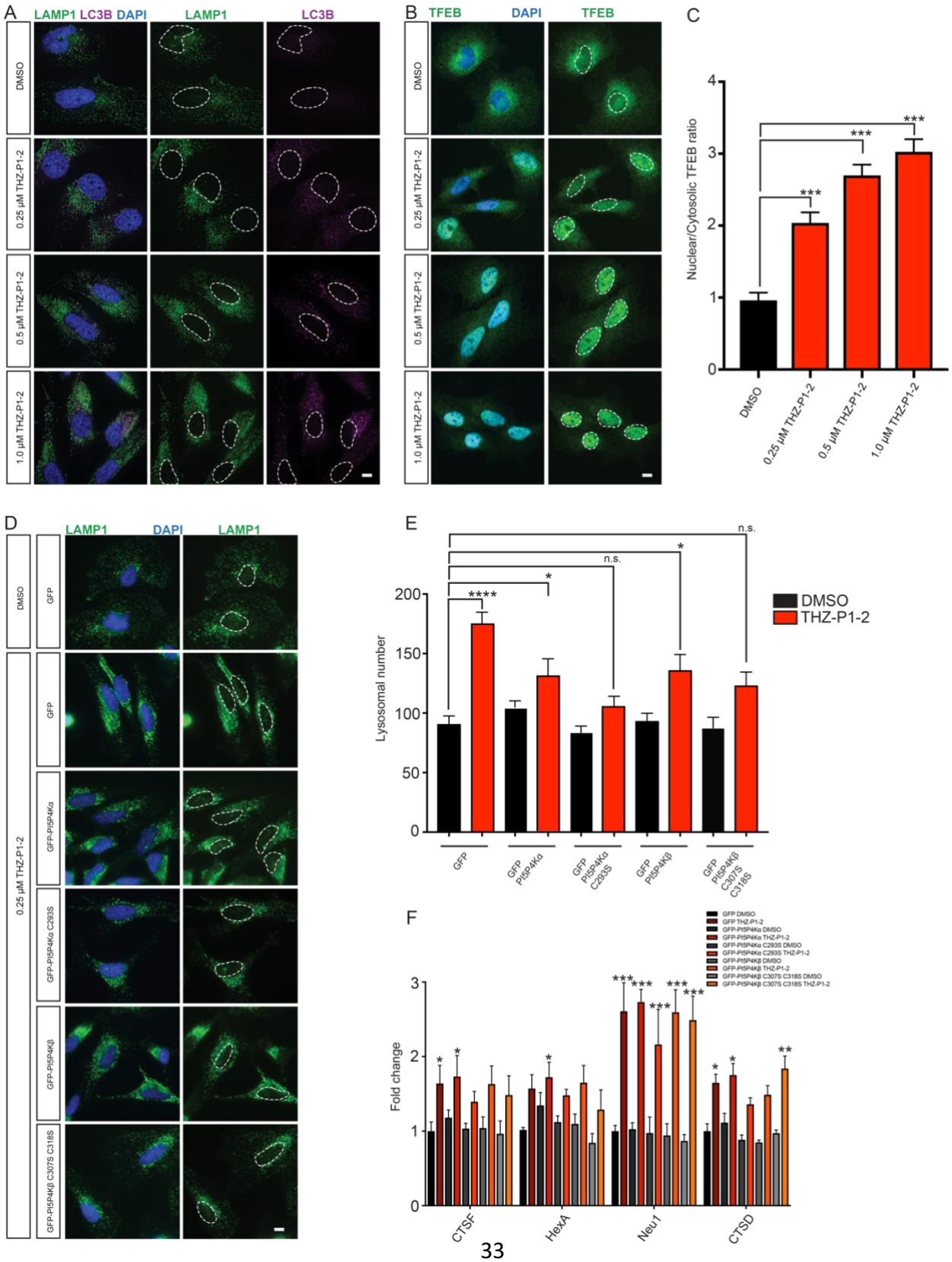

Structure-Activity Relationships (SAR) of the THZ-scaffold on the PI5P4Ks

The THZ-P1-2 scaffold has been studied and characterized widely, being the core scaffold for previously published inhibitors THZ1, THZ-5-31, JNK-IN-7, and JZ128. To further explore the functionality of the scaffold as it pertains to PI5P4K activity, we embarked on a medicinal chemistry campaign to explore the SAR of these compounds with PI5P4K. We designed a series of new analogs inspired by a series of compounds available for *in silico* screening from the ICCB-Longwood facility, particularly with functional group modifications in the head group region to take advantage of the deep hydrophobic pocket in PI5P4K (Fig. 2.6A) . We proceeded to dock these designs into our resolved co-crystal structure of PI5P4Kα in complex with THZ-P1-2 using Schrodinger's Glide XP workflow in order to rank and prioritize analogs according to predicted binding affinity (Fig. 2.6B). Upon determining compounds that bound in the correct orientation to the kinase, we narrowed down the list of modification design ideas and incorporated them into the current THZ-P1-2 scaffold.

The main objective in probing the SAR of this scaffold was to hopefully obtain a next-generation compound possessing superior potency and selectivity for PI5P4K. The added knowledge from continued modifications on the scaffold would also be useful for directing selectivity towards alternative targets (as we will discuss in Chapter 3 with PIKfyve). Although the co-crystal structure did not resolve the cysteine-containing loop and covalent bond, the structure very clearly revealed key reversible interactions, notably two hydrogen bonds between the aminopyrimidine and Asp-198, a hydrogen

bond between the pyrimidine and Val-199, as well as π-stacking interactions between the phenyl group and Phe-200 in the hinge region.

A

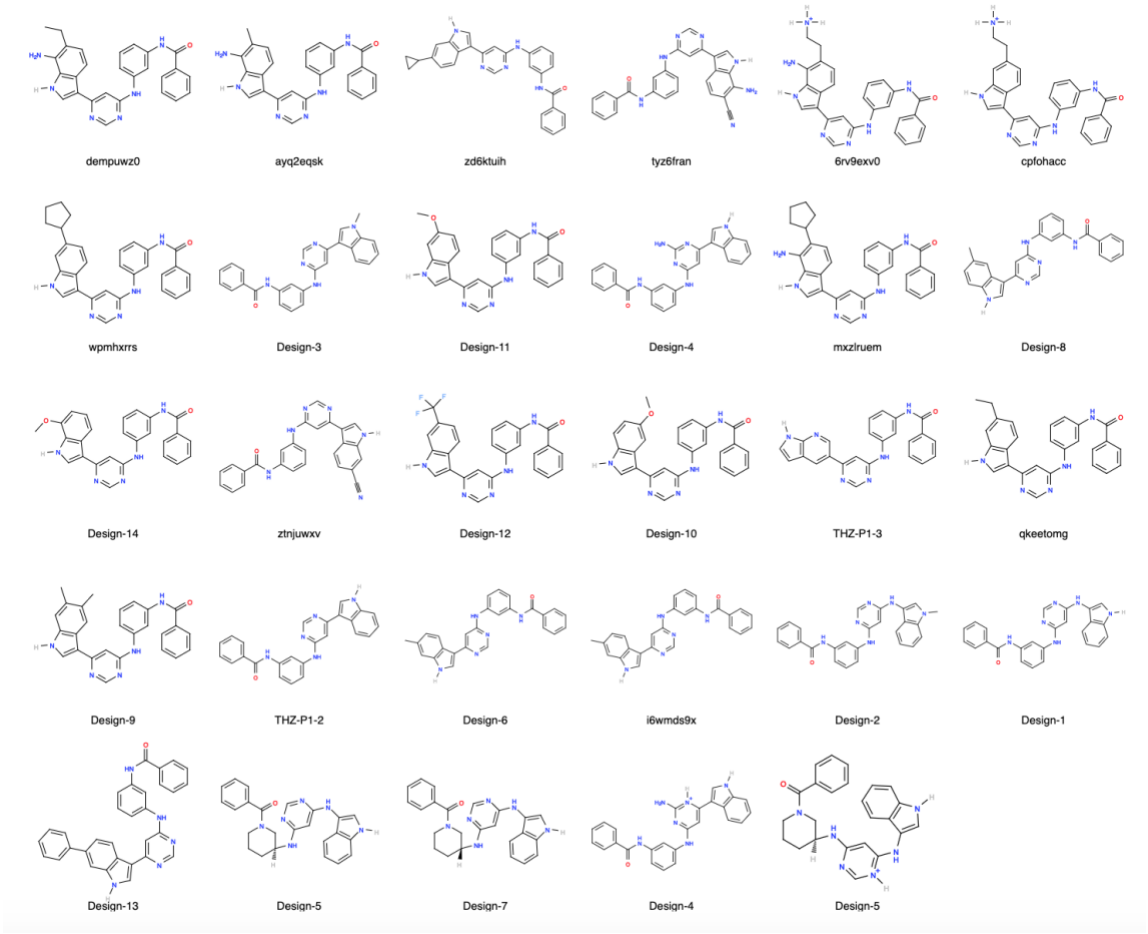

B

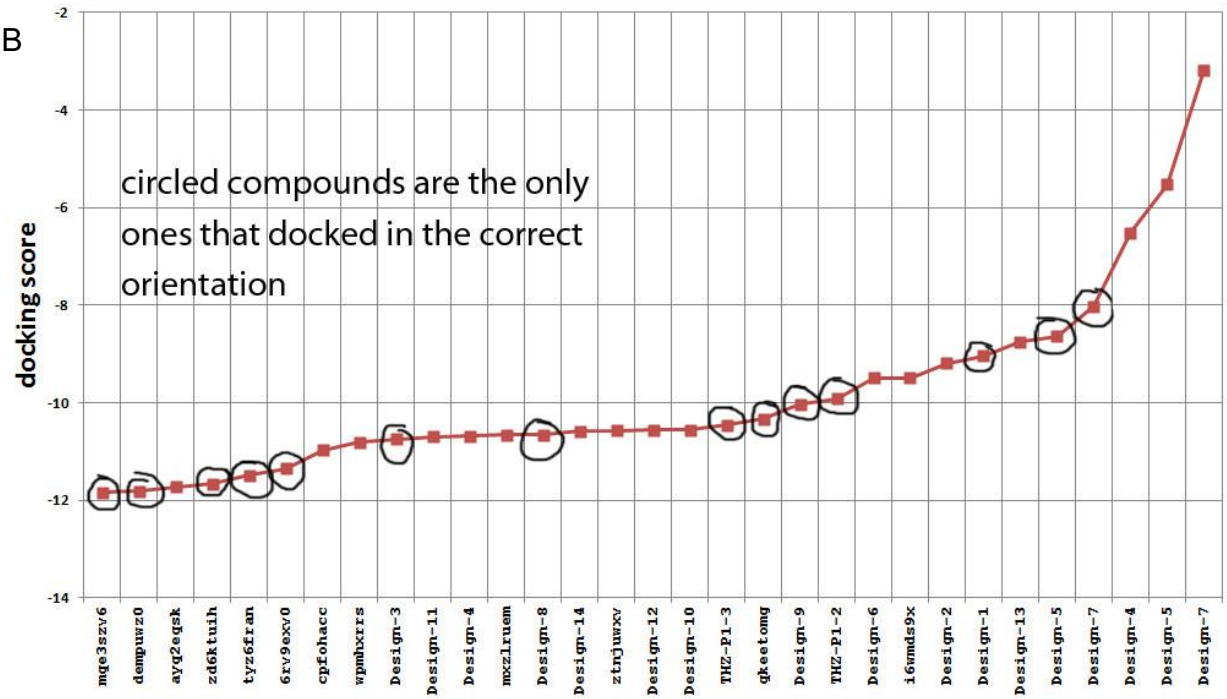

Figure 2.6. Computational analysis of potential new THZ-P1-2 analog designs
(A) Series of compound designs obtained from the ICCB-Longwood Screening Facility with similarity to THZ-P1-2 scaffold. All compounds within ICCB collections and libraries were ligprepped using EPIK generating a maximum of 32 stereoisomers per compound.
(B) Docking scores of new compound designs in Schrodinger Glide. Higher scores represent favored docked conformations.

It was also evident that hydrophobic interactions between the compound indole head group and the PI5P4K pocket under the P-loop contributed to overall affinity. The acrylamide moiety was appropriately positioned towards the solvent exposed region for undergoing a Michael addition reaction with the targetable cysteines, but further SAR studies might allow us to design compounds that covalently bind the loop cysteines in a crystallizable manner. We first synthesized a series of analogs containing variations of the indole ring system, with mono- or bi-aromatic six-membered rings to first understand and investigate the tolerability of the hydrophobic pocket of PI5P4K, as also exemplified by the higher/better docking scores indicating that modifications at the indole were preferred (Table 1).

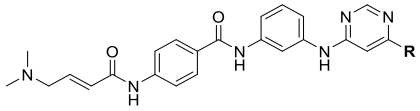

Table 2. IC_{50} evaluation of first batch of analogs

Compound Name	R	IC_{50} (μM) PI5P4Kα	PI5P4Kβ
THZ-P1-2		0.947 ±0.341	5.857 ±5.433
THZ-CE-A4		2.120 ±0.000	10.853 ±3.952
THZ-P1-16	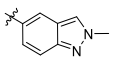	3.500 ±0.242	15.817 ±7.527
TM-02-170-01	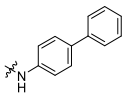	1.270 ±0.364	6.277 ±2.627
HAB001-127		1.343 ±0.155	6.163 ±1.287
TM-02-128-01	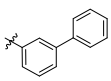	17.363 ±4.837	30.387 ±32.771

The primary synthetic strategy revolved around the key 4,6-dichloropyrimidine, which underwent either a Suzuki coupling reaction with aromatic boronic acids/esters, or an SN_2 nucleophilic substitution reaction with aromatic amines. The second chloride group was then substituted with *m*-phenylenediamine which was extended through an amide bond with 4-aminobenzoic acid, containing a free amino group for acrylamide transformation, as the final step.

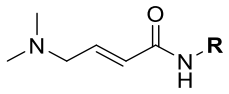

Table 3. IC_{50} evaluation of second batch of analogs

Compound Name	R	IC50 (μM) PI5P4Kα	PI5P4Kβ
TM-02-182-01	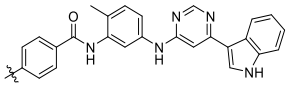	5.307 ±3.925	33.640 ±8.175
THZ-P1-14	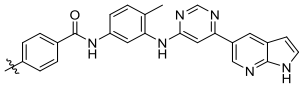	6.497 ±0.895	20.530 ±11.934
THZ-P1-5	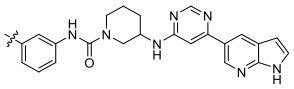	inactive	inactive
THZ-P1-12	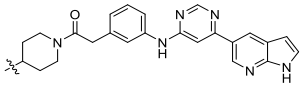	2.563 ±0.756	10.103 ±10.228
THZ-P1-10	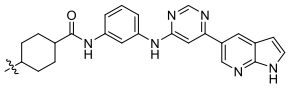	2.013 ±1.166	31.847 ±4.059
THZ-P1-3	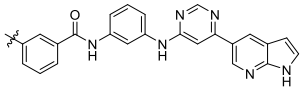	2.130 ±0.778	8.867 ±2.856
THZ-P1-18	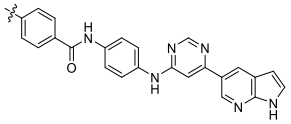	1.987 ±0.355	35.580 ±2.408
TM-02-087-01	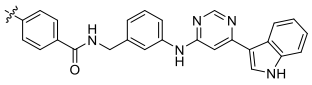	5.197 ±2.825	29.810 ±12.124
TM-02-137-01	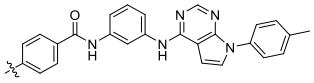	1.343 ±0.155	9.920 ±2.765

We also explored the SAR for the middle linker region and the solvent exposed region of the compound by designing a second group of THZ-P1-2 analogs (Table 2) where the chloro at the 6-position of the pyrimidine was substituted with aromatic amines through SN_2 reactions, which were then further conjugated with either 3- or 4-nitro benzoic acid, 4-aminocyclohexane-1-carboxylic acid or 4-aminopiperidine through amide bond formation. We further diversified this series with THZ-P1-5, possessing a piperidyl-carboxamide middle linker region. All of these compounds were appended with an acrylamide warhead with varying linkers.

An ADP-Glo assay and Transcreener assay for PI5P4Kα and PI5P4Kβ respectively were employed (assays run by NCATS group at NIH) to produce IC_{50} values guiding initial biochemical SAR observations. THZ-P1-2 showed sub-micromolar potency of 950 nM as IC_{50} regarding PI5P4Kα – slightly increased from initial THZ-P1-2 testing likely due to a different ADP-Glo assay format, nonetheless within nanomolar range - as well as an IC_{50} of 5.9 μM in regards to PI5P4Kβ in our assay formats – also higher than the 50% inhibition observed at 700 nM in the radiometric TLC, which may also be due to assay differences. For modifications at the head group region, the pyrrolo[2,3-b]pyridine group installed in THZ-CE-A4 led to a slight decrease in potency on both isoforms, while the 2-methyl-indazole on THZ-P1-16 diminished the activity even further to 3.5 μM/15.8 μM for PI5P4Kα/β respectively. The introduction of an amine linker connecting the pyrimidine with a phenyl group substituted with a 4-methyl group or a 4-phenyl group (4-phenylaniline and 4-methylaniline R groups in TM-02-170-01/ HAB001-027) was well tolerated and kept IC_{50} values of around 1.3 μM and 6.2-6.3 μM for the α- and β-isoform of the PI5P4Ks respectively. However, conjugating the

pyrimidine with a 3-phenylbenzene group (TM-02-128-01) resulted in a more than 10-fold loss in activity, suggesting some steric clash by the bulky phenyl group which can be circumvented via extension of the head group with the amine linker in place of the phenyl group (Fig. 2.7A).

For the middle linker regions, we found that introducing a methyl group to either carbon-4 (TM-02-182-01) or carbon-6 (THZ-P1-14) of the phenylenediamine dramatically increased the IC_{50}, likely due to a loss of the π-stacking interaction with Phe-200. We saw a similar loss of affinity using a non-aromatic piperidine ring in 20, lending confidence to the our conclusion that this specific interaction was being disrupted. A scan of different linkers containing the acrylamide warhead demonstrated high tolerability and retained overall activity on PI5P4Kα, with compounds 12, 16 and 17 losing activity significantly on PI5P4Kβ. Both piperidyl- and cyclohexyl-containing compounds (THZ-P1-12 and 10, respectively) showed almost identical activity compared to THZ-P1-2 with IC_{50} values of 2.0-2.5 μM on PI5P4Kα, while PI5P4Kβ seemed to be more sensitive to changes in this motif. Similarly, the stereochemical variation of THZ-P1-2 in THZ-P1-3 and 18, attaching the acrylamide residue in either *meta* or *para* positions, reduced the inhibitory activity on PI5P4Kα, with THZ-P1-18 showing an almost 6-fold higher IC_{50} value for the β-isoform. Lastly, an extended linker via insertion of a methylene group in TM-02-087-01 saw a loss in activity on both PI5P4Kα and PI5P4Kβ as well (Fig. 2.7A).

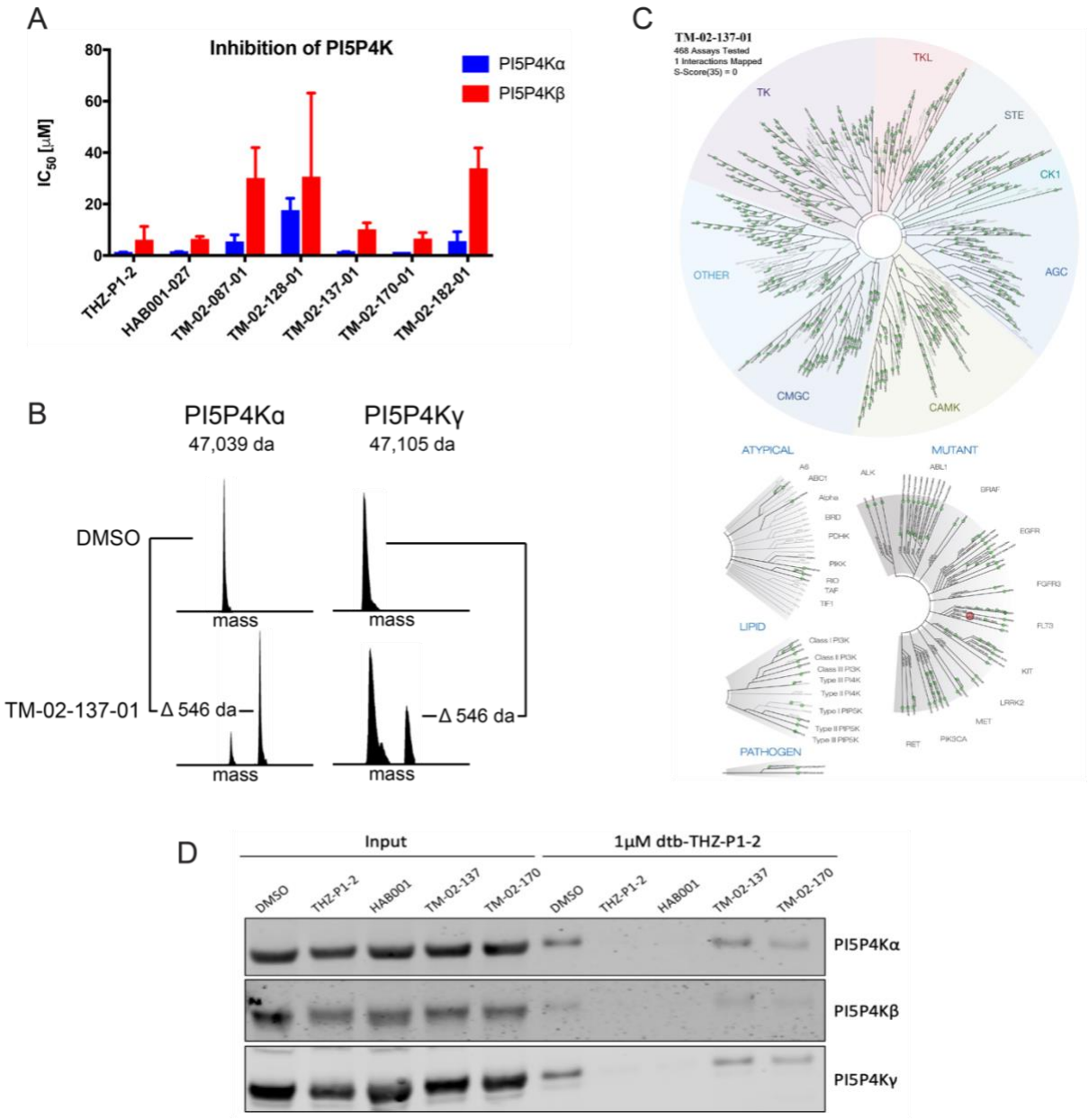

Figure 2.7. SAR of THZ-P1-2 analogs. (A) Summary of IC_{50}s of representative THZ-P1-2 analogs on pI5P4Kα/β. (B) Intact mass spectrometry showing covalent labeling of PI5P4Ks by TM-02-137-01. (C) DiscoverX KINOMEScan selectivity profiling of TM-02-137-01. Full data to be submitted as ETD. (D) Competitive streptavidin pulldown of three chosen analogs alongside THZ-P1-2 to assess on-target engagement in live HEK293T cells.

Inspired by the SAR information we obtained above, as well as the co-crystal structure of our inhibitor THZ-P1-2 with PI5P4Kα, we additionally cyclized the pyrimidine ring from carbon-4 and -5 to yield a bicyclic pyrrolo[2,3-d]pyrimidine in place of the 4,6-pyrimidine, and introduced a toluene head group, a favorable modification as observerd in HAB001-127, attached to the N-atom of the pyrrolo ring system. This led to TM-02-137-01 with an IC_{50} value of 1.3 μM and 9.9 μM for PI5P4Kα and PI5P4Kβ respectively, demonstrating satisfactory retention of biochemical potency. We confirmed PI5P4K labeling by TM-02-137-01 using mass spectrometry as well (Fig. 2.7A-B).

The selectivity profiling of THZ-P1-2 with KINOMEScan described previously exhibited some cross activity on the type I lipid kinases PI4P5K, as well as some protein kinases including BRK, TYK and ABL that we followed up on using biochemical assays and cellular pulldowns. We questioned whether the bicyclic pyrrolo[2,3-d]pyrimidine scaffold on TM-02-137-01 could dial out these off-targets, becoming a more selective PI5P4K inhibitor given its demonstrated biochemical potency. At a concentration of 1 μM, the inhibitor loses almost all off-targets seen with THZ-P1-2. An ADP-Glo-based lipid kinase panel commercial profiling (Carna) for TM-02-137-01 also demonstrated an IC_{50} for PIKfyve of over 10 μM, indicating a loss of activity caused by the chosen head group design which exploited more conformational space in the deep hydrophobic pocket of PI5P4K likely contributed to the improved selectivity (Fig. 2.7C).

To assess if the biochemical potency was retained in the native cellular context, we looked the cellular activity of the THZ-P1-2 analogs with our previously established

competitive streptavidin pulldown assay. We screened all compounds showing a biochemical IC_{50} on PI5P4Kα below 5 μM in the target engagement assay, once again using a dtb-THZ-P1-2 as a probe to immunoprecipitate the PI5P4Ks from HEK293T cells. Although TM-02-137-01 proved to have an exquisite selectivity profile across the kinome, the engagement of cellular PI5P4Ks was less than THZ-P1-2 (Fig. 2.7D); in fact, several other compounds that showed potent biochemical activity also showed compromised cellular activity, revealed by little to no ability to compete with the desthiobiotinylated probe. We hypothesize that this failure to engage the PI5P4K isoforms in cells might be due to an inability to bind covalently to the native protein. While these compounds exhibit inhibition in the biochemical setting, which does not accurately assay covalency (as determined by a small IC_{50} shift between THZ-P1-2 and THZ-P1-2-R in the ADP-Glo assay), and show the ability to bind covalently to purified protein (as observed with TM-02-137-01), the slight modifications in chemical structure might result in a loss of covalent binding in cells evidenced by pulldown results. However, HAB001-127, which showed decent biochemical inhibition of PI5P4Kα/β also performed about equally as THZ-P1-2 in preventing pulldown by dtb-THZ-P1-2, indicating that the toluene head group was a tolerable modification for covalent binding *in cellulo*. In summary, our SAR study provided insight into examples of structure variations that improved selectivity as well as modifications that retained on-target engagement.

A high-throughput screening approach towards identifying new scaffolds for PI5P4K inhibitor development

As an orthogonal approach to our structure-guided rational design strategy towards obtaining PI5P4K inhibitors, we also pursued a high-throughput screen in the hopes of discovering novel scaffolds to serve as new starting points for PI5P4K inhibitor design. The challenges of designing a screening strategy for lipid kinases with difficult-to-handle lipid substrates have fortunately been addressed previously with the development of a homogenous, robust, miniaturizable ADP-Glo-based assay, which served as the basis for in-house inhibitor biochemical testing on PI5P4Kα (Davis et al., 2013).

We sought to screen our internal kinase inhibitor library of approximately 6000 compounds. This library contains pharmacologically active compounds biased towards kinase-binding. Upon initial optimization of the assay with regards to PI5P4Kα enzyme concentration and ADP-Glo reagent volumes to obtain a robust signal:background ratio, stable Z' factor (0.725), and low CV (0.098) (Fig. S5A-B), we proceeded to screen our kinase inhibitor library of 15 plates in 384-well format (Fig. 2.8).

We screened at a relatively high final concentration of 66 μM after doing a trial screen with two plates and observing the hit rate (defined as >90% inhibition) to be relatively low. We obtained approximately 50 hits by setting a cutoff of 90% inhibition. We cherry-picked a subset of compounds from this collection based on diversity of scaffold and potential for compound optimization via design, and proceeded to obtain

full 12-point dose-response curves (Fig. 2.8). As expected, some selected compounds demonstrated inhibition only at high concentrations with relatively high IC_{50}s, likely because those compounds caused aggregation or precipitation at high concentrations, while other compounds proved to be *bona fide* inhibitors with nanomolar IC_{50}s (Fig. 2.8, Fig. S5C-D). We counterscreened this collection of compounds to investigate any potential compound interference with components of the ADP-Glo kit. The counterscreen was an assay where a fixed concentration of ADP/ATP, representing 20% conversion, is present in the absence of the PI5P4Kα enzyme and lipid substrate. All cherry-picked hit compounds were free of effects against the detection in the ADP-Glo assay, recording a fixed luminescence for 20% ATP-to-ADP conversion, indicating that the compound IC_{50} values obtained in the screen were due to the effect of the compound on the PI5P4Kα enzyme reaction itself and not nonspecific effects on the detection reagents (Fig. S5E).

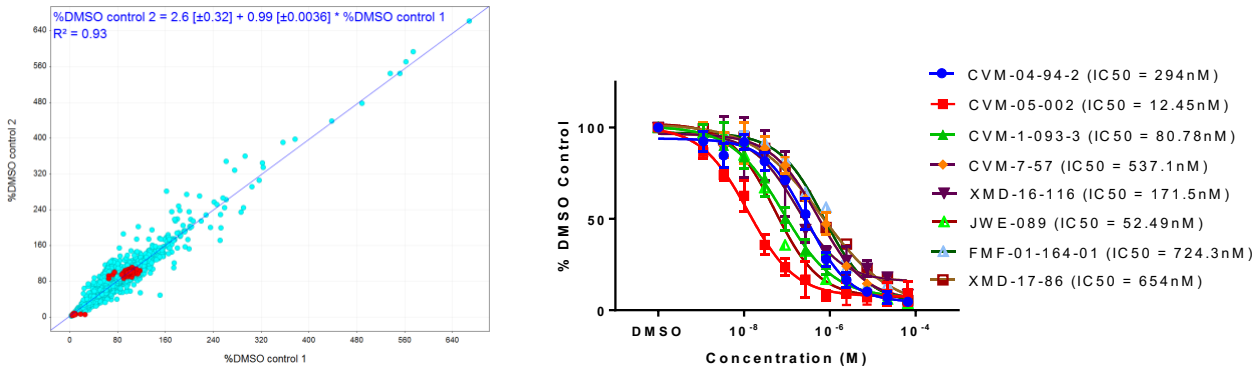

Figure 2.8 High-throughput screening on PI5P4Kα in search of novel scaffolds. A scatter plot showing the replicates of the screen and dose curves for the cherry-picked hits. Full dataset to be submitted as ETD.

We moved forward with the most potent of the identified hits, noticing an enrichment of benzodiazepinones and thiazolidinedione (TZD) derivatives with double or triple digit nanomolar IC_{50}s. We honed in on compound JWE-089 because it had a benzodiazepinone core, which has previously been studied by the lab in development of LRRK2 and ERK5 inhibitors (Deng, Dzamko, et al., 2011; Deng, Yang, et al., 2011; Williams et al., 2016), but with a slight difference of an additional 5-membered ring. We did some initial testing with several analogs of JWE-089 already available in our kinase inhibitor library database, but none were found to inhibit PI5P4Kα.

We turned our attention towards the TZD class of compounds, prioritizing CVM-05-002 as the top hit emerging from the screen. There is a general negative connotation of rhodanine-based compounds as being pan-assay interference (PAINs) compounds and frequent hitters in high-throughput screens due to their properties as aggregators and ability to interfere non-specifically with assay components (Tomašić & Peterlin Mašič, 2012). The negative reputation of these five-membered multiheterocyclic (FMMH) compounds is in stark contrast to their employment as probes that possess a variety of biological activities. They represent moieties often used as “privileged scaffolds” due to their ability to interact with a multitude of targets (Mendgen, Steuer, & Klein, 2012). Our interest in this compound class stemmed firstly from the exquisite potency we observed with these FMMH compounds, but also from the consideration that the selectivity of these rhodamine-based inhibitors could potentially be tuned in subsequent development. Furthermore, the multitargeted nature of this scaffold type could lead to meaningful polypharmacology that can be explored.

CVM-05-002 was profiled in the KiNativ profiling platform and surprisingly, found to be not very PAINs-like. CVM-05-002 had three major targets – ZC2/TNIK, RIPK2, and PI5P4Kγ -- and a range of other targets, however the compound did not seem to bind promiscuously to every single kinase on the panel as would be expected from a PAINs compound (Fig. 2.9).

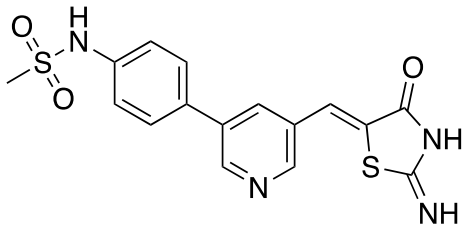

Compound	CVM-05-002
Kinase(s)	1 μM
ZC2/TNIK	>96
RIPK2	>90
PIP4K2C	97.3
MAP3K1	82.8
PIP5K3	82.8
LOK	79.7
ZAK	75.5
ZC1/HGK, ZC2/TNIK, ZC3/MINK	72.9
SLK	63.6
GSK3A	61.4
LOK	59.3
NLK	54.4
PIP4K2A	54.0
KHS1	52.4

Figure 2.9 Structure of CVM-05-002 and top hits from KiNativ selectivity profiling in THP1 cells. Full list submitted as ETD.

We proceeded to screen our kinase inhibitor library collection for analogs of CVM-05-002 containing a rhodamine derivative. We set a structural similarity limit of 55% and above, narrowed down compounds based on their similarity to CVM-05-002, and systematically approximately 30 analogs in the ADP-Glo assay. To our surprise, none of the compounds tested came close potency-wise to CVM-05-002, despite sharing most of CVM-05-002's structure with minor changes. CVM-05-002 was again by far the most potent, with an IC_{50} of around 9 nM (Fig. 2.10). This led us to believe that the binding of this pharmacophore to PI5P4Kα was very sensitive to chemical modifications.

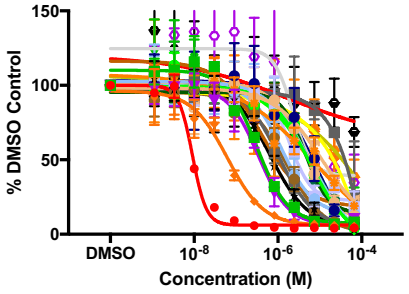

- CVM-05-002
- CVM-6-063-2
- GSK1059615
- CVM-04-133-1
- CVM-06-140-1
- CVM-06-048
- CVM-6-012
- CVM-06-041
- CVM-05-150-1
- CVM-6-039
- CVM-7-100-1
- CVM-7-100-2
- CVM-04-133-2
- CVM-05-85
- CVM-6-060-1
- CVM-08-045-C
- CVM-6-056-1
- CVM-05-144-1
- CVM-05-142-1
- CVM-05-001
- ALV-02-020-02
- CVM-05-004
- CVM-08-037-1

	IC50
CVM-05-002	9.106e-009
GSK1059615	6.272e-008
CVM-04-133-1	3.133e-007
CVM-06-140-1	3.445e-007
CVM-06-048	7.627e-006
CVM-6-012	6.557e-007
CVM-06-041	1.533e-006
CVM-05-150-1	7.536e-006
CVM-6-060-1	4.45e-006
CVM-08-045-C	1.078e-005
CVM-6-056-1	5.913e-006
CVM-05-144-1	6.306e-006
CVM-6-063-2	4.452e-006
CVM-6-039	8.079e-006
CVM-7-100-1	1.237e-006
CVM-7-100-2	1.957e-006
CVM-04-133-2	1.001e-006
CVM-05-85	~ 0.001226
CVM-05-142-1	~ 2.28
CVM-05-001	4.037e-007
CVM-05-004	2.279e-006
CVM-08-037-1	~ 15.93
ALV-02-020-02	1.785e-006

Figure 2.10 Biochemical testing of available CVM-05-002 analogs in Gray lab kinase inhibitor collection. Full dataset of all analogs to be submitted as ETD.

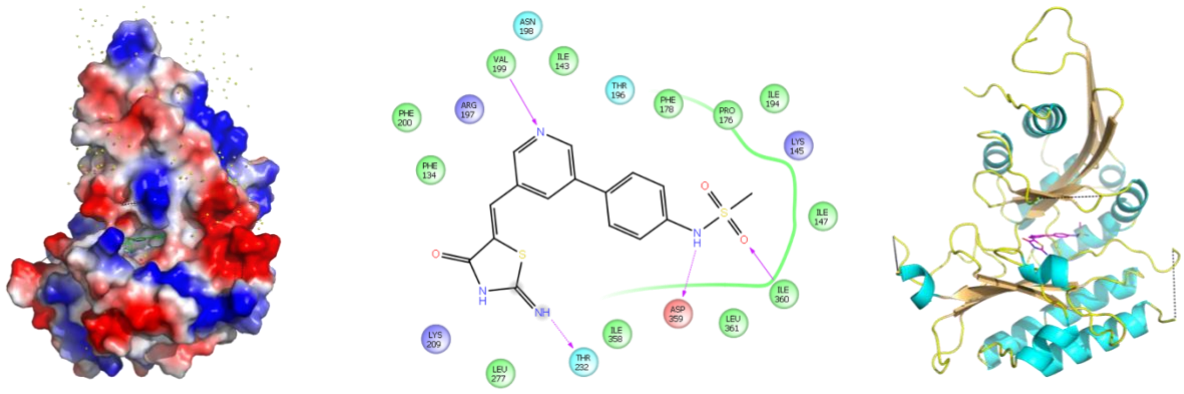

Figure 2.11 Crystal structure and ligand interaction map of PI5P4Kα with CVM-05-002. See Table S2 for diffraction data collection and refinement statistics.

We were able to obtain a crystal structure of PI5P4Kα in complex with CVM-05-002 (Fig. 2.11). The structure illuminated important hydrogen-bonding interactions between the FMMH, sulfonamide, and pyridine linker. The interactions justified why even a pyridine orientation switch, as seen with the analogs tested, led to a loss in binding activity. Using this structural information, we were able to rationally design one analog (among several inactive compounds) that not only retained activity, but actually increased potency relative to CVM-05-002 (Fig. 2.12). These compounds were tested in the live cell streptavidin pulldown assay, where they demonstrated mild competition with the desthiobiotinylated probe (Fig. 2.13). We reason that this could be because of the polarity of the compounds, causing them to have a poor cLogP (0.4-0.5) and consequently poor cell permeability, compared to THZ-P1-2 with a cLogP of around 5.

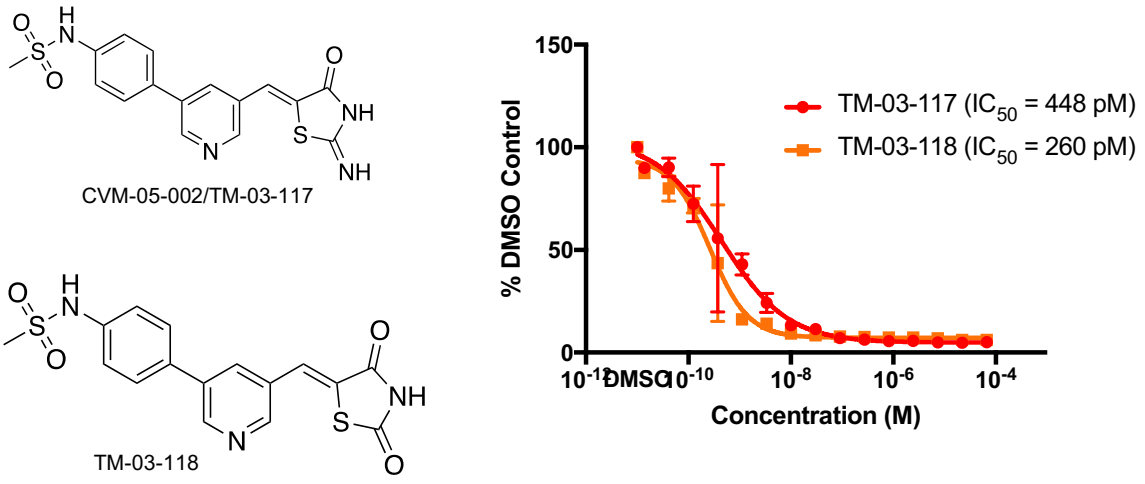

Figure 2.12 Structure-guided rational design leads to improved PI5P4K inhibitor TM-03-118. TM-03-117 refers to a new batch of CVM-05-002, which displays picomolar IC_{50}, indicating that the previous screening batch was old or had undergone degradation.

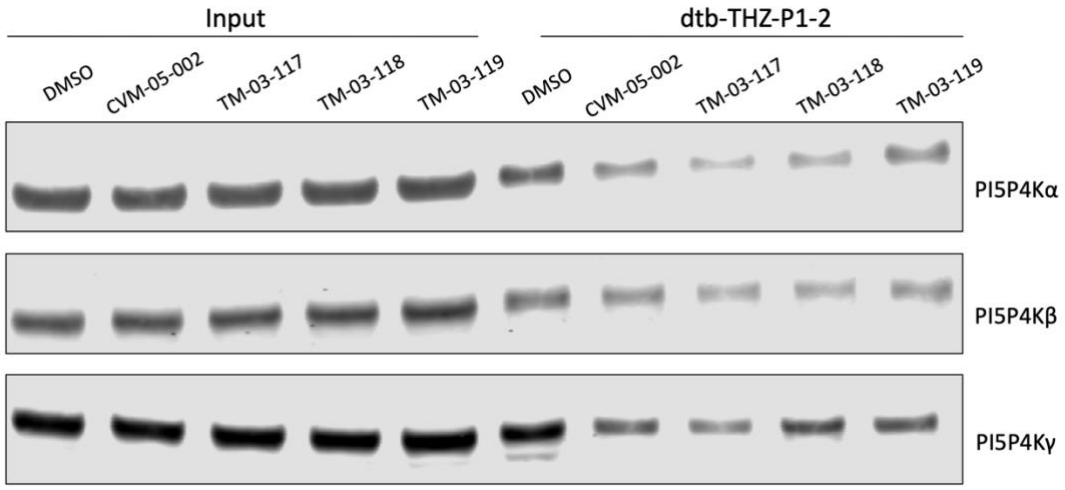

Figure 2.13 Streptavidin pulldown with CVM analogs

A targeted protein degradation approach to PI5P4K

To complement our inhibition approach, we also pursued a degradation strategy for PI5P4K. There are clear drawbacks to genetic methodologies such as RNAi and CRISPR for determining the consequence of the loss of a particular target, specifically

limitations in looking at acute changes and potential compensatory mechanisms coming into play upon long-term depletion which may be difficult to unravel. Small-molecule degradation allows for quick assessments of biological mechanisms (Nabet et al., 2018). We looked to the degradation tag (dTAG) chemical genetic system for probing PI5P4K degradation.

The dTAG system is a hybrid chemical biology technology that leverages the short-term benefits of small molecule treatment with the precision of genetic approaches. This technique builds on previously described proteostasis tag-based technologies and comprises two components (Fig. 2.14):

(1) A fusion protein of the target with $FKBP^{F36V}$, the allele-sensitive FKBP

(2) An FKBP mutant-selective bifunctional degrader molecule (termed dTAGs)

The advantage of this tagging system is the generalizability it confers, with the tag being able to be applied to virtually any target, and the exquisite selectivity of the degradation, since the dTAG degrader compound would only bind to the mutant FKBP and not the wild-type, inducing rapid and specific of the fusion protein. The F36V mutation introduces a “hole” into the FKBP12 binding site that recognizes the “bump” on the dTAG molecule. The heterobifunctional dTAG molecules are synthesized by conjugating $FKBP^{F36V}$ binders (AP1867 or a novel regioisomer ortho-AP1867) to thalidomide which binds the E3 ubiquitin ligase cereblon or CRBN (Erb et al., 2017; Huang et al., 2017; Nabet et al., 2018). Several heterobifunctional dTAG molecules were synthesized with varying linker lengths and composition.

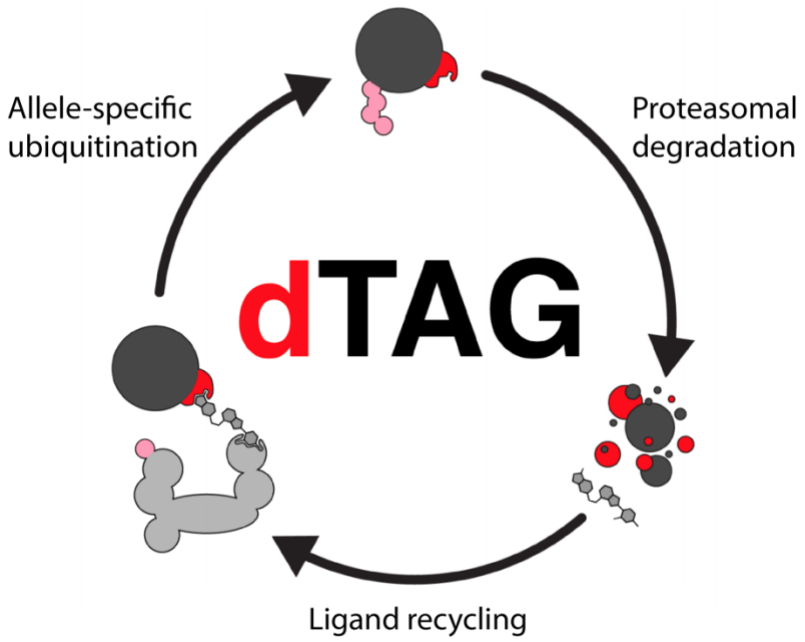

Figure 2.14 Schematic of the dTAG technology. Image modified from Nabet et al. (2018).

We employed the dTAG system with PI5P4Kα/β by generating $FKBP^{F36V}$-PI5P4K fusions, which also include a HA tag for easy Western blotting, and stably expressing them in cell lines. We started with HEK293Ts, our workhorse cell line for target engagement, but upon treating with three top dTAG candidate molecules, no degradation was observed. We looked at two additional cell lines, MDA-MB-468, chosen for its amenability to degradation with dTAG (Huang et al., 2017), and THP1, which had previously been reported to have a dependency on *PIP4K2A* (Jude et al., 2014). Both cell lines showed degradation of both exogenously expressed targets preferentially by dTAG-13 at concentrations of 50, 250 and 500 nM at 24h timepoints

(Fig. 2.15). Thus, we were able to demonstrate using dTAG the inherent degradability of PI5P4K.

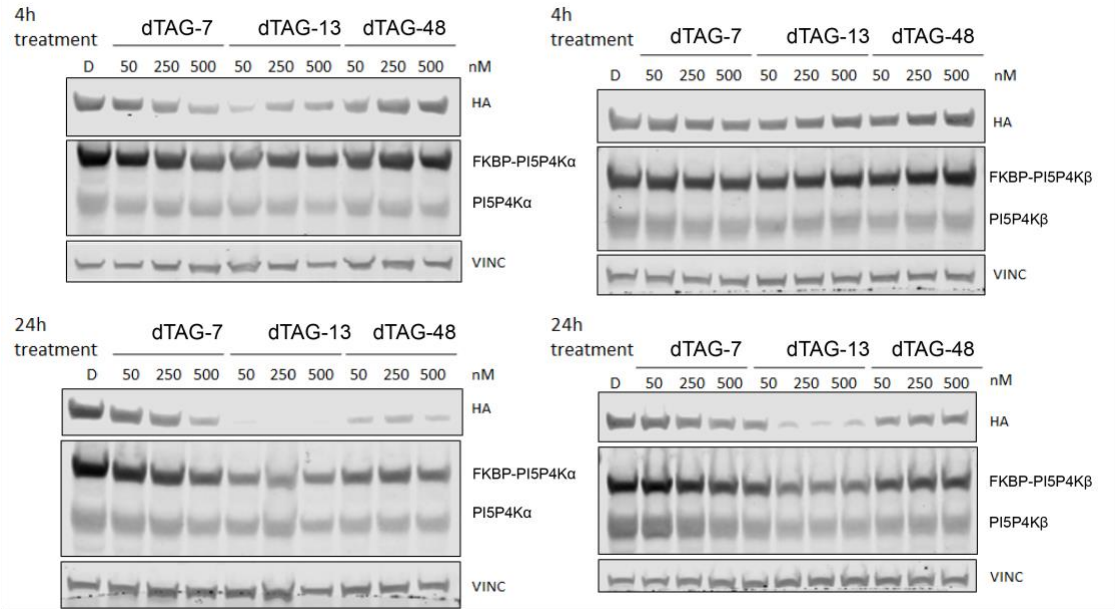

Figure 2.15 Western blot analysis of dTAG-mediated degradation of PI5P4Kα/β in MDA-MB-468.

Building on these initial observations, we pursued a PROTAC approach in designing bifunctional molecules with PI5P4K-targeting moiety and CRBN-targeting moieties to address the limitations of dTAG – namely, the need to genetically tag the target in every cell line. We synthesized bifunctional molecules, this time fusing the PI5P4K-targeting component (THZ-P1-2 or analogs) to the phthalimide CRBN-targeting moiety (Fig. 2.16). We tested these PROTACs in the ADP-Glo and Transcreener assays, finding that some of them retained some potency, while some dramatically lost activity, for instance TM-03-073-02 and TM-03-076-02 (Fig. 2.17).

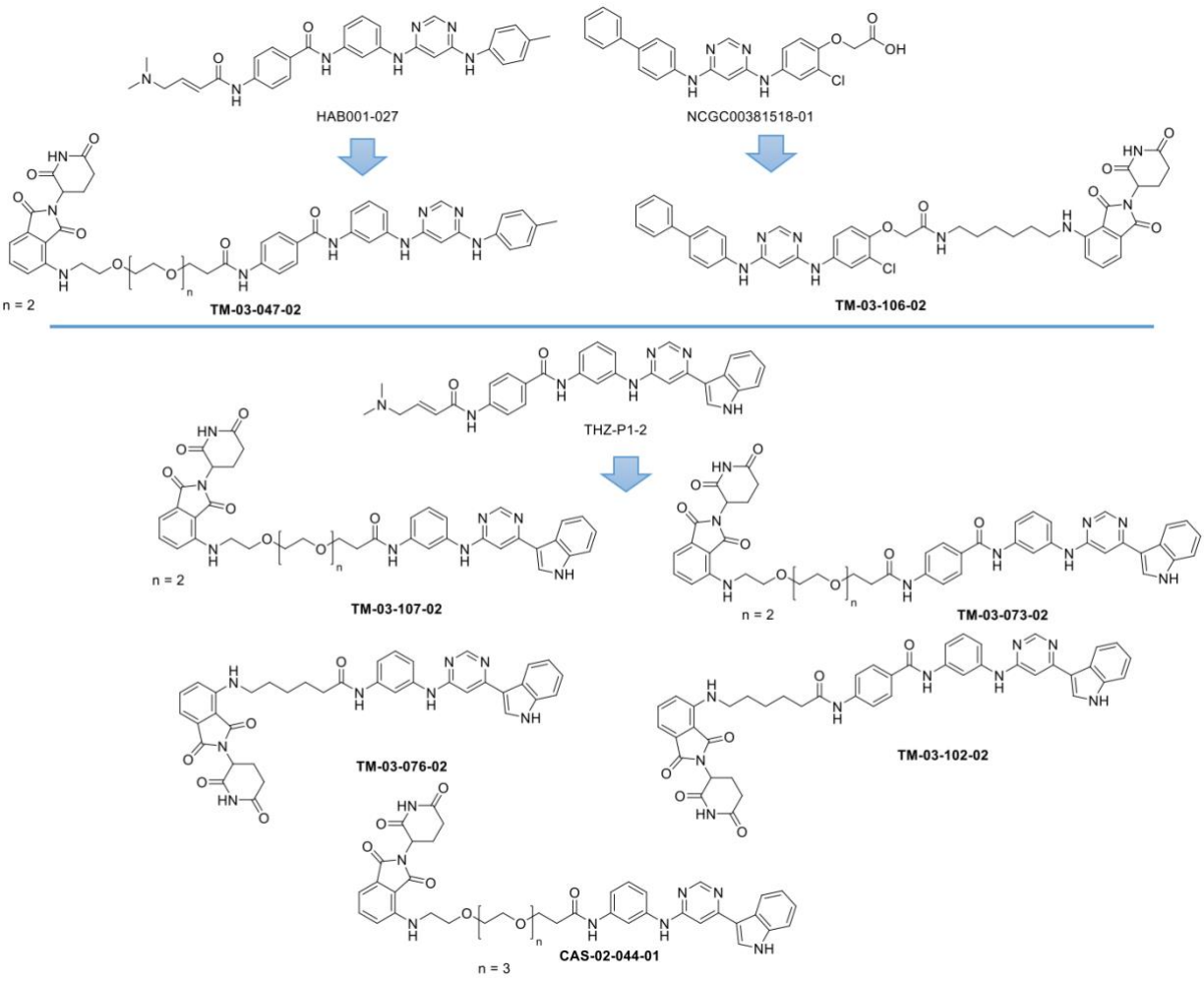

Figure 2.16 Design and synthesis strategy for PI5P4K PROTAC approach.

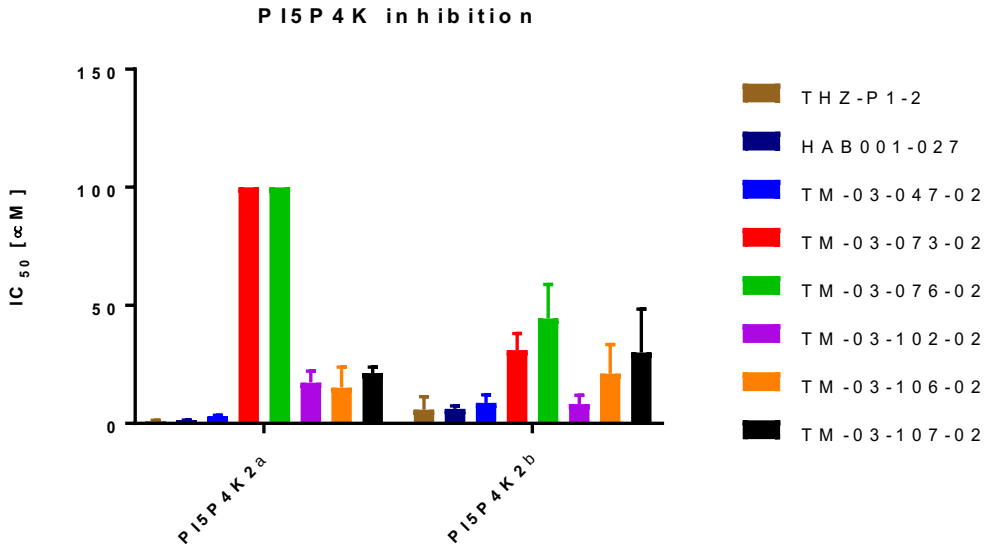

Figure 2.17 Evaluated IC_{50}s for PROTACS in ADP-Glo and Transcreener assays.

We tested two PROTACS in MDA-MB-468 cells in a time-course at two doses, and saw moderate degradation of the PI5P4Ks – for instance, TM-03-107-02 seemed to induce some degradation at time points after 2h, while TM-03-106-02 seemed to induce

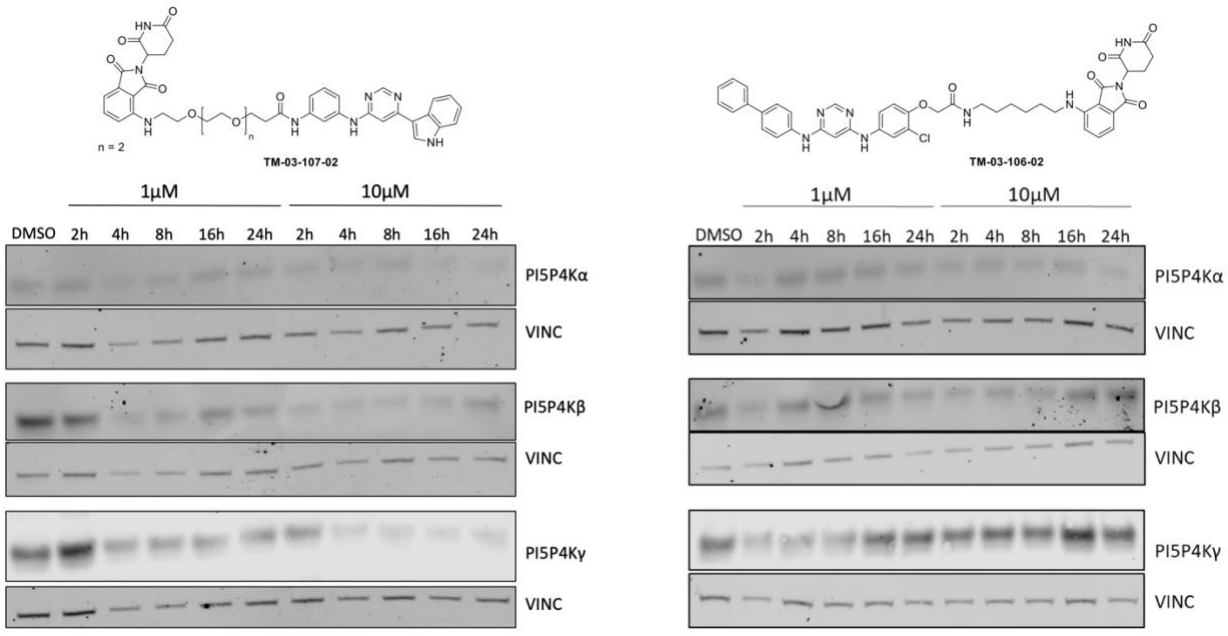

Figure 2.18 Western blot analysis of PROTAC-mediated degradation of PI5P4Ks

minimal degradation at shorter time points. We also saw no degradation in Jurkat cells, indicating that the designed PROTACS are not sufficiently effective at inducing degradation and need to be optimized further.

Discussion

The PI5P4Ks comprise a family of lipid kinases that regulate levels of their substrate and product PI-5-P and PI-4,5-P_2, maintaining compartment-specific concentrations of these phosphoinositides at a subcellular level. Initially thought to be mainly a PI-5-P modulator within a noncanonical PI-4,5-P_2 generation pathway, the PI5P4Ks have garnered a lot of interest in recent years because of their purported importance in specific disease contexts, spurring efforts to develop PI5P4K inhibitors. In this study, we designed and characterized THZ-P1-2, a first-in-class covalent inhibitor of the PI5P4K family. THZ-P1-2, a small molecule containing an electrophilic acrylamide moiety capable of undergoing a Michael addition, bound in the active site and irreversibly inhibited the enzymatic activity of these kinases. A covalent targeting strategy with THZ-P1-2 resulted in prolonged on-target engagement in cells and modest anti-proliferative activity in a panel of AML and ALL cell lines, while retaining a reasonable selectivity across the kinome. Lastly, we found that THZ-P1-2 treatment phenocopied the effects of genetic deletion of PI5P4K $\alpha/\beta/\gamma$ in mice by causing autophagy defects in HeLa cells.

Our initial point of compound development was JNK-IN-7, a previously reported covalent JNK inhibitor that was found to be capable of binding to PI5P4Kγ by KiNativ

profiling. Originally inspired by the imatinib core structure, this “privileged” kinase scaffold served as a promising starting point for developing a selection of analogs with chemical modifications with which to explore structure-activity relationships. Among this panel of molecules, we found a critical feature resulting in superior potency to be a switch from a 2,4-pyrimidine to a 4,6-pyrimidine hinge-interacting motif. We established THZ-P1-2’s inhibitory activity with an apparent IC_{50} of 190 nM on PI5P4Kα in a fixed time-point assay, the isoform with the highest kinase activity and thus easiest to analyze using an ATPase assay (ADP-Glo). We confirmed that THZ-P1-2 specifically prevents phosphate transfer to the PI-5-P substrate at nanomolar concentrations for all isoforms with an orthogonal TLC assay measuring radiolabeled PI-4,5-P_2 formation.

THZ-P1-2 covalently labels all three PI5P4K isoforms, with the reactive cysteine residues located on analogous disordered loops of unknown function outside the kinase domain. There has been a resurgence of interest in covalent inhibitors, especially with recent clinical successes of cysteine-directed covalent BTK inhibitor ibrutinib (Pan et al., 2007), EGFR inhibitors neratinib (Rabindran et al., 2004), afatinib (Li et al., 2008), and osimertinib (Cross et al., 2014). Covalent irreversible inhibitors characteristically exhibit an enhanced potency and prolonged pharmacodynamics due to permanent disabling of kinase enzymatic activity, and high selectivity as covalent inhibitors will only bind irreversibly to a kinase with an appropriately placed cysteine, within the trajectory of the electrophilic warhead (Liu et al., 2013). Our approach in developing probes THZ1 against CDK7 (Kwiatkowski et al., 2014), TH531 against CDK12/13 (Zhang et al., 2016) and most recently JZ128 against PKN3 (Browne et al., 2018) showcased to great effect the modification of a reactive cysteine residue outside the active site, widening the

scope of “accessible” cysteines. We sought to apply these principles and strategies towards PI5P4K. Our study validates the PI5P4Ks as additional candidate kinases with cysteines that are distant from the active site in sequence but brought close to the ATP-binding site due to kinase tertiary structure, rendering them amenable to covalent targeting. Moreover, our approach in targeting these unique cysteines provides a proof-of-concept in using a combination of inhibitor covalent and noncovalent affinities to achieve selectivity, due to a lack of equivalent off-target cysteines across the kinome.

Structural insights into the binding mode of THZ-P1-2 with PI5P4Kα were obtained through a co-crystal structure. Besides the noncovalent interactions highlighted in the results, hydrogen-bonding between the backbone of Val199 and the 4,6-pyrimidine may account for the increased potency compared to analogs with a 2,4-pyrimidine, especially if they contain substituents on the heterocycle linker. Notably, the Phe205 residue that engages in aromatic π-stacking interactions with the phenylenediamine moiety of THZ-P1-2 is conserved among the PI5P4Ks and has been identified as the residue responsible for the GTP-sensing ability of PI5P4Kβ (Sumita et al., 2016). This co-crystal structure also serves as an important resource for the scientific community, enabling structure-guided design of PI5P4K inhibitors with improved properties. Cell permeability and dose-dependent on-target engagement of THZ-P1-2 was validated in HEK293T cells, chosen for their robust expression of all three PI5P4K isoforms, and the necessity for covalency verified through observing effects after washout and in anti-proliferation assays alongside THZ-P1-2-R.

Our biochemical profiling (Invitrogen) of THZ-P1-2 indicates that though the compound exhibits satisfactory selectivity, there are some off-targets observed. The most potent off-targets, such as ABL1, PIKfyve and BRK, were not engaged by dtb-THZ-P1-2 in a cellular pull-down assay. PIKfyve was inhibited by THZ-P1-2 only at concentrations of 10 μM or greater, higher than concentrations relevant for observable PI5P4K targeting. These results indicate that THZ-P1-2 does have some off-target activity on PIKfyve, but maintains a higher preference for the PI5P4Ks, again possibly due to a combination of covalent and non-covalent binding modes.

A principal part of our study was to further confirm novel functions of the PI5P4Ks beyond their asserted primary role of non-canonical PI-4,5-P_2 generation. Treatment with THZ-P1-2 phenocopied genetic deletion of PI5P4K in causing autophagosome and lysosome disruption, TFEB nuclear localization and TFEB target gene upregulation, indicating that PI5P4K kinase activity is required for the role of these kinases in autophagy. Cancer cell line profiling demonstrates AML/ALL cancer cell lines to be sensitive to THZ-P1-2 covalent targeting. Consistent with findings that PI5P4K mediates autophagy in times of nutrient stress (Lundquist et al., 2018) our studies using THZ-P1-2 as a tool suggest that the PI5P4Ks display an induced essentiality by facilitating autophagy as an energy source in a metabolically-stressed environment such as cancer (Kimmelman & White, 2017). Additional studies are required to fully dissect the connection between PI5P4K inhibition, autophagy disruption and subsequent effects on cell viability, as well as investigate the sensitivities of various cancer types to specific PI5P4K inhibition. THZ-P1-2 may be a useful probe of the pharmacological consequences of covalent inhibition of PI5P4K that can complement genetic

approaches (such as CRISPR- or RNAi-based screening) to identify unique vulnerabilities in cancer.

Our SAR studies based on structure-guided rational design did not yield compounds superior to THZ-P1-2 overall, which suggests that we may need to take a step backwards to the original scaffold and make smaller modifications from there. The SAR study did however provide critically useful information on modifications that were tolerated for retaining PI5P4K activity, for instance the toluene head group in HAB001-027, and regions for modifications to improve selectivity, such as the head group/middle linker region in TM-02-137. The high-throughput screen provided us a promising new scaffold to continue developing inhibitors with. We aim to take advantage of the differing activity profiles to hopefully achieve isoform-selective inhibitors or degraders, and to improve selectivity by appending a covalent warhead onto the noncovalent FMMH core. Lastly, we hope to improve our PROTAC approach with further “linkerology” exploration and with VHL-targeted ligands in parallel.

In conclusion, we have characterized a novel potent and selective covalent PI5P4K inhibitor that exhibits durable cellular pharmacodynamics, disruption of autophagy, and modest anti-proliferative activity against leukemia-derived cell lines. THZ-P1-2, THZ-P1-R and the inhibitor resistant PI5P4K Cys to Ser mutants described in this manuscript provide a chemical biology toolbox serving as a valuable resource with which to investigate the pharmacological consequences of covalent inhibition of PI5P4Ks. Our discovery of THZ-P1-2 may be used as a model for targeting other understudied gene families, especially those bearing targetable cysteines in unique

sites. Lastly, our small-molecule strategy for disrupting autophagy through covalent PI5P4K inhibition exposes a new Achilles heel and indicates that exploiting this metabolic vulnerability may be a viable therapeutic strategy in cancer and potentially other autophagy-addicted disorders.

Author contributions:

Lewis Cantley, Hyeseok Shim, Tinghu Zhang, and Nathanael Gray conceived original project. Sindhu Carmen Sivakumaren led the project, designed and performed biochemical and cellular experiments (exceptions below) and conducted the majority of analyses. Tinghu Zhang synthesized initial THZ compounds and provided chemistry guidance and expertise. Fleur Ferguson provided overall project guidance and assay development advice. Theresa Manz synthesized TM compounds (THZ-P1-2 and CVM analogs). Hyuk-Soo Seo and Sirano Dhe-Paganon (DFCI Structural and Chemical Biology Center) conducted docking studies, protein purification and crystallography efforts. Christopher Browne (Jarrod Marto lab) collected and analyzed mass spectrometry data (samples prepared by Sindhu Carmen Sivakumaren). Marcia Paddock and Mark Lundquist (Lewis Cantley lab) conducted TLC and autophagy assays respectively. Nick Kwiatkowski provided overall biology guidance. NCATS (NIH) conducted ADP-Glo/Transcreener assays in the SAR study.

Materials & Methods:

Chemistry

All solvents and reagents were used as obtained. ^{1}H-NMR spectra were recorded with a Varian Inova 600 NMR spectrometer and referenced to DMSO. Chemical shifts are expressed in ppm. Mass spectra were measured with Waters Micromass ZQ using an ESI source coupled to a Waters 2525 HPLC system operating in reverse mode with a Waters Sunfire C18 5 μm, 4.6 x 50 mm column. Purification of compounds was performed with either a Teledyne ISCO CombiFlash Rf system or a Waters Micromass ZQ preparative system. The purity was analyzed on a Waters LC-MS Symmetry (C18 column, 4.6 x 50 mm, 5 μM) using a gradient of 5%–95% methanol in water containing 0.05% trifluoroacetic acid (TFA). Schemes shown in Appendix 1.

Cell Culture

All cell culture was performed using standard techniques. HEK293T and HeLa cells were cultured in Dulbecco's Modified Eagle's medium (DMEM) supplemented with 10% FBS and 1% penicillin/streptomycin (Gibco). Leukemia cells were cultured according to ATCC or DSMZ recommendations. All cells were cultured at 37°C and 5% CO_2.

ADP-Glo kinase assays

ADP-Glo assay protocol was modified from Davis et al. (2013). DPPS and PI5P (Echelon Biosciences) were dissolved in DMSO (333 μL/mg) and mixed by sonication and vortexing in a ratio of 2:1 DPPS:P15P. First, 63 μL of DMSO was added to 1255 μL

of buffer 1 (30 mM Hepes pH 7.4, 1 mM EGTA, 0.1% CHAPS) and 2868 µL of buffer 2 (46 mM Hepes pH 7.4, 0.1% CHAPS). Volumes were multiplied according to number of assays to be run. PI5P4Kα enzyme was added to the buffer mixture at 32 nM concentration (predetermined on a batch-by-batch basis to give maximal signal to background). 10 µL was dispensed into white 384-well plates (Corning #3824). Then, 100 nL of compounds in DMSO were transferred by a pintool (JANUS, PerkinElmer). To initiate the reaction, 5 µL of ATP (Promega) at 15 µM (final assay concentration of 5 µM) and PI5P/DPPS (at concentrations of 0.06 µg/µL and 0.12 µg/µL respectively) in buffer 3 (20 mM Hepes pH 7.4, 60 mM $MgCl_2$, 0.015 mM ATP and 0.1% CHAPS) was added to each well. The final concentration of DMSO in the reaction was less than 5%. The resulting mixture was incubated at room temperature in the dark for one hour, at which time 5 µL of ADP-Glo reagent 1 were added to stop the reaction and remove any remaining ATP. After a 45-minute incubation, 10 µL of the ADP-Glo reagent 2 were added and allowed to incubate for 30 minutes. The luminescence was then read on an EnVision 2104 Multilabel Plate Reader (PerkinElmer). IC_{50}s were determined using the GraphPad Prism nonlinear regression curve fit.

Radiometric kinase assays

The PI5P4K assay was carried out as described in Rameh et al. (1997). Briefly, the kinase reaction was carried out in a total of 70 µL of kinase buffer (50 mM HEPES pH 7.4, 10 mM $MgCl_2$) with 0.1 µg of purified PI5P4K protein (preincubated with DMSO or compound at various concentrations), followed by addition of 20 µL of the resuspended lipids (sonicated and vortexed), 10 µM non-radiolabeled ATP, and 10 µCi [γ-^{32}P]-ATP

for 10 minutes at room temperature. The reaction was terminated by adding 50 µL of 4 N HCl. Phosphoinositides were extracted by adding 100 µL of methanol/chloroform (approximately 1:1, vol:vol) mix and subjected to TLC (thin-layer chromatography) separation using heat-activated 2% oxaloacetate-coated silica gel 60 plates (20 cmx20 cm, EMD Millipore) and a 1-propanol/2 M acetic acid (65:35, vol:vol) solvent system. The radiolabeled product, $PI(4,5)P_2$, was quantified with a Phosphorimager (Molecular Dynamics, STORM840, GE Healthcare).

Immunoblotting

Cells were lysed with Pierce IP Lysis buffer supplemented with a cOmplete™ Mini Protease Inhibitor Cocktail tablet (Roche) on ice for 60 min. Lysates were clarified by centrifugation at 20,000 × *g* for 15 min at 4°C. Protein concentration was determined by a BCA assay (Pierce), and all samples were run with equal total protein content. The following antibodies were used in this study: PI5P4Kα (5527; Cell Signaling), PI5P4Kβ (9694; Cell Signaling), PI5P4Kγ (HPA058551**;** Sigma-Aldrich),PI4P5Kα (9693; Cell Signaling), PI4P5Kβ (12541-1-AP; Proteintech), PI4P5Kγ (3296; Cell Signaling), PIKfyve (MABS522; EMD Millipore), c-Abl (sc-56887; Santa Cruz), Brk (ab137563; Santa Cruz), IRAK1 (4504; Cell Signaling), PKN3 (NBP1-30102; Novus Biologicals), SAP/JNK (9252; Cell Signaling), CDK7 (2916; Cell Signaling), CDK12 (11973; Cell Signaling), LAMP1 (9091; Cell Signaling), LC3B (2773; Cell Signaling), tubulin (3873; Cell Signaling). Imaging was performed by detection of fluorescently labeled infrared secondary antibodies (IRDye) on the Odyssey CLx Imager (LI-COR).

Pulldown assays

HEK293T cells were lysed with Pierce IP Lysis buffer supplemented with a cOmplete™ Mini Protease Inhibitor Cocktail tablet (Roche) on ice for 60 min. Lysates were clarified by centrifugation at 20,000 × *g* for 15 min at 4°C. Protein concentration was determined by a BCA assay (Pierce), and all samples were equalized for protein content. DMSO or 1 μM dtb-THZ-P1-2 was added and rotated overnight at 4°C. Samples were rotated for 2h at room temperature to enhance covalent binding and then incubated with streptavidin resin for 2h at 4°C. Beads were washed with lysis buffer five times, resuspended in 1x LDS sample buffer, boiled at 95°C for 10 min and subjected to immunoblotting. For competitive pulldowns, HEK293T cells were grown to 90-95% confluence, pretreated for 6h with DMSO or varying concentrations of THZ-P1-2, washed twice with cold PBS, lysed, and streptavidin pulldown conducted as described above with normalized samples.

Mass Spectrometry

For intact MS analysis, recombinant PI5P4K protein was incubated with DMSO or 5 μM inhibitor for 2 h at 37°C and analyzed by LC-ESI-MS essentially as described in Zhang et al. (2012). In each analysis, 5 μg protein was injected onto a self-packed reversed phase column (1/32" O.D. × 500 um I.D., 5 cm of POROS 10R2 resin). After desalting for four minutes, protein was eluted with an HPLC gradient (0–100% B in 4 min, A = 0.2M acetic acid in water, B = 0.2 M acetic acid in acetonitrile, flow rate = 10 μL/min)

into an LTQ ion trap mass spectrometer (ThermoFisher). Mass spectra were deconvoluted using MagTran1.03b2 software. To determine the site of modification, the samples used for intact analysis were reduced with TCEP (10 mM final concentration), alkylated with iodoacetamide (22.5 mM final concentration) and digested with Asp-N or Glu-C (37 °C, overnight) and analyzed by nanoLC-MS. Digested peptides were injected onto the precolumn (4 cm POROS 10R2, Applied Biosystems) and eluted with an HPLC gradient (NanoAcquity UPLC system, Waters, Milford, MA; 10–70% B in 60 min; A = 0.1 M acetic acid in water, B = 0.1M acetic acid in acetonitrile). Peptides were resolved on a self-packed analytical column (50 cm Monitor C18, Column Engineering, Ontario, CA) and introduced to the mass spectrometer (LTQ Orbitrap XL) at a flow rate of ~30 nL/min (ESI spray voltage = 3.2 kV). The mass spectrometer was programmed to perform data-dependent MS/MS on the five most abundant precursors (35% collision energy) in each MS1 scan (image current detection, 30K resolution, *m*/*z* 300–2000). MS/MS spectra were matched to peptide sequences using Mascot (version 2.2.1) after conversion of raw data to .mgf using multiplierz scripts. Precursor and peptide ion mass tolerances were 10 ppm and 0.6 Da, respectively.

Protein expression and purification

A construct of human PI5P4Kα covering residues 35-405 in the pNIC28Bsa4 vector (Addgene #42494) was overexpressed in E. coli BL21 (DE3) in TB medium in the presence of 50 µg/ml of kanamycin. Cells were grown at 37°C to an OD of 0.7, induced overnight at 17°C with 400 µM isopropyl-1-thio-D-galactopyranoside, collected by centrifugation, and stored at -80°C. Cell pellets were resuspended in buffer A (50 mM

sodium phosphate, pH 7.4, 500 mM NaCl, 10% glycerol, 20 mM Imidazole, and 14 mM BME), lysed by sonication, and the resulting lysate was centrifuged at 16,000 xg for 30 min. ~5mL Ni-NTA beads (Qiagen) were mixed with lysate supernatant for 45 min, washed with buffer A, and eluted with buffer B (50 mM sodium phosphate, pH 7.4, 500 mM NaCl, 10% glycerol, 300 mM Imidazole, and 14 mM BME). The eluted sample was gel-filtered through a Superdex-200 16/600 column in buffer C (20 mM HEPES, pH 7.5, 500 mM NaCl, 10% glycerol, 10mM DTT, and 1mM TCEP). Protein fractions were pooled, concentrated, and stored at -80°C.

Co-crystallization, data collection, and structure determination

A twofold excess of 10 mM inhibitor in DMSO was mixed with 500 µM PI5P4Kα protein and crystallized by sitting-drop vapor diffusion at 20°C in the following crystallization buffer: 2 M NH_4 citrate, pH 6.5. Crystals were transferred briefly into crystallization buffer containing 25% glycerol prior to flash-freezing in liquid nitrogen. Diffraction data from complex crystals were collected at beamline 24ID of the NE-CAT at the Advanced Photon Source (Argonne National Laboratory). Data sets were integrated and scaled using XDS (Kabsch, 2010). Structures were solved by molecular replacement using the program Phaser (McCoy et al., 2007). The ligand was positioned manually and refined using Buster and Rhofit (Smart et al., 2012). Iterative manual model building and refinement using Phenix (Adams et al., 2010) and Coot (Emsley and Cowtan, 2004) led to a model with excellent statistics, including a maximum diffraction of 2.21Å (Table S1 and S2). The PI5P4Kα/THZ-P1-2 and CVM-05-002 co-crystal structures are being deposited into the NCBI Database.

Proliferation assays

Cells were plated in 96-well or 384-well format and treated with indicated compounds at varying concentrations for 72h. Anti-proliferative effects of compounds were assessed using the Cell Titer Glo assay kit (Promega) with luminescence measured on an EnVision 2104 Multilabel Plate Reader (PerkinElmer). IC_{50}s were determined using the GraphPad Prism nonlinear regression curve fit.

qRT-PCR

Total RNA was prepared using RNeasy (Qiagen). cDNA was synthesized using Superscript Vilo (Thermo) and qRT-PCR performed utilizing Fast SYBR green (Thermo) and the Realplex Mastercycler (Eppendorf). Isolation of mRNA and qPCR was performed as follows. 200,000 cells were plated in 6-well plastic dishes. 24 hours later, the RNA in the lysates was extracted using the RNeasy protocol. The RNA was resuspended in 50 µl H_2O at a concentration of 1 μg/μL. cDNA was transcribed using the SuperScript Vilo.. The genes that were quantified here were previously shown to be regulated by TFEB.

Fluorescence microscopy

HeLa were grown on glass coverslips pre-treated with poly-d-lysine. When indicated cells were treated with 250-1000 nM THZ-P1-2 for 16 hours. Adherent cell lines were rinsed with phosphate-buffered saline, pH 7.4 (PBS) and fixed with 4% paraformaldehyde (PFA) in PBS for 15 minutes at room temperature. After fixation, the

cells were permeabilized for 10 minutes with PBS/0.1% Triton X-100, blocked for 30 minutes in blocking buffer (PBS with 3% BSA) and labeled with primary antibodies in blocking buffer for 1 hour at room temperature or overnight at 4°C. Alternatively, for staining, LC3B and LAMP1 (ab25245; Abcam) cells were fixed/permeabilized in -20 MeOH for 20 minutes. Coverslips were washed three times with blocking buffer and incubated with Alexa Fluor-conjugated goat secondary antibodies in blocking buffer for 1 hour at room temperature. After incubation with secondary antibodies, coverslips were washed three times with PBS, once with water, and then mounted on a glass microscope slide with Prolong Gold with DAPI (Thermo). The following primary antibodies were used: TFEB (SAB4503154; Sigma), LC3B (3868; Cell Signaling), LAMP1 (ab25245; Abcam). Alexa Fluor-conjugated secondary antibodies (Thermo) were used at 1:1000. Fluorescent and phase contrast images were acquired on a Nikon Eclipse Ti microscope equipped with an Andor Zyla sCMOS camera. Within each experiment, exposure times were kept constant and in the linear range throughout. When using the 60x and 100x oil immersion objectives, stacks of images were taken and deconvoluted using AutoQuant (Media Cybernetics).

Generation and transduction of GFP PIP4K2 lentiviral constructs

Replication-deficient lentiviruses were prepared using a third-generation lentiviral system. GFP was inserted by itself or upstream of either human PIP4K2A or PIP4K2B in a lentiviral vector. Cysteine to Serine point mutations were made using the Quikchange XL II site-directed mutagenesis kit (Agilent). Virus was generated by cotransfecting three helper plasmids (pLP1, pLP2, pVSV-G) and the vector containing

the gene of interest with *cis*-acting sequences for proper packaging were used to generate pseudovirions. A subconfluent culture of HEK293T cells was transfected using the CalPhos Mammalian Transfection Kit (Clontech). The titer of each virus was determined using HEK293T cells. Viral supernatant was then used to express PIP4K2s in MEFs.

Virus production and infection

293T packaging cell line was used for retroviral amplification. In brief, viruses were collected 48 hours after infection, filtered, and used for infecting cells in the presence of 8μg/ml polybrene (Sigma), prior to puromycin selection or upon cell sorting for GFP. The packaging plasmid used for retroviral infection was pCL-Eco.

Chapter 3. Targeting the PIKfyve lipid kinase using small molecules

Development of novel covalent PIKfyve inhibitors in cancer

Abstract

PIKfyve, a related understudied lipid kinase, has also been proposed as a potential therapeutic target in Non-Hodgkin lymphoma and Ebola viral infection. We observed that THZ-P1-2 was also capable of covalently binding to PIKfyve, albeit at a much lower preference than PI5P4K. We reengineered compound selectivity towards PIKfyve and identified a class of compounds from the THZ-P1-2 scaffold exhibiting picomolar-to-nanomolar biochemical and cellular inhibition. These inhibitors exhibit cellular on-target engagement and induce vacuolar enlargement, a well-established PIKfyve inhibitory phenotype. Docking/modeling studies and mass spectrometry revealed a similar distant cysteine, Cys1970, to be covalently labeled by these compounds. Lastly, this THZ-family of inhibitors, particularly two top compounds MFH-5-3 and MFH-5-4, exhibit potent antiproliferative activity in lymphoma cell lines and inhibition of Ebola viral infectivity.

Introduction

PIKfyve is another important player in the phosphoinositide regulation landscape that has been characterized over the year. PIKfyve is a 250 kDa lipid kinase that phosphorylates PI and PI-3-P on the 5-position to yield both PI-5-P and PI-3,5-P_2 respectively (Sbrissa, Ikonomov, & Shisheva, 1999). This lipid kinase is thought to be one of the best examples of both a PI-binding and PI-synthesizing enzyme, through its association with membrane PI-3-P via its FYVE domain (Shisheva, 2008). The

interaction of the FYVE domain with PI-3-P is crucial for the targeting of PIKfyve to the membranes of late endosomes, where this localization is dependent on the presence of an intact FYVE finger (Sbrissa, Ikonomov, & Shisheva, 2002).

PI-5-P synthesis by PIKfyve, as discussed previously in Chapter 2, is crucial as a substrate for PI5P4K. Autophagy was classically considered to be PI-3-P-dependent, produced by the class III phosphatidylinositol 3-kinase (also known as VPS34), but noncanonical autophagy was found to proceed via PI-5-P production by PIKfyve. PI-5-P regulates autophagosome biogenesis, being a key regulator when VPS34 is inhibited. PI-5-P also plays roles in chromatin organization, bacteria invasion, and cytoskeletal remodeling (Shisheva, 2008; Vicinanza et al., 2015). Through its PI-3,5-P_2 synthesis, PIKfyve is responsible for maintaining endosomal and lysosomal morphology and homeostasis, and this endosome processing regulation affects overall endocytic cargo transport. PIKfyve forms a regulatory complex with Vac14 (also called ArPIKfyve, for *A*ssociated *r*egulator of *PIKfyve*) and the Sac-domain containing Sac3 phosphatase, and this complex is required to form to control endosomal phosphoinositide metabolism. The physical assembly of this tri-member complex is directly coupled to the machinery for PI-3,5-P_2 synthesis and turnover, although Vac14 and Sac3 can associate independently of PIKfyve. PI-3,5-P_2 signaling mediated by PIKfyve is also integral to other biological processes such as GLUT4 translocation and retroviral budding (Shisheva, 2008).

PIKfyve has also garnered attention in recent years as a key player in Toll-like receptor (TLR) signaling. Apilimod, a small molecule inhibitor of IL-12/13, had been in clinical trials for Crohn's disease, psoriasis and rheumatoid arthritis, but its direct target

was unknown. A group at Novartis used a chemical genetic approach and identified PIKfyve to be the target bound by apilimod with an IC_{50} of 10 nM, specifically blocking its PI-5-P and PI-3,5-P_2 phosphoinositide activity and causing selective IL-12/13 inhibition. This was confirmed by genetic deletion of PIKfyve (Murphy et al., 2013). Apilimod has also been characterized in the context of endomembrane dilation caused by a reduction of PI-3,5-P_2 due to PIKfyve inhibition, where this phenotype was found to be reversible with bafilomycin A1 (Sbrissa, Naisan, Ikonomov, & Shisheva, 2018). Another PIKfyve inhibitor, YM201636, was also discovered a few years back through a drug discovery programme directed at PI3K. YM201636 was found to have an IC_{50} of 33 nM, preferentially inhibiting PI-5-P production at low doses (10 –25 nM) and inhibiting both phosphoinositide products at higher doses (Jefferies et al., 2008; Sbrissa, Ikonomov, Filios, Delvecchio, & Shisheva, 2012; Vicinanza et al., 2015). Together, these two most well-known PIKfyve inhibitors have unraveled roles of PIKfyve in modulating TLR immune signaling as well as differential phosphotransferase activity in the context of noncanonical autophagy (Fig 3.1).

As previously mentioned, the use of apilimod had been restricted to mainly the autoimmune space, with anticancer strategies being minimally explored. PIKfyve inhibition with apilimod has been tested in non-small lung cancer cell lines, and PIKfyve has been shown to play a role in controlling tumor cell migration and invasiveness, with MTMR3 and NPM-ALK (Krishna et al., 2016; Oppelt et al., 2014; Ramel, Saland, & Payrastre, 2011).

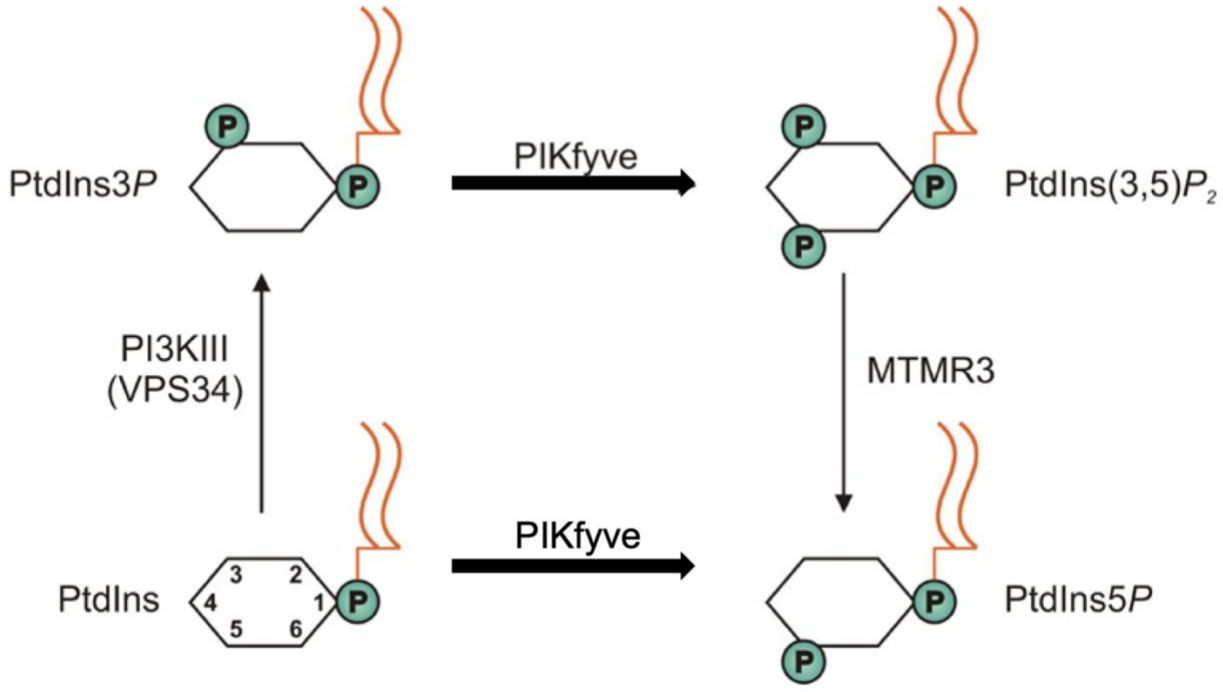

Figure 3.1 Phosphoinositide signaling pathway overview of PIKfyve.

Recently, apilimod was used to validate PIKfyve as a target in B-cell Non-Hodgkin lymphoma (B-NHL) via specific disruption of lysosomal homeostasis. Expression of key players TFEB, CLCN7, OSTM1 and SNX10 were found to be the main determinants of apilimod sensitivity, where loss of each gene was sufficient to confer >100-fold apilimod resistance (Gayle et al., 2018). This was the first in-depth study linking disruption of nutrient signaling and metabolism to antiproliferative activity in cancer due to PIKfyve inhibition. Other PIKfyve inhibitors have also been developed and assessed in the context of autophagy-dependent cancer due to disruption of lysosomal homeostasis (Sharma et al., 2019). These findings prove the importance of targeting PIKfyve in the context of cancer, and while there are two high-quality probes for studying PIKfyve

biology, diversifying the small molecule space especially with inhibitors of novel mechanism such as covalent inhibitors or degraders could be informative and valuable.

When developing our PI5P4K inhibitor THZ-P1-2, we observed that though PIKfyve was not engaged through streptavidin pulldown, THZ-P1-2 had potent biochemical activity on the kinase with an IC_{50} of 40 nM (Carna). As also noted in Chapter 2, we perceived that THZ-P1-2 showed vacuolar enlargement, a PIKfyve inhibitory phenotype, and concentrations of 10 μM. This suggested to us that THZ-P1-2 had some off-target activity on PIKfyve despite preferential activity on its intended target, the PI5P4Ks, and that we could potentially modulate activity away from PI5P4K and towards PIKfyve to generate a new series of PIKfyve inhibitors. Given the relevance of PIKfyve in cancer, we employed our established chemical biology approach to obtain PIKfyve inhibitors from our THZ-P1-2 scaffold starting point. By mining our compound database for inhibitors with the same structural core, we were able to narrow down and identify a series of compounds with potent PIKfyve biochemical activity. We confirmed the ability of these compounds to bind covalently to PIKfyve and found the labeled cysteine, Cys1970, to be outside the kinase domain similar to PI5P4K, using protein modeling and mass spectrometry approaches. We confirmed on-target engagement of these inhibitors and profiled them in a panel of lymphoma cell lines, showing them to have potencies on par with or superior to apilimod. From our studies, we obtained two top compounds that serve as promising starting points for further optimization for studying and targeting PIKfyve.

Results

We started by first strategizing to prioritize compounds that shared the same pharmacophore as THZ-P1-2. Firstly, we observed that compound THZ-2-72-1, also known as PIP4Kin1 in Shim et al. (Harvard, 2015), had potent activity on PIKfyve biochemically (Fig 3.2A.) and also had a 0% control value when profiled in KINOMEScan (Fig. 3.2B). We also observed that kinome profiling by KiNativ previously done for THZ-P1-3 showed decent selectivity for PIKfyve in THP1 cell lysate (Fig. 3.2C-D). Together with the biochemical and cellular PIKfyve activity observed with THZ-P1-2, we reasoned that these three observations presented promising starting points for PIKfyve inhibitor development. We once again harnessed our rich internal collection of kinase inhibitors and curated a collection of approximately 50 compounds by setting a parameter of 70% structural similarity and above to THZ-2-72-1 and THZ-P1-2/3. We cherry-picked and screened a selection of these compounds against purified PIKfyve protein in the radiometric TLC assay.

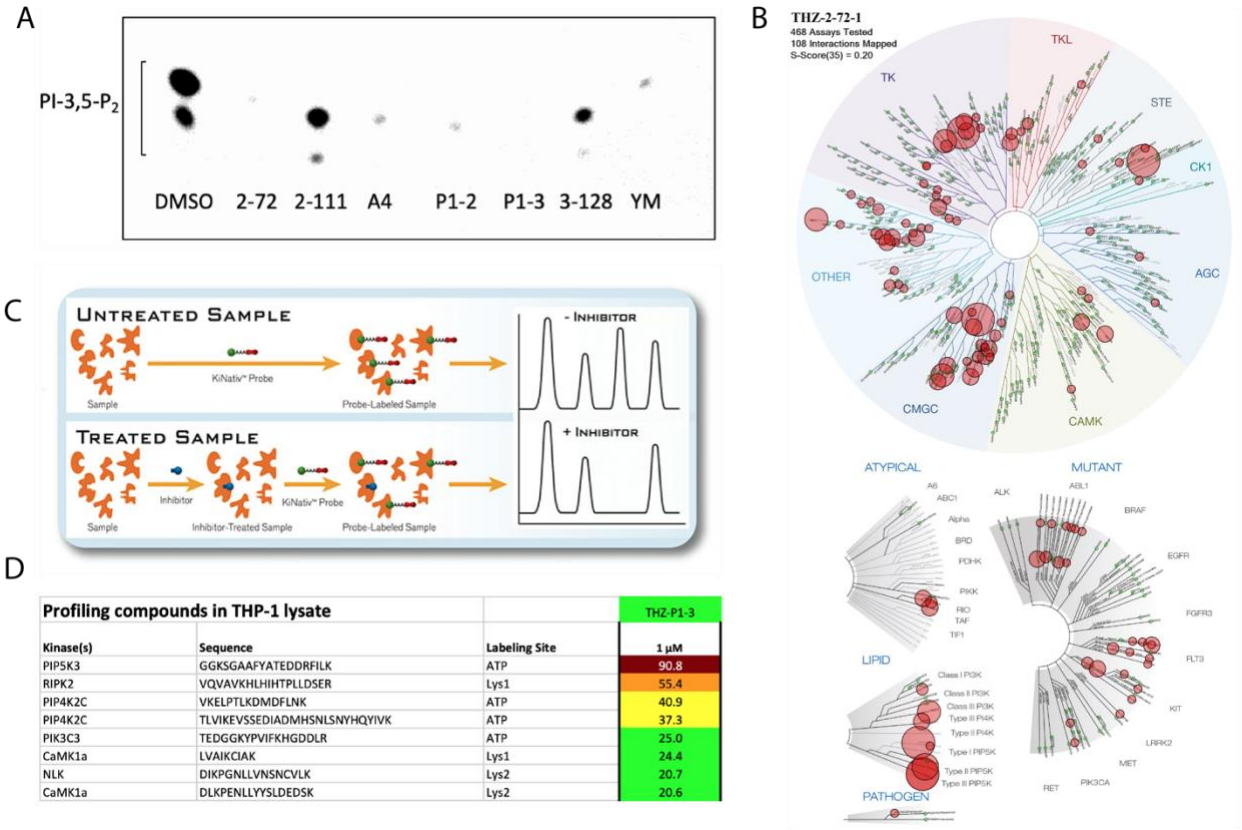

Profiling compounds in THP-1 lysate			THZ-P1-3
Kinase(s)	Sequence	Labeling Site	1 μM
PIP5K3	GGKSGAAFYATEDDRFILK	ATP	90.8
RIPK2	VQVAVKHLHIHTPLLDSER	Lys1	55.4
PIP4K2C	VKELPTLKDMDFLNK	ATP	40.9
PIP4K2C	TLVIKEVSSEDIADMHSNLSNYHQYIVK	ATP	37.3
PIK3C3	TEDGGKYPVIFKHGDDLR	ATP	25.0
CaMK1a	LVAIKCIAK	Lys1	24.4
NLK	DIKPGNLLVNSNCVLK	Lys2	20.7
CaMK1a	DLKPENLLYYSLDEDSK	Lys2	20.6

Figure 3.2 Identification of starting points for PIKfyve inhibitor development. (A) Radiometric TLC analysis of THZ-P1-2 analogs. (B) DiscoverX KINOMEScan profiling of THZ-2-72-1 at 1 μM. Full data to be submitted as ETD. (C) Schematic of KiNativ profiling platform. (D) Top hits from THZ-P1-3 KiNativ profiling in THP1 lysate. Full list included as ETD submission.

We noticed a trend of compounds with more reactive warheads (such as the enamide acrylamide in a few compounds in the ZG series) having a higher potency on PIKfyve, achieving almost 100% inhibition or close at 100 nM concentrations (Fig. 3.3A). We proceeded to test a few of these compounds in the vacuolar assay in Vero cells to see if these biochemically active compounds were able to induce vacuolar enlargement. We confirmed that the ZG-9 and ZG-11 compounds were able to cause the PIKfyve inhibitory phenotype in a dose-dependent manner, down to concentrations of 200 nM. Here, we also looked at three additional compounds that were analogs of

THZ-P1-2, 3 and 18, identical apart from the warhead – while the P1 series bore N,N-dimethyl-butenoic amide acrylamide warheads, these compounds, called the MFH series, were appended with chloroacetamide linkers. These compounds, named MFH-5-2, MFH-5-3 and MFH-5-4 were also able to induce vacuolar enlargement with concentrations as low as 250 nM (Fig. 3.4).

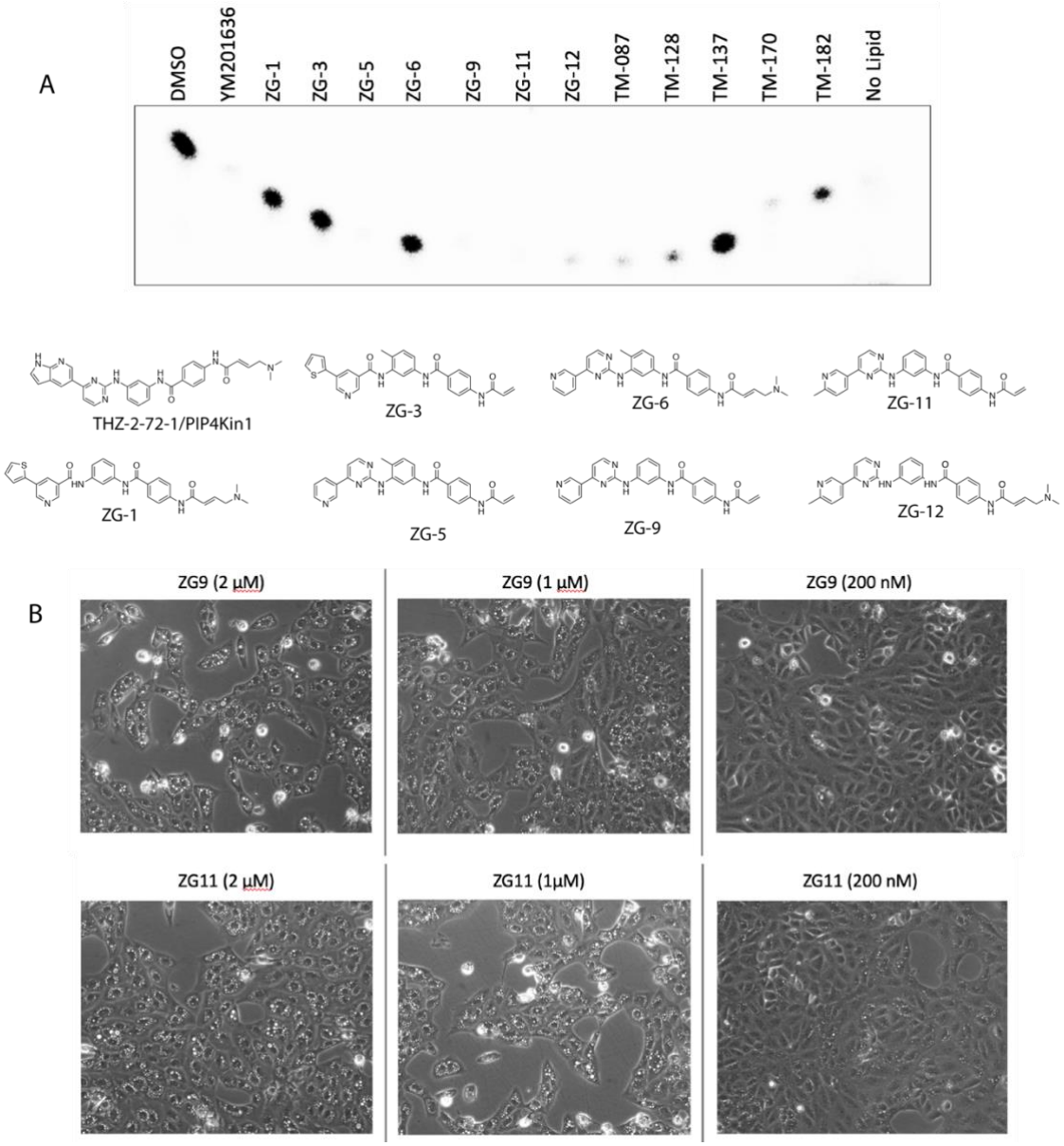

Figure 3.3 Biochemical and cellular testing of PIKfyve inhibitors. (A) TLC and structures of PIKfyve inhibitors. (B) Vacuolar assay of top PIKfyve inhibitors. All vacuolar assays were done with DMSO and apilimod at 10 nM as negative and positive controls.

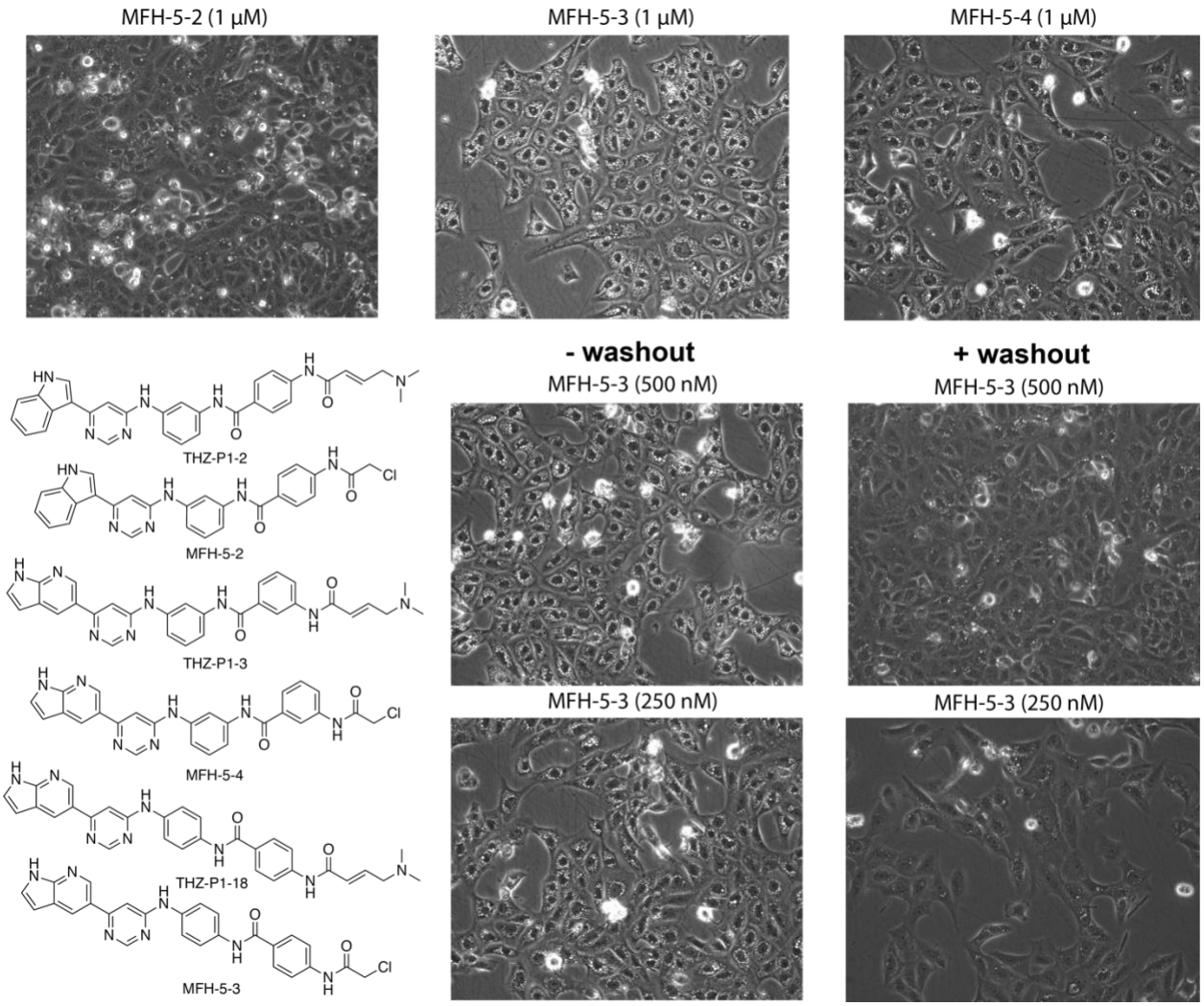

Figure 3.4 Vacuolar assay with MFH compounds with and without washout. All vacuolar assays were done with DMSO and apilimod at 10 nM as negative and positive controls.

MFH-5-3 proved to be the superior compound in the cellular context, able to sustain this phenotype upon washout, characteristic of the prolonged pharmacodynamics conferred by covalent binding with slight vacuolization still visible at 250 nM after washout at 2h.

To ascertain whether these compounds were binding in a covalent manner, we compared the structure of PIKfyve with PI5P4K. Because there is no reported structure

for PIKfyve, we modeled and aligned the PIKfyve sequence with our high-resolution structure of PI5P4Kα/THZ-P1-2 using the Protein Model Portal (Fig 3.5). We observed that there was one cysteine residue, Cys1970, similarly to PI5P4K, outside the kinase domain but theoretically within reach of the covalent warhead. We performed mass spectrometry on purified PIKfyve protein (Carna) incubated with top compound MFH-5-3. Because the GST-tagged protein was not compatible with our intact mass spectrometry instrument (potential glutathionylation adducts add a large amount of heterogeneity to the protein, splitting the signal and rendering it undetectable), we proceeded with the digest and tandem mass spectrometry. We detected a peptide fragment with the labeled Cys1970, confirming that MFH-5-3 indeed was able to covalently bind and inhibit PIKfyve, both biochemically and in cells (Fig. 3.5).

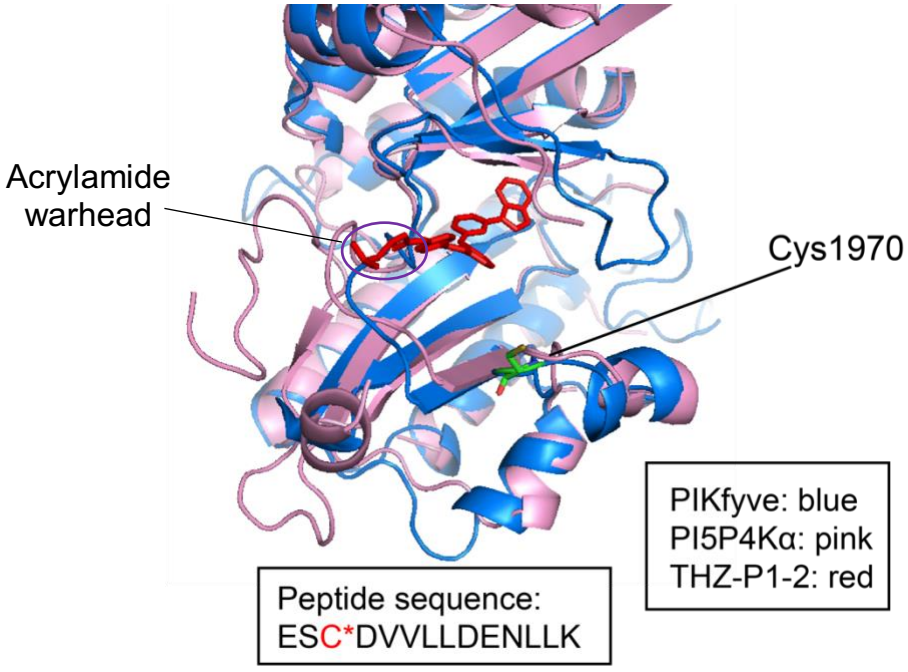

Figure 3.5 Structural modeling and mass labeling of compound with PIKfyve

We sought to also confirm on-target engagement of the MFH series by performing a competitive streptavidin pulldown in HEK293T cells. The pulldown was conducted in competition with dtb-THZ-2-72-1 that we established previously was able to immunoprecipitated PIKfyve. We found that the chloroacetamide MFH compounds, along with their acrylamide P1 counterparts, were able to compete and block PIKfyve pulldown, but not their reversible analogs (difference seen more clearly with MFH-5-3 and the reversible equivalent) (Fig. 3.6).

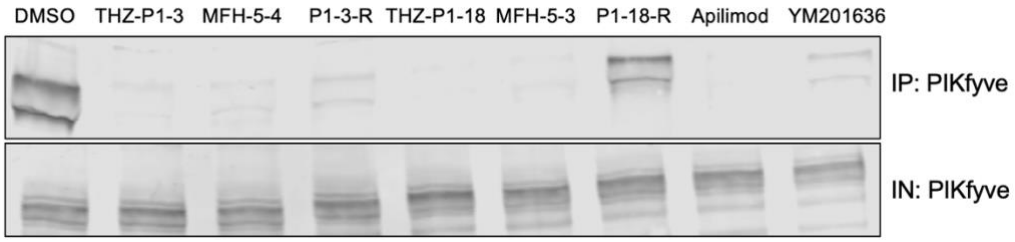

Figure 3.6 Streptavidin pulldown with acrylamide, chloroacetamide, and reversible PIKfyve inhibitors. All compounds were treated at 1 μM concentrations for 6h in HEK293T cells before subjecting to pulldown.

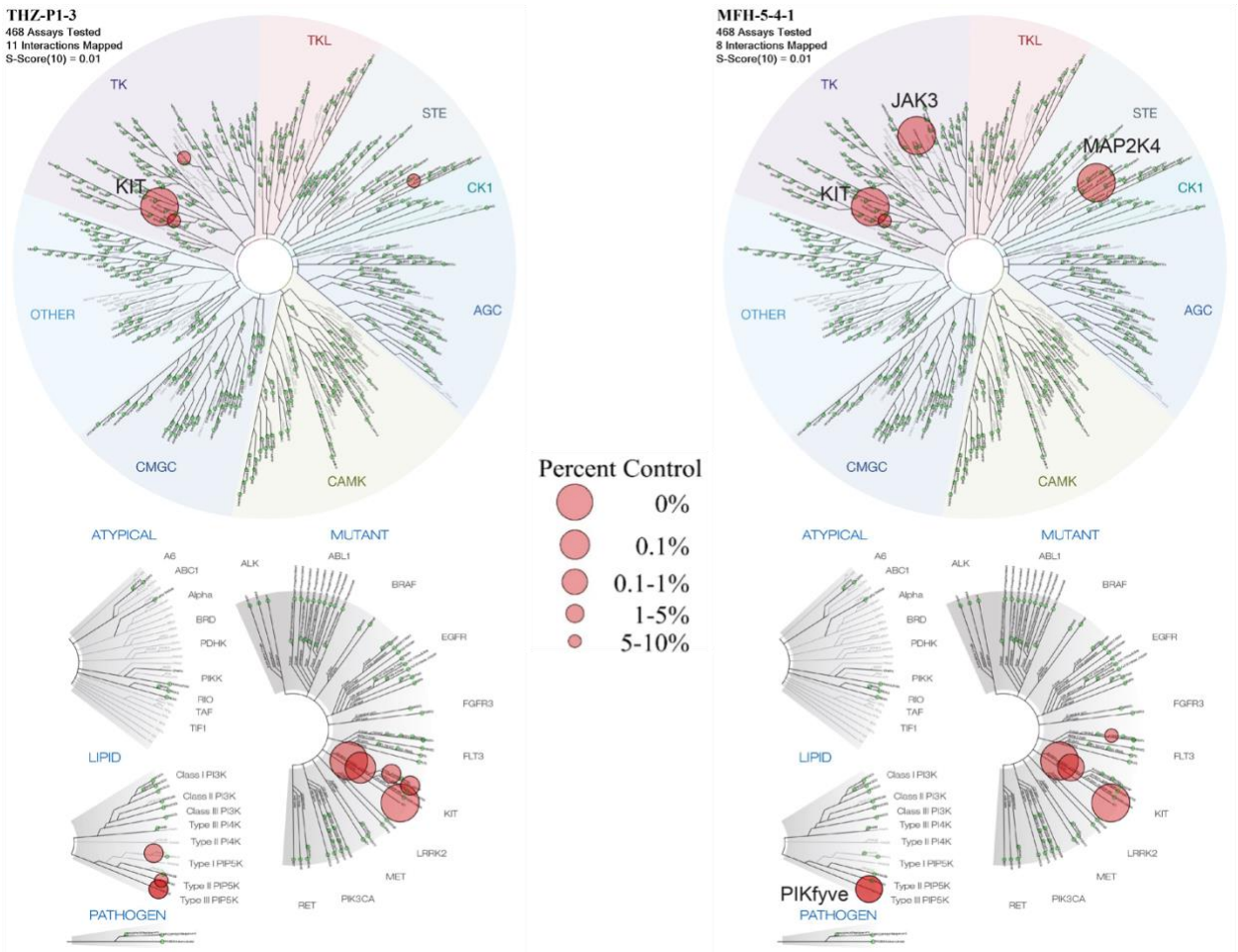

Figure 3.7 DiscoverX KINOMEScan selectivity profiling of THZ-P1-3 and MFH-5-4. Full data submitted as ETD.

Given the reactivity of the chloroacetamide warhead, we were concerned about the increased potency coming at a cost to selectivity. Looking at the selectivity profile of representative compounds THZ-P1-3 and MFH-5-4, we saw that only two major off-targets were gained (JAK3 and MAP2K4) while selectivity was actually improved within the lipid kinase family, with only PIKfyve appearing as a hit (Fig. 3.7).

We next decided to profile some of these identified PIKfyve inhibitors in the context of B-cell lymphoma. We found that our selected inhibitors displayed IC_{50}s mostly

in the double and triple digit nanomolar range across a range of lymphoma cell lines (Table 3). Some of these cell lines were used in Gayle et al. (2018) and compared well with the apilimod values. Notably, the WSU-DLCL2 cell line, which had reported to be exquisitely dependent on PIKfyve by comparing with an apilimod-resistant mutant, displayed sensitivity to all compounds. MFH-5-3 once again stood out as being the most potent compound consistently across cell lines, with values on par with or superior to apilimod, particulary in WSU-DLCL2 with an IC_{50} of 15 nM (Fig. 3.8). This activity was confirmed to be covalent dependent, with no inhibition by the reversible analogs.

Table 3. IC_{50} evaluation of PIKfyve inhibitors in lymphoma cell lines

IC_{50} (M)	Apilimod	YM201636	THZ-P1-2	MFH-5-2	MFH-5-3	MFH-5-4	THZ-2-71	THZ-P1-3	ZG11	ZG9
BCWM.1	N/A	1.55E-06	1.33E-06	1.41E-07	4.84E-08	1.95E-07	2.20E-07	1.59E-06	3.00E-07	6.26E-08
MWCL-1	1.55E-06	1.58E-06	N/A	9.40E-07	3.01E-07	7.55E-07	6.35E-07	3.46E-06	5.69E-07	3.89E-07
TMD8	2.69E-07	3.19E-06	7.35E-06	6.99E-07	2.54E-07	6.61E-07	4.75E-07	3.79E-06	4.39E-07	2.05E-07
HBL-1	1.75E-07	4.43E-07	1.57E-05	7.42E-07	1.22E-07	5.61E-07	8.63E-07	2.05E-06	7.15E-07	3.07E-07
OCI-Ly7	8.52E-08	1.33E-06	4.89E-07	2.19E-07	4.95E-08	9.96E-08	3.73E-07	1.15E-07	4.98E-07	2.18E-07
OCI-Ly19	7.72E-08	8.48E-07	6.87E-07	1.46E-07	1.44E-08	9.12E-08	3.93E-07	2.64E-07	3.74E-07	1.08E-07
Ramos	2.81E-07	8.17E-07	2.50E-07	2.26E-07	2.34E-08	2.55E-07	5.86E-07	2.48E-07	6.39E-07	3.01E-07
RPMI-8226	1.54E-07	2.06E-06	5.46E-06	8.34E-07	1.37E-07	4.81E-07	7.91E-07	1.23E-06	1.01E-06	3.47E-07
SU-DHL-6	5.79E-08	4.34E-07	2.53E-06	1.27E-07	2.24E-08	7.56E-08	3.27E-07	2.94E-07	6.18E-07	2.00E-07
JeKo-1	6.94E-08	9.41E-07	1.24E-06	2.13E-07	5.59E-08	2.19E-07	4.40E-07	1.14E-06	5.97E-07	3.03E-07

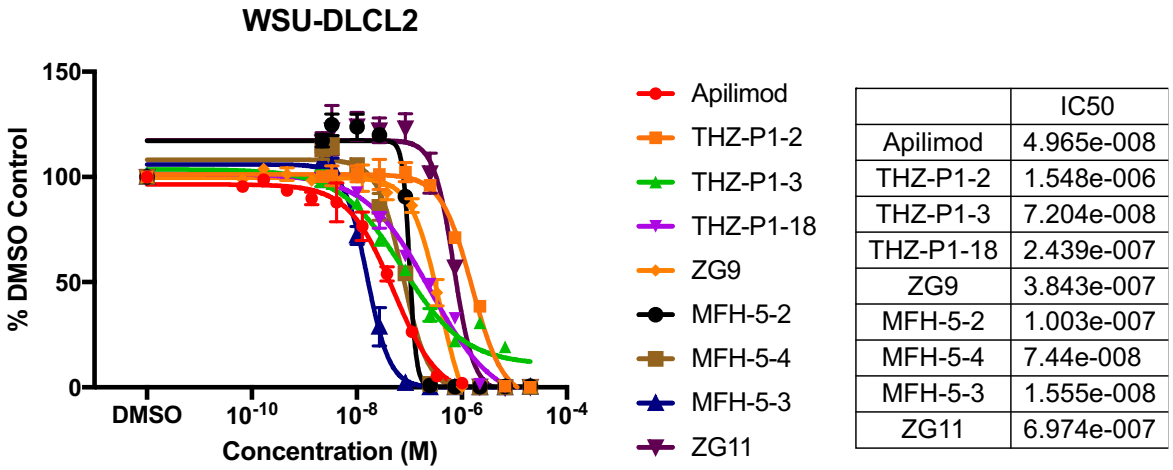

	IC50
Apilimod	4.965e-008
THZ-P1-2	1.548e-006
THZ-P1-3	7.204e-008
THZ-P1-18	2.439e-007
ZG9	3.843e-007
MFH-5-2	1.003e-007
MFH-5-4	7.44e-008
MFH-5-3	1.555e-008
ZG11	6.974e-007

Figure 3.8 Antiproliferation assay of PIKfyve inhibitors in WSU-DLCL2.

Application of novel covalent PIKfyve inhibitors towards Ebola viral infectivity

The Ebola virus (EBOV), thought to be transmitted by fruit bats as animal reservoirs, is a negative-sense, single-stranded RNA filovirus that causes hemorrhagic fever in humans that can be deadly. The Ebola 2013-2016 epidemic was devastating in its impact, starting in Guinea and spreading to Sierra Leona and Liberia, resulting in over 28,000 cases and over 11,000 deaths. The extreme magnitude and rapidness of EBOV spreading was due to an unprecedented number of mutations in the virus glycoprotein (GP) that occurred over successive transmission events. These amino acid mutations confer an increased tropism for human cells and decreased tropism for fruit bat cells, enhancing the spread of the virus among humans in the Western African region. One particular GP mutant, A82V, had specifically heightened ability to infect primate cells, and thus dominated the outbreak (Diehl et al., 2016; Dudas et al., 2016; Urbanowicz et al., 2016). The mechanism of this increased infectivity was further demonstrated using a variety of biochemical assays to be caused by a decrease in the

threshold for activation of membrane fusion activity triggered by host factors cathepsin B and EBOV receptor Niemann-Pick C1 (NPC1) upon EBOV GP binding. It was also discovered that this increase in infectivity came at a cost of decreased virus stability, conferring a net advantage to the virus for extremely fast transmission (Wang et al., 2017).

The most recent EBOV outbreak occurred throughout 2018 in Central Africa, mostly in the Democratic Republic of the Congo (DRC), and the number of cases and deaths, over 800 and 400 respectively, is continuing to rise steadily despite the end of the epidemic being reported several times. The persistence of EBOV highlights the urgent need for therapeutics that can combat the infectious disease, in a manner that is practical for resource-poor areas globally. Studies have previously shown that EBOV infectivity can be halted with PIKfyve inhibition, using apilimod as a tool compound. PIKfyve's involvement in EBOV was discovered through a haploid genetic screen (Nelson et al., 2017). Apilimod was able to block trafficking of EBOV-GP virus-like particles (VLPs) to endolysosomes containing the EBOV receptor NPC1. Since it was demonstrated that PI-3,5-P_2 is crucial for the proper maturation of late endosomes, PIKfyve seems to play an important role in facilitating virus trafficking towards their port of entry, NPC1 (Nelson et al., 2017; Qiu et al., 2018). Most importantly, these findings suggest that PIKfyve inhibitors need to be developed and further explored to study and treat EBOV and potentially other filoviral infections.

Results

We tested a panel of PIKfyve inhibitors, already narrowed down from cancer cell line profiling, in a GFP assay with GFP-encoding murine leukemia virus (MLV) pseudotyped with the EBOV GP. We found that the compounds had activity mostly in the micromolar range, with MFH-5-3 top-performing at approximately 200 nM IC_{50} (Fig. 3.9). We ensured that the decrease in signal was due inhibition of infectivity and not due to cell death, as some compounds only induced cell death at high concentrations (Fig. 3.10). We also performed a washout assay to investigate if MFH compounds could perform better than apilimod in a prolonged setting. Interestingly, apilimod was able to sustain better potency even over the course of three days (Fig. 3.11) compared to the MFH compounds. This suggested that apilimod's potency was able to bestow upon it prolonged effects which are not reflected in the vacuolar assay alone, and maybe fusing our designs with apilimod could lead to improved properties.

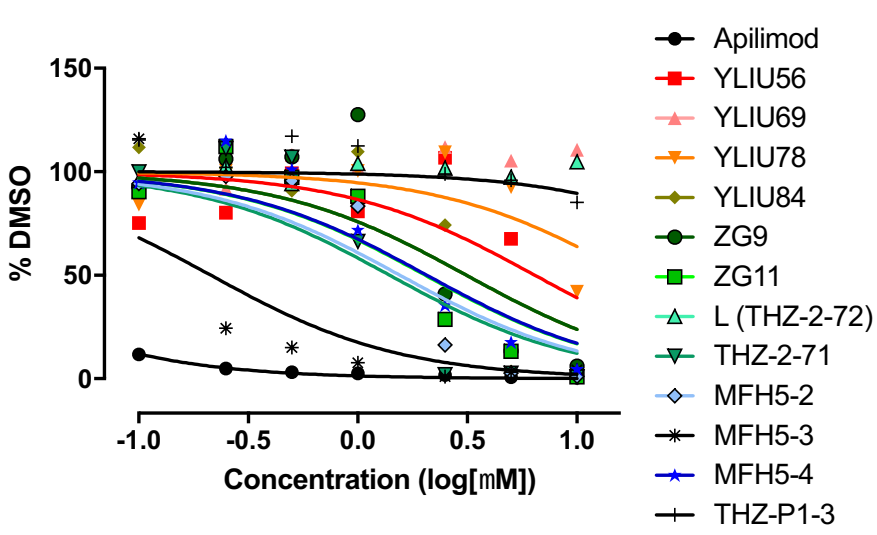

	IC50
Apilimod	0.01364
YLIU56	6.421
YLIU69	inactive
YLIU78	17.63
YLIU84	3.128
ZG9	3.129
ZG11	2.028
L (THZ-2-72)	inactive
THZ-2-71	1.396
MFH5-2	1.555
MFH5-3	0.2131
MFH5-4	2.065
THZ-P1-3	85.42

Figure 3.9 EBOV infectivity assay with PIKfyve inhibitors

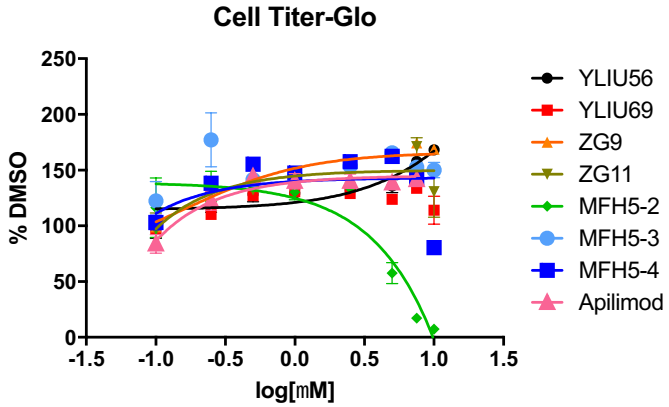

Figure 3.10 Antiproliferation assay with PIKfyve inhibitors in Vero cells

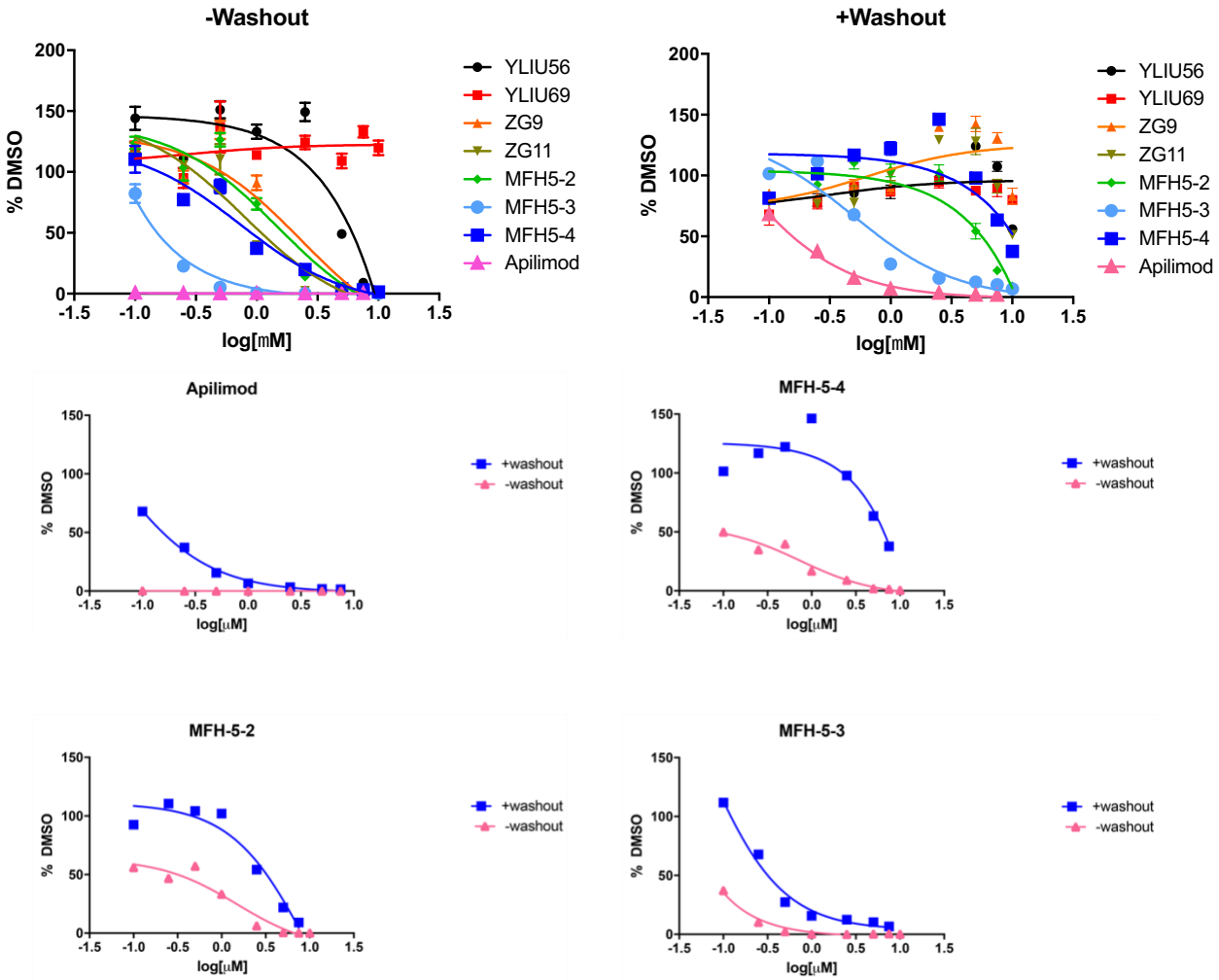

Figure 3.11 EBOV infectivity assay with and without washout with PIKfyve inhibitors. Vero cells were preincubated with compound 1h before infection as usual, with or without PBS washout performed at the 2h timepoint, and GFP readout at 7h.

Discussion

PIKfyve has also garnered attention in recent years as a key player in Toll-like receptor (TLR). Apilimod, a small molecule inhibitor of IL-12/13, had been in clinical trials for Crohn's disease, psoriasis and rheumatoid arthritis, but its direct target was unknown. A group at Novartis used a chemical genetic approach and identified PIKfyve to be the target bound by apilimod with an IC_{50} of 10 nM, specifically blocking its PI-5-P and PI-3,5-P_2 phosphoinositide activity and causing selective IL-12/13 inhibition. Since

then, apilimod has been an incredibly useful tool for dissecting the role of PIKfyve within the complex web of phosphoinositide signaling. Together with another PIKfyve inhibitor YM201636, these two most well-known PIKfyve inhibitors have unraveled functions of PIKfyve in modulating TLR immune signaling as well as differential phosphotransferase activity in the context of noncanonical autophagy.

As previously mentioned, PIKfyve as a target had been restricted to mainly the autoimmune space, but has been validated in the context of both cancer (B-NHL specifically) and Ebola viral disease. In both cases, PIKfyve's crucial role in maintaining the integrity of endosomes through its generation of the important phosphoinositide PI-3,5-P_2 seems to be the key factor. In lymphoma, a clear dependency on lysosomal homeostasis for nutrient access, and in EBOV, a dependency on a well-functioning endosomal pathway to allow viral entry, makes these diseases extremely susceptible to PIKfyve inhibition.

We capitalized on the slight off-target activity of THZ-P1-2 on PIKfyve to obtain PIKfyve inhibitors from our THZ-P1-2 scaffold starting point by employing our established chemical biology approach. By mining our compound database for inhibitors with the same structural core, we were able to narrow down and identify a series of compounds with potent PIKfyve biochemical activity. We confirmed the ability of these compounds to bind covalently to PIKfyve and found the labeled cysteine, Cys1970, to be outside the kinase domain similar to PI5P4K, using protein modeling and mass spectrometry approaches. We confirmed on-target engagement of these inhibitors and profiled them in a panel of lymphoma cell lines, showing them to have potencies on par with or superior to apilimod. From our studies, we obtained two top compounds, MFH-5-

3 and MFH-5-4, that serve as promising starting points for further optimization for studying and targeting PIKfyve.

The potent activity of our developed PIKfyve inhibitors in lymphoma cell lines compare well with that of apilimod. As this activity has yet to be validated as on-target with cysteine-to-serine mutants, we can speculate that some of the activity may be due to polypharmacology, with main off-target KIT and other milder off-targets such as FLT3 and PDGFRB. We hope to improve this selectivity by pursuing fusions of the apilimod and MFH scaffolds, to take advantage of apilimod's exquisite selectivity profile. We also observe that apilimod is still superior in the viral infectivity assays, which may be again due to its potency, or the covalent binding of MFH inhibitors rendering them unavailable to bind to more PIKfyve targets. Again, the PIKfyve inhibitor series could be improved on and also used as degrader starting point to be pursued in parallel. More studies need to be done with the covalent inhibitor approach in looking at inhibition of multiple rounds of infection, versus just the first or second cycle of virus production, in which case the covalent strategy may prove to be advantageous.

Author contributions:

Sindhu Carmen Sivakumaren and Nathanael Gray conceived original project. Sindhu Carmen Sivakumaren led the project, designed and performed biochemical and cellular experiments (exceptions below), conducted the majority of analyses and oversaw all collaborations. Tinghu Zhang synthesized initial THZ compounds and provided chemistry guidance and expertise. Ming-Feng Hao synthesized MFH compounds.

Christopher Browne (Jarrod Marto lab) collected and analyzed mass spectrometry data (samples prepared by Sindhu Carmen Sivakumaren). Guang Yang (Treon lab) conducted lymphoma cell line proliferation study in Table 3. May Wang (Cunningham lab) conducted EBOV viral infectivity assays.

Materials and Methods

Cell Culture

All cell culture was performed using standard techniques. HEK293T cells were cultured in Dulbecco's Modified Eagle's medium (DMEM) supplemented with 10% FBS and 1% penicillin/streptomycin (Gibco). Leukemia cells were cultured according to ATCC or DSMZ recommendations. All cells were cultured at 37°C and 5% CO_2.

Radiometric kinase assays

The PIKfyve assay was carried out as described in Rameh et al. (1997). Briefly, the kinase reaction was carried out in a total of 70 µL of kinase buffer (50 mM HEPES pH 7.4, 10 mM $MgCl_2$) with 0.1 µg of purified PIKfyve protein (Carna) preincubated with DMSO or compound at various concentrations, followed by addition of 20 µL of the resuspended PI-3-P lipids (sonicated and vortexed), 10 µM non-radiolabeled ATP, and 10 µCi [γ-^{32}P]-ATP for 10 minutes at room temperature. The reaction was terminated by adding 50 µL of 4 N HCl. Phosphoinositides were extracted by adding 100 µL of methanol/chloroform (approximately 1:1, vol:vol) mix and subjected to TLC (thin-layer chromatography) separation using heat-activated 2% oxaloacetate-coated silica gel 60

plates (20 cmx20 cm, EMD Millipore) and a 1-propanol/2 M acetic acid (65:35, vol:vol) solvent system. The radiolabeled product, $PI(3,5)P_2$, was quantified with a Phosphorimager (Molecular Dynamics, STORM840, GE Healthcare).

Immunoblotting

Cells were lysed with Pierce IP Lysis buffer supplemented with a cOmplete™ Mini Protease Inhibitor Cocktail tablet (Roche) on ice for 60 min. Lysates were clarified by centrifugation at 20,000 × *g* for 15 min at 4°C. Protein concentration was determined by a BCA assay (Pierce), and all samples were run with equal total protein content. Imaging was performed by detection of fluorescently labeled infrared secondary antibodies (IRDye) on the Odyssey CLx Imager (LI-COR).

Pulldown assays

HEK293T cells were lysed with Pierce IP Lysis buffer supplemented with a cOmplete™ Mini Protease Inhibitor Cocktail tablet (Roche) on ice for 60 min. Lysates were clarified by centrifugation at 20,000 × *g* for 15 min at 4°C. Protein concentration was determined by a BCA assay (Pierce), and all samples were equalized for protein content. DMSO or 1 μM dtb-THZ-P1-2 was added and rotated overnight at 4°C. Samples were rotated for 2h at room temperature to enhance covalent binding and then incubated with streptavidin resin for 2h at 4°C. Beads were washed with lysis buffer five times, resuspended in 1x LDS sample buffer, boiled at 95°C for 10 min and subjected to immunoblotting. For competitive pulldowns, HEK293T cells were grown to 90-95%

confluence, pretreated for 6h with DMSO or varying concentrations of THZ-P1-2, washed twice with cold PBS, lysed, and streptavidin pulldown conducted as described above with normalized samples.

Mass Spectrometry

Recombinant GST-PIKfyve protein (Carna) was incubated with DMSO or 5 μM inhibitor for 2 h at 37°C. Because GST-tagged proteins are not suitable for intact analysis, the samples prepared were immediately moved forward for site modification analysis. Samples were reduced with TCEP (10 mM final concentration), alkylated with iodoacetamide (22.5 mM final concentration) and digested with Asp-N or Glu-C (37 °C, overnight) and analyzed by nanoLC-MS. Digested peptides were injected onto the precolumn (4 cm POROS 10R2, Applied Biosystems) and eluted with an HPLC gradient (NanoAcquity UPLC system, Waters, Milford, MA; 10–70% B in 60 min; A = 0.1 M acetic acid in water, B = 0.1M acetic acid in acetonitrile). Peptides were resolved on a self-packed analytical column (50 cm Monitor C18, Column Engineering, Ontario, CA) and introduced to the mass spectrometer (LTQ Orbitrap XL) at a flow rate of ~30 nL/min (ESI spray voltage = 3.2 kV). The mass spectrometer was programmed to perform data-dependent MS/MS on the five most abundant precursors (35% collision energy) in each MS1 scan (image current detection, 30K resolution, *m*/*z* 300–2000). MS/MS spectra were matched to peptide sequences using Mascot (version 2.2.1) after conversion of raw data to .mgf using multiplierz scripts. Precursor and peptide ion mass tolerances were 10 ppm and 0.6 Da, respectively.

GFP Transduction Assays with Pseudotyped Virus

MLV pseudotyped viruses were added to Vero cells in serial 10-fold dilutions and assayed 72 hr later using fluorescence microscopy. An infectious unit (IU) is defined as one GFP-expressing cell within a range where the change in GFP-positive cells is directly proportional to the virus dilution. In experiments involving inhibitors, stock solutions of inhibitors (10 mM) in DMSO were diluted to a final concentration of 1% DMSO in media. Vero cells at 50% confluency and plated in 48-well plates were pre-incubated for 1 hr with the indicated concentrations of inhibitors prior to challenge with equal infectious units of MLV pseudotyped with the indicated GPs. 7 h post-infection, the number of GFP positive cells was counted. IC_{50} values were calculated in GraphPad Prism by fitting to a single-slope dose response curve. All assays were done in triplicate (Wang et al., 2017).

Proliferation assays

Cells were plated in 96-well or 384-well format and treated with indicated compounds at varying concentrations for 72h. Anti-proliferative effects of compounds were assessed using the Cell Titer Glo assay kit (Promega) with luminescence measured on an EnVision 2104 Multilabel Plate Reader (PerkinElmer). IC_{50}s were determined using the GraphPad Prism nonlinear regression curve fit.

Chapter 4. Summary and Future Directions

The work presented in this thesis takes a multipronged chemical biology strategy, bringing together methods in organic synthesis, biochemistry, cellular biology, crystallography and mass spectrometry, to devise novel small-molecule modulators (inhibitors and degraders) for the PI5P4K and PIKfyve lipid kinases. Though inhibitors exist for both these Type 2 and 3 lipid kinases, in some cases (e.g. for PI5P4K) the properties such as selectivity and potency can be improved upon with new compounds. For PIKfyve on the other hand, where a probe of superlative potency and selectivity already exists (apilimod), diversifying the compound space with new molecules can still have advantages, as we saw in Chapter 3 with prolonged pharmacodynamics due to irreversible inhibitors. This thesis aims to highlight how phosphoinositide kinases outside of PI3K can be targeted using a rational chemical biology approach and reveals the development of inhibitors of the PI5P4K/PIKfyve family of enzymes with the goal of studying these kinases in more detail in the context of cancer and Ebola.

In Chapter 2, we developed a covalent inhibitor of PI5P4K from a scaffold originally inhibiting the JNK family of kinases. In this study, we demonstrated the strength of building upon known pharmacophore knowledge, with having a starting point from JNK-IN-7 that led to the identification of a potent and selective pan-PI5P4K inhibitor. We obtained a nanomolar IC_{50} covalent PI5P4K inhibitor THZ-P1-2 that possesses few off-targets and is able to induce antiproliferative activity and autophagy dysfunction in cancer cells in a covalent manner.

Our current model is that THZ-P1-2's anticancer activity comes from its ability to induce autophagy dysfunction through PI5P4K inhibiton. More work is needed to fully elucidate the link between anticancer effects and the autophagy phenotype. We have

performed rescue experiments in cancer cell lines treated with THZ-P1-2 and supplemented with dimethyl α-ketoglutarate (DMKG) to provide acetyl-coA, or autophagy inhibitor 3-methyladenine, and observed mild attenuation of compound effects. This suggests that the cell killing mediated by THZ-P1-2 may be autophagy-dependent, and effects may be more substantial in heavily autophagic cancers, such as pancreatic cancer (Chude & Amaravadi, 2017).

One major goal of developing such tool compounds is being able to include them in large scale cancer cell line screens to identify potential new PI5P4K dependencies. This can be done in parallel with typical genetic approaches (such as CRISPR- or RNAi-based screening) to identify unique vulnerabilities in a cheaper, faster, less labor-intensive manner. In fact, THZ-P1-2 has been included in the Broad PRISM and Lab of Systems Pharmacology (LSP) LINCS screens for hematological malignancies and breast cancer respectively, and found to have broad activity in both screens. We already observed sensitivity of leukemia and lymphoma cell lines to THZ-P1-2 and plan on narrowing down into hematological malignancy subtypes. We also followed up with two of the most sensitive cell lines from the LINCS screen (MCF7 and T47D) and found that THZ-P1-2 induces potent cell cycle effects (G_1/S phase block) at nanomolar concentrations. MCF7 and T47D are also known to be heavily macropinocytic, from the work of Dr. Aimee Edinger presented at Keystone Tumor Metabolism 2019 (unpublished). This reliance on an “extrinsic” form of autophagy for nutrient access and cell survival may trigger an induced essentiality on the PI5P4Ks as autophagy mediators, thus exhibiting sensitivity to PI5P4K inhibitor THZ-P1-2. More work is needed to fully expound upon this connection once again, perhaps using a lipidomics/

phosphoinositomics and transcriptional profiling approach as well. One of the major advantages of covalent compounds, besides improved potency and selectivity, is the ability to verify on-target activity through inhibitor-resistant cysteine-to-serine mutations. As always, it is challenging to perform rescue experiments for every single cell line, especially for a family of enzymes like PI5P4K which has three isoforms. This is where the utility of having both covalent and reversible compounds comes into play. Both compounds can be used together to broadly assess PI5P4K dependency across cancer types, with follow-up studies to verify the PI5P4K contribution once the scope is narrowed down.

We performed preliminary chemoproteomic analysis of THZ-P1-2 in HEK293T cells using the CITe-Id platform in competition with dtb-THZ-P1-2 (Browne et al., 2018). This methodology allows us to identify specifically labeled cysteine residues by looking at dose-dependent competition, i.e. if a residue is labeled but does not show dose-dependent competition with the desthiobiotinylated probe, it is a nonspecifically labeled residue. We identified only three hits from this method: PI5P4Kγ, PIKfyve, and TEX264. TEX264 was previously an unknown protein, only known to be highly expressed in the testis, but two recent studies identified it as a receptor of ER-phagy (An et al., 2019; Chino, Hatta, Natsume, & Mizushima, 2019). More work is needed especially with regards to optimizing the assay for live-cell treatment, as lysate incubations may remove the effect of organelle compartmentalization, leading to false positives or overrepresentation of some off-targets. Either way, if TEX264 is a *bona fide* off-target of THZ-P1-2, this could shed some light onto THZ-P1-2's mechanism of action and also explain the partial rescue seen with the cysteine-to-serine mutants in the autophagy

assays. This polypharmacology of THZ-P1-2 could be responsible for the autophagy dysfunction observed, with TEX264 inhibition leading to ER-phagy-specific disruption. We sincerely hope to continue exploring new PI5PK and autophagy dependencies using these compounds – as mentioned, pancreatic ductal adenocarcinoma (PDAC) having a clearly defined dependency on autophagy could be a promising next move, with THZ-P1-2 and next-generation compounds either as single agents or in combination with Ras- and/or MEK-targeting agents (Bryant et al., 2019; Kinsey et al., 2019).

The high-throughput screening approach gave us a novel scaffold to work with, yielding a picomolar inhibitor TM-03-118 from structure-guided rational design. Though the cell permeability properties could be improved by continuing the medicinal chemistry campaign, there are also other strategies for utilizing this compound. We are interested in appending a covalent warhead to improve selectivity, by taking advantage of the unique targeted cysteines. We also aim to turn these compounds into degraders and see if we can achieve pan- or isoform-selective degradation.

With our PROTAC approach, we aim to continue exploring linker lengths and other E3 ligase targeting moieties, such as VHL, to hopefully achieve rapid and efficacious degradation. We also aim to investigate the applicability of the Lysosome Targeting Chimera (LYTAC) platform for PI5P4K targeting (Banik et al., 2019). Because loss of PI5P4K leads to lysosome accumulation, we are interested in exploring if a LYTAC-based degradation approach will lead to a positive feedback loop and consequently increased efficacy.

In Chapter 3, we proved the versatility of our chemical biology platform that was used to generate PI5P4K compounds by pivoting towards a new target, PIKfyve. We observed that a key determining factor for potency, especially in cells, was the reactivity of the covalent warhead. The chloroacetamide-containing MFH compounds demonstrated potent and long-lasting PIKfyve inhibitor both in biochemical and cellular assays.

While it is encouraging that the reactivity of the warhead does not seem to come at a cost of selectivity, the overall selectivity profile needs improvement. We plan to pursue apilimod-MFH fusion compound designs, taking advantage of apilimod's unique three-pronged binding mode, illuminated by docking studies into our PIKfyve model. We will continue to use WSU-DLCL2 as our main model for lymphoma, given an already established PIKfyve dependency and apilimod-resistant mutation. We aim to perform cysteine-to-serine mutant rescues for PIKfyve in our various models. We also plan to look at other cell lines that have high PIKfyve expression but no dependency, such as Karpas422 and MDA-PCA-2b according to the CancerDepMap. Our PIKfyve inhibitors alongside apilimod could be used to further uncover differences in PIKfyve, TFEB, and overall lysosomal homeostasis in these different environments. We also hope to discover settings where irreversible inhibition could be advantageous compared to apilimod.

In the context of EBOV, we plan on testing our compounds with various EBOV GP mutants to see if they are sensitive to PIKfyve covalent inhibition, especially if they confer resistance to apilimod or NPC1 inhibitors. We hope to further characterize where our inhibitors come into play during the trafficking process of virus particles to the

endosomes and NPC1, especially if there are potential advantages to inhibiting the viral infection mechanism prior to receptor fusion. One method we hope to explore is single-cell RNA-seq (with Pardis Sabeti lab) to detect host and Ebola virus RNA reads from infected cells harvested from healthy humans or non-human primates to assess host and viral transcriptomes in individual immune cell types. Given apilimod's initial application in the context of immune signaling, we believe this investigation of host and viral immune signaling, which could be differentially affected by PIKfyve inhibition, would be extremely informative in dissecting the antiviral mechanism of these inhibitors.

We hope to assess the potential for PIKfyve inhibitors to have broad or pan-filoviral activity, and if there is synergy or potential for combination with NPC1 inhibitors or other current EBOV inhibitors. Because of the dire need for better therapeutic options and the advantages of temperature stable, orally bioavailable inhibitors in resource-poor settings, we hope to improve pharmacokinetic parameters of these inhibitors for testing in EBOV animal models and eventually humans.

In summary, we hope this thesis has sufficiently highlighted the targetability of PI5P4Ks and PIKfyve, with our developed inhibitors serving as useful tools to further interrogate the therapeutic potential of these noncanonical lipid kinases and inform drug discovery campaigns in the context of cancer, Ebola, and potentially other autophagy-dependent diseases. The tool compound development using a chemical biology approach in this thesis opens up several more doors for further study and validation of these target kinases, and we hope that this advances even more uncovering of hidden gems within the understudied proteome.

Bibliography

Al-ramahi, I., Srinivas, S., Giridharan, P., Chen, Y., Patnaik, S., Safren, N., … Marugan, J. J. (2017). Inhibition of PIP4K g ameliorates the pathological effects of mutant huntingtin protein, 1–25.

An, H., Ordureau, A., Paulo, J. A., Shoemaker, C. J., Denic, V., & Harper, J. W. (2019). TEX264 Is an Endoplasmic Reticulum-Resident ATG8-Interacting Protein Critical for ER Remodeling during Nutrient Stress. *Molecular Cell*, 1–18. https://doi.org/10.1016/j.molcel.2019.03.034

Balla, T. (2013). Phosphoinositides: Tiny Lipids With Giant Impact on Cell Regulation. *Physiological Reviews*, *93*(3), 1019–1137. https://doi.org/10.1152/physrev.00028.2012

Balla, T., Szentpetery, Z., & Kim, Y. J. (2009). Phosphoinositide Signaling: New Tools and Insights. *Physiology*, *24*(4), 231–244. https://doi.org/10.1152/physiol.00014.2009

Banik, S., Pedram, K., Wisnovsky, S., Riley, N., Bertozzi, C., & Banik, C. (2019). Lysosome Targeting Chimeras (LYTACs) for the Degradation of Secreted and Membrane Proteins. https://doi.org/10.26434/chemrxiv.7927061.v1

Browne, C. M., Jiang, B., Ficarro, S. B., Doctor, Z. M., Johnson, J. L., Card, J. D., … Marto, J. A. (2018). Article A Chemoproteomic Strategy for Direct and Proteome-wide Covalent Inhibitor Target-site Identification. https://doi.org/10.1021/jacs.8b07911

Bryant, K. L., Stalnecker, C. A., Zeitouni, D., Klomp, J. E., Peng, S., Tikunov, A. P., … Der, C. J. (2019). Combination of ERK and autophagy inhibition as a treatment approach for pancreatic cancer. *Nature Medicine*, *25*(April). https://doi.org/10.1038/s41591-019-0368-8

Bulley, S. J., Clarke, J. H., Droubi, A., Giudici, M. L., & Irvine, R. F. (2015). Exploring phosphatidylinositol 5-phosphate 4-kinase function. *Advances in Biological Regulation*, *57*, 193–202. https://doi.org/10.1016/j.jbior.2014.09.007

Bulley, S. J., Droubi, A., Clarke, J. H., Anderson, K. E., Stephens, L. R., Hawkins, P. T., & Irvine, R. F. (2016). In B cells, phosphatidylinositol 5-phosphate 4-kinase-α synthesizes PI(4,5)P2 to impact mTORC2 and Akt signaling. *Proceedings of the National Academy of Sciences of the United States of America*, *113*(38), 10571–10576. https://doi.org/10.1073/pnas.1522478113

Cantley, L. C., & Ph, D. (2018). Phosphatidylinositol 3-Kinase, Growth Disorders, and Cancer. https://doi.org/10.1056/NEJMra1704560

Chino, H., Hatta, T., Natsume, T., & Mizushima, N. (2019). Intrinsically Disordered Protein TEX264 Mediates ER-phagy. *Molecular Cell*, 1–13. https://doi.org/10.1016/j.molcel.2019.03.033

Chude, C. I., & Amaravadi, R. K. (2017). Targeting autophagy in cancer: Update on clinical trials and novel inhibitors. *International Journal of Molecular Sciences*, *18*(6). https://doi.org/10.3390/ijms18061279

Craene, J. De, Bertazzi, D. L., Bär, S., & Friant, S. (2017). Phosphoinositides , Major Actors in Membrane Trafficking and Lipid Signaling Pathways. https://doi.org/10.3390/ijms18030634

Davis, M. I., Sasaki, A. T., Shen, M., Emerling, B. M., Thorne, N., Michael, S., … Simeonov, A. (2013). A Homogeneous, High-Throughput Assay for Phosphatidylinositol 5-Phosphate 4-Kinase with a Novel, Rapid Substrate Preparation. *PLoS ONE*, *8*(1). https://doi.org/10.1371/journal.pone.0054127

Deng, X., Dzamko, N., Prescott, A., Davies, P., Liu, Q., Yang, Q., … Gray, N. S. (2011). Characterization of a selective inhibitor of the Parkinson's disease kinase LRRK2. *Nature Chemical Biology*, *7*(4), 203–205. https://doi.org/10.1038/nchembio.538

Deng, X., Yang, Q., Kwiatkowski, N., Sim, T., Mcdermott, U., Settleman, E., … Gray, N. S. (2011). Xianming Deng, † , || Qingkai Yang, ‡ , || Nicholas Kwiatkowski, † Taebo Sim, † Ultan McDermott, § Je ff rey E. Settleman, § Jiing-Dwan Lee,* , ‡ and Nathanael S. Gray* , † †, *6*, 195–200.

Diehl, W. E., Lin, A. E., Grubaugh, N. D., Andersen, K. G., Sabeti, P. C., Diehl, W. E., … Kyawe, P. P. (2016). Ebola Virus Glycoprotein with Increased Infectivity Article Ebola Virus Glycoprotein with Increased Infectivity Dominated the 2013 – 2016

Epidemic. *Cell*, *167*(4), 1088–1097.e6. https://doi.org/10.1016/j.cell.2016.10.014

Dudas, G., Carvalho, L. M., Bedford, T., Tatem, A. J., Baele, G., Faria, N., … Rambaut, A. (2016). Virus genomes reveal the factors that spread and sustained the West African Ebola epidemic. *BioRxiv*, (February 2014), 071779. https://doi.org/10.1101/071779

Emerling, B. M., Hurov, J. B., Poulogiannis, G., Tsukazawa, K. S., Choo-Wing, R., Wulf, G. M., … Cantley, L. C. (2013). XDepletion of a putatively druggable class of phosphatidylinositol kinases inhibits growth of p53-Null tumors. *Cell*, *155*(4), 844–857. https://doi.org/10.1016/j.cell.2013.09.057

Erb, M. A., Scott, T. G., Li, B. E., Xie, H., Paulk, J., Seo, H. S., … Bradner, J. E. (2017). Transcription control by the ENL YEATS domain in acute leukaemia. *Nature*, *543*(7644), 270–274. https://doi.org/10.1038/nature21688

Fedorov, O., Müller, S., & Knapp, S. (2010). The (un)targeted cancer kinome. *Nature Chemical Biology*, *6*(3), 166–169. https://doi.org/10.1038/nchembio.297

Ferguson, F. M., & Gray, N. S. (2018). Kinase inhibitors: The road ahead. *Nature Reviews Drug Discovery*, *17*(5), 353–376. https://doi.org/10.1038/nrd.2018.21

Fiume, R., Stijf-Bultsma, Y., Shah, Z. H., Keune, W. J., Jones, D. R., Jude, J. G., & Divecha, N. (2015). PIP4K and the role of nuclear phosphoinositides in tumour suppression. *Biochimica et Biophysica Acta - Molecular and Cell Biology of Lipids*, *1851*(6), 898–910. https://doi.org/10.1016/j.bbalip.2015.02.014

Gayle, S., Landrette, S., Beeharry, N., Conrad, C., Hernandez, M., Beckett, P., … Lichenstein, H. (2018). Identi fi cation of apilimod as a fi rst-in-class PIKfyve kinase inhibitor for treatment of B-cell non-Hodgkin lymphoma, *129*(13), 1768–1779. https://doi.org/10.1182/blood-2016-09-736892.

Hamann, B. L., & Blind, R. D. (2017). Nuclear phosphoinositide regulation of chromatin. *Journal of Cellular Physiology*, (February). https://doi.org/10.1002/jcp.25886

Harvard, T. (2015). Biology of Type 2 Phosphatidylinositol-5- Phosphate 4-Kinase.

Hasegawa, J., Strunk, B. S., & Weisman, L. S. (2017). PI5P and PI(3,5)P₂: Minor, but Essential Phosphoinositides. *Cell Structure and Function*, *42*(1), 49–60. https://doi.org/10.1247/csf.17003

Hu, A., Zhao, X.-T., Tu, H., Xiao, T., Fu, T., Wang, Y., … Song, B.-L. (2018). PIP4K2A regulates intracellular cholesterol transport through modulating PI(4,5)P 2 homeostasis . *Journal of Lipid Research*, *59*(3), 507–514. https://doi.org/10.1194/jlr.m082149

Huang, H.-T., Seo, H.-S., Zhang, T., Wang, Y., Jiang, B., Li, Q., … Gray, N. S. (2017). MELK is not necessary for the proliferation of basal-like breast cancer cells. *ELife*, *6*. https://doi.org/10.7554/elife.26693

Isserlin, R., Bader, G. D., Edwards, A., Frye, S., & Willson, T. (2011). Human genome and drug discovery - paths not taken. Retrieved from papers2://publication/uuid/9D5509EE-B482-4F47-A54A-18B8196F241F

Jefferies, H. B. J., Cooke, F. T., Jat, P., Boucheron, C., Koizumi, T., Hayakawa, M., … Parker, P. J. (2008). A selective PIKfyve inhibitor blocks PtdIns(3,5)P2 production and disrupts endomembrane transport and retroviral budding. *EMBO Reports*, *9*(2), 164–170. https://doi.org/10.1038/sj.embor.7401155

Jude, J. G., Spencer, G. J., Huang, X., Somerville, T. D. D., Jones, D. R., Divecha, N., & Somervaille, T. C. P. (2014). A targeted knockdown screen of genes coding for phosphoinositide modulators identifies PIP4K2A as required for acute myeloid leukemia cell proliferation and survival. *Oncogene*, *34*(10), 1–10. https://doi.org/10.1038/onc.2014.77

Keune, W. J., Jones, D. R., Bultsma, Y., Sommer, L., Zhou, X. Z., Lu, K. P., & Divecha, N. (2012). Regulation of phosphatidylinositol-5-phosphate signaling by Pin1 determines sensitivity to oxidative stress. *Science Signaling*, *5*(252), 1–13. https://doi.org/10.1126/scisignal.2003223

Keune, W. J., Jones, D. R., & Divecha, N. (2013). PtdIns5P and Pin1 in oxidative stress signaling. *Advances in Biological Regulation*, *53*(2), 179–189. https://doi.org/10.1016/j.jbior.2013.02.001

Kinsey, C. G., Camolotto, S. A., Boespflug, A. M., Guillen, K. P., Foth, M., Truong, A.,

… Mcmahon, M. (2019). Protective autophagy elicited by RAF → MEK → ERK inhibition suggests a treatment strategy for RAS-driven cancers. *Nature Medicine*, *25*(April). https://doi.org/10.1038/s41591-019-0367-9

Kitagawa, M., Liao, P., Lee, K. H., Wong, J., Shang, S. C., Minami, N., … Lee, S. H. (2017). mitotic pathways leads to cancer-selective lethality. *Nature Communications*. https://doi.org/10.1038/s41467-017-02287-5

Krishna, S., Palm, W., Lee, Y., Yang, W., Bandyopadhyay, U., Xu, H., … Overholtzer, M. (2016). PIKfyve Regulates Vacuole Maturation and Nutrient Recovery following Engulfment. *Developmental Cell*, *38*(5), 536–547. https://doi.org/10.1016/j.devcel.2016.08.001

Kutateladze, T. G. (2010). Translation of the phosphoinositide code by PI effectors. *Nature Chemical Biology*, *6*(7), 507–513. https://doi.org/10.1038/nchembio.390

Liu, Q., Sabnis, Y., Zhao, Z., Zhang, T., Buhrlage, S. J., Jones, L. H., & Gray, N. S. (2013). Developing irreversible inhibitors of the protein kinase cysteinome. *Chemistry and Biology*, *20*(2), 146–159. https://doi.org/10.1016/j.chembiol.2012.12.006

Lundquist, M. R., Goncalves, M. D., Loughran, R. M., Possik, E., Vijayaraghavan, T., Yang, A., … Emerling, B. M. (2018). Phosphatidylinositol-5-Phosphate 4-Kinases Regulate Cellular Lipid Metabolism By Facilitating Autophagy. *Molecular Cell*, *70*(3), 531–544.e9. https://doi.org/10.1016/j.molcel.2018.03.037

Ma, G., Duan, Y., Huang, X., Qian, C. X., Chee, Y., Mukai, S., … Lei, H. (2016). Prevention of proliferative vitreoretinopathy by suppression of phosphatidylinositol 5-phosphate 4-kinases. *Investigative Ophthalmology and Visual Science*, *57*(8), 3935–3943. https://doi.org/10.1167/iovs.16-19405

Mendgen, T., Steuer, C., & Klein, C. D. (2012). Privileged scaffolds or promiscuous binders: A comparative study on rhodanines and related heterocycles in medicinal chemistry. *Journal of Medicinal Chemistry*, *55*(2), 743–753. https://doi.org/10.1021/jm201243p

Murphy, L., Cai, X., Xu, Y., Cheung, A. K., Tomlinson, R. C., Alca, A., … Huang, Q. (2013). Article PIKfyve , a Class III PI Kinase , Is the Target of the Small Molecular

IL-12 / IL-23 Inhibitor Apilimod and a Player in Toll-like Receptor Signaling, 912–921. https://doi.org/10.1016/j.chembiol.2013.05.010

Nabet, B., Roberts, J. M., Buckley, D. L., Paulk, J., Dastjerdi, S., Yang, A., … Bradner, J. E. (2018). specific protein degradation. *Nature Chemical Biology*, *14*(May). https://doi.org/10.1038/s41589-018-0021-8

Nelson, E. A., Dyall, J., Hoenen, T., Barnes, A. B., Zhou, H., Liang, J. Y., … White, J. M. (2017). The phosphatidylinositol-3-phosphate 5-kinase inhibitor apilimod blocks filoviral entry and infection. *PLoS Neglected Tropical Diseases*, *11*(4), 1–22. https://doi.org/10.1371/journal.pntd.0005540

Oppelt, A., Haugsten, E. M., Zech, T., Danielsen, H. E., Sveen, A., Lobert, V. H., … Wesche, J. (2014). PIKfyve, MTMR3 and their product PtdIns5 P regulate cancer cell migration and invasion through activation of Rac1 . *Biochemical Journal*, *461*(3), 383–390. https://doi.org/10.1042/bj20140132

Qiu, S., Leung, A., Bo, Y., Kozak, R. A., Priya, S., Warkentin, C., … Kobinger, G. (2018). Ebola virus requires phosphatidylinositol (3 , 5) bisphosphate production for e ffi cient viral entry. *Virology*, *513*(October 2017), 17–28. https://doi.org/10.1016/j.virol.2017.09.028

Rameh, L. E., & Cantley, L. C. (1999). Minireview The Role of Phosphoinositide 3-Kinase Lipid Products in, *2*(30), 8347–8350. https://doi.org/10.1074/jbc.274.13.8347

Rameh, L. E., Tolias, K. F., Duckworth, B. C., & Cantley, L. C. (1997). A new pathway for synthesis of phosphatidylinositol-4,5-bisphosphate. *Nature*, *390*(6656), 192–196. https://doi.org/10.1038/36621

Ramel, D., Saland, E., & Payrastre, B. (2011). The Nucleophosmin-Anaplastic Lymphoma Kinase Oncogene Interacts , Activates , and Uses the Kinase PIKfyve to Increase, *286*(37), 32105–32114. https://doi.org/10.1074/jbc.M111.227512

Sbrissa, D., Ikonomov, O. C., Filios, C., Delvecchio, K., & Shisheva, A. (2012). Functional dissociation between PIKfyve-synthesized PtdIns5P and PtdIns(3,5)P 2 by means of the PIKfyve inhibitor YM201636 . *American Journal of Physiology-Cell Physiology*, *303*(4), C436–C446. https://doi.org/10.1152/ajpcell.00105.2012

Sbrissa, D., Ikonomov, O. C., & Shisheva, A. (1999). PIKfyve, a mammalian ortholog of yeast Fab1p lipid kinase, synthesizes 5-phosphoinositides. Effect of insulin. *Journal of Biological Chemistry*, *274*(31), 21589–21597. https://doi.org/10.1074/jbc.274.31.21589

Sbrissa, D., Ikonomov, O. C., & Shisheva, A. (2002). Phosphatidylinositol 3-Phosphate-interacting Domains in PIKfyve. *Journal of Biological Chemistry*, *277*(8), 6073–6079. https://doi.org/10.1074/jbc.m110194200

Sbrissa, D., Naisan, G., Ikonomov, O. C., & Shisheva, A. (2018). Apilimod, a candidate anticancer therapeutic, arrests not only PtdIns(3,5)P2 but also PtdIns5P synthesis by PIKfyve and induces bafilomycin A1-reversible aberrant endomembrane dilation. *PLoS ONE*, *13*(9), 1–22. https://doi.org/10.1371/journal.pone.0204532

Sharma, G., Guardia, C. M., Roy, A., Vassilev, A., Saric, A., Griner, L. N., … DePamphilis, M. L. (2019). A Family of PIKFYVE Inhibitors with Therapeutic Potential Against Autophagy-Dependent Cancer Cells Disrupt Multiple Events in Lysosome Homeostasis. *Autophagy*, *0*(0), 15548627.2019.1586257. https://doi.org/10.1080/15548627.2019.1586257

Shim, H., Wu, C., Ramsamooj, S., Bosch, K. N., Chen, Z., & Emerling, B. M. (2016). Deletion of the gene Pip4k2c , a novel phosphatidylinositol kinase , results in hyperactivation of the immune system, *113*(27), 7596–7601. https://doi.org/10.1073/pnas.1600934113

Shisheva, A. (2008). PIKfyve: Partners, significance, debates and paradoxes. *Cell Biology International*, *32*(6), 591–604. https://doi.org/10.1016/j.cellbi.2008.01.006

Stijf-Bultsma, Y., Sommer, L., Tauber, M., Baalbaki, M., Giardoglou, P., Jones, D. R., … Divecha, N. (2015). The basal transcription complex component TAF3 transduces changes in nuclear phosphoinositides into transcriptional output. *Molecular Cell*, *58*(3), 453–467. https://doi.org/10.1016/j.molcel.2015.03.009

Thapa, N., Tan, X., Choi, S., Lambert, F., Rapraeger, A. C., & Anderson, R. A. (2016). The Hidden Conundrum of Phosphoinositide Signaling in Cancer, *xx*, 1–13.

Tomašić, T., & Peterlin Mašič, L. (2012). Rhodanine as a scaffold in drug discovery: a critical review of its biological activities and mechanisms of target modulation. *Expert Opinion on Drug Discovery*, *7*(7), 549–560. https://doi.org/10.1517/17460441.2012.688743

Urbanowicz, R. A., Mcclure, C. P., Rey, A., Simon-loriere, E., Ball, J. K., Urbanowicz, R. A., … Holmes, E. C. (2016). Human Adaptation of Ebola Virus during the West Article Human Adaptation of Ebola Virus during the West African Outbreak, 1079–1087. https://doi.org/10.1016/j.cell.2016.10.013

Vicinanza, M., D 'angelo, G., Campli, A. Di, & De Matteis, M. A. (2008). Function and dysfunction of the PI system in membrane trafficking. *The EMBO Journal*, *27*(19), 2457–2470. https://doi.org/10.1038/emboj.2008.169

Vicinanza, M., Korolchuk, V. I., Ashkenazi, A., Puri, C., Menzies, F. M., Clarke, J. H., & Rubinsztein, D. C. (2015). PI(5)P regulates autophagosome biogenesis. *Molecular Cell*, *57*(2), 219–234. https://doi.org/10.1016/j.molcel.2014.12.007

Wang, M. K., Lim, S., Lee, S. M., Cunningham, J. M., Wang, M. K., Lim, S., … Cunningham, J. M. (2017). Biochemical Basis for Increased Activity of Ebola Article Biochemical Basis for Increased Activity of Ebola Glycoprotein in the 2013 – 16 Epidemic. *Cell Host and Microbe*, *21*(3), 367–375. https://doi.org/10.1016/j.chom.2017.02.002

Williams, C. A. C., Fernandez-Alonso, R., Wang, J., Toth, R., Gray, N. S., & Findlay, G. M. (2016). Erk5 Is a Key Regulator of Naive-Primed Transition and Embryonic Stem Cell Identity. *Cell Reports*, *16*(7), 1820–1828. https://doi.org/10.1016/j.celrep.2016.07.033

Zhang, J., Yang, P. L., & Gray, N. S. (2008). Targeting cancer with small molecule kinase inhibitors. *Nature Reviews Cancer*, *9*(1), 28–39. https://doi.org/10.1172/JCI76094.genomically

Zhang, T., Inesta-Vaquera, F., Niepel, M., Zhang, J., Ficarro, S. B., MacHleidt, T., … Gray, N. S. (2012). Discovery of potent and selective covalent inhibitors of JNK. *Chemistry and Biology*, *19*(1), 140–154. https://doi.org/10.1016/j.chembiol.2011.11.010

Zheng, L., & Conner, S. D. (2018). PI5P4Kγ functions in DTX1-mediated Notch signaling. *Proceedings of the National Academy of Sciences*, *115*(9), E1983–E1990. https://doi.org/10.1073/pnas.1712142115

Appendix 1: Supplemental Materials

A

Kinase	Labeling site	% Inhibition (%)
JNK1, JNK2, JNK3	Lys2	99.7
p38a	Lys2	16.4
p38a	Other	14.7
GSK3A	Lys2	20.4
GSK3B	Lys2	12.3
PFTAIRE1	Lys1	75.3
CDK9	Lys2	16.6
ROCK1	Other	-11.9
ROCK1, ROCK2	Lys2	-21.5
PIP5K3	ATP	91.8
PIK3C3	ATP	77.5
PIK3C3	ATP	74.2
PIP4K2C	ATP	77.2
PIP4K2C	ATP	84.3

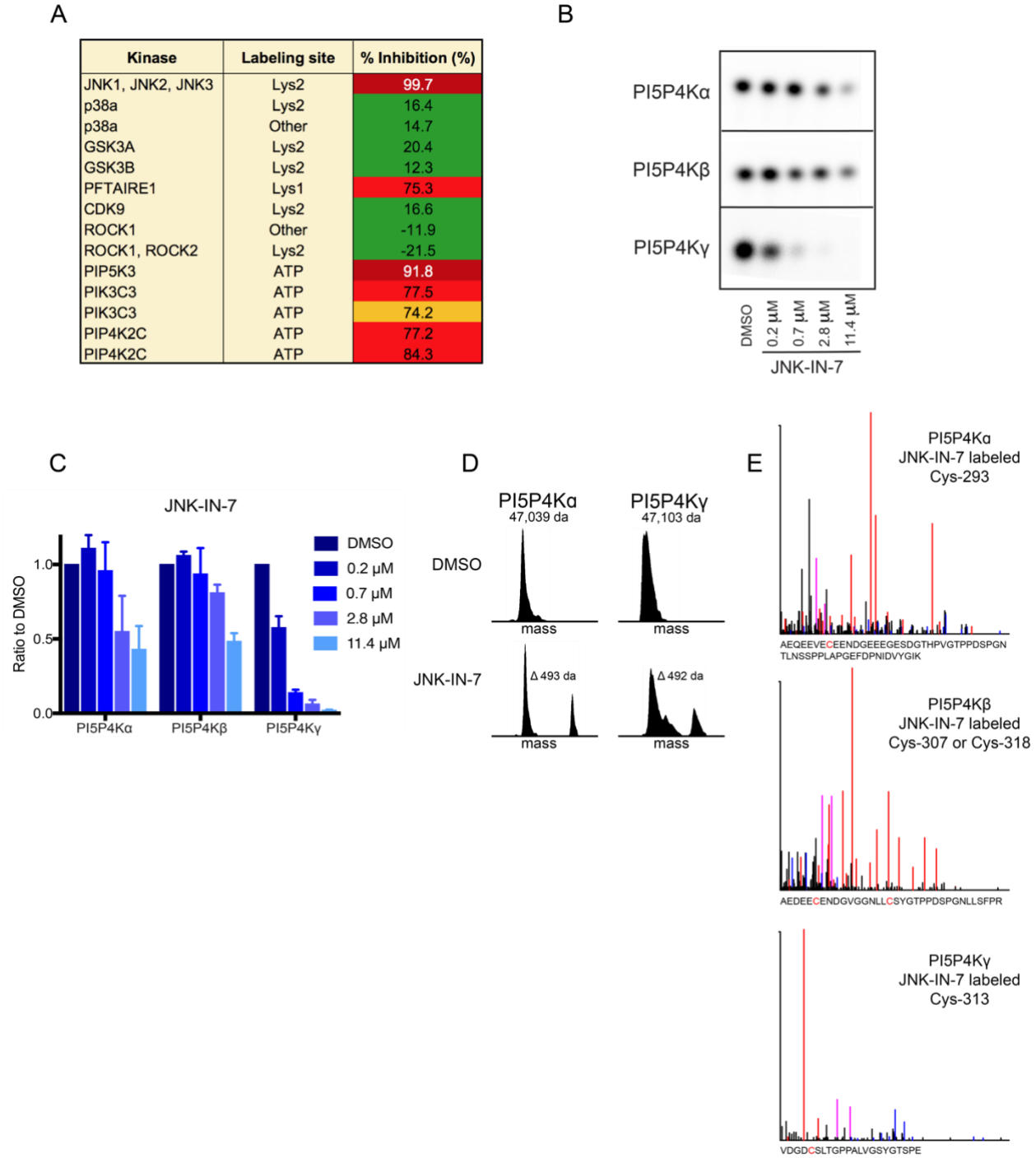

Figure S1. Characterization of JNK-IN-7 on PI5P4K. (A) A list of selected targets, including PI5P4Kγ (PIP4K2C), from KiNativ profiling of JNK-IN-7. Full list is available in Zhang et al. (2012). (B) JNK-IN-7 inhibits kinase activity of all three PI5P4K isoforms in a radiometric TLC assay measuring radiolabeled PI-4,5-P_2. (C) Quantification of (B). Radiolabeled PI-4,5-P_2 spots were imaged by autoradiography and quantified by densitometry. (D) Covalent labeling of PI5P4K isoforms as determined by intact mass spectrometry. (E) Subsequent protease digestion and tandem mass spectrometry confirms that THZ-P1-2 covalently labels cysteine residues on all three PI5P4K isoforms. The peptide for PI5P4Kβ was exclusively observed to be singly labeled at either Cys-307 or Cys-318.

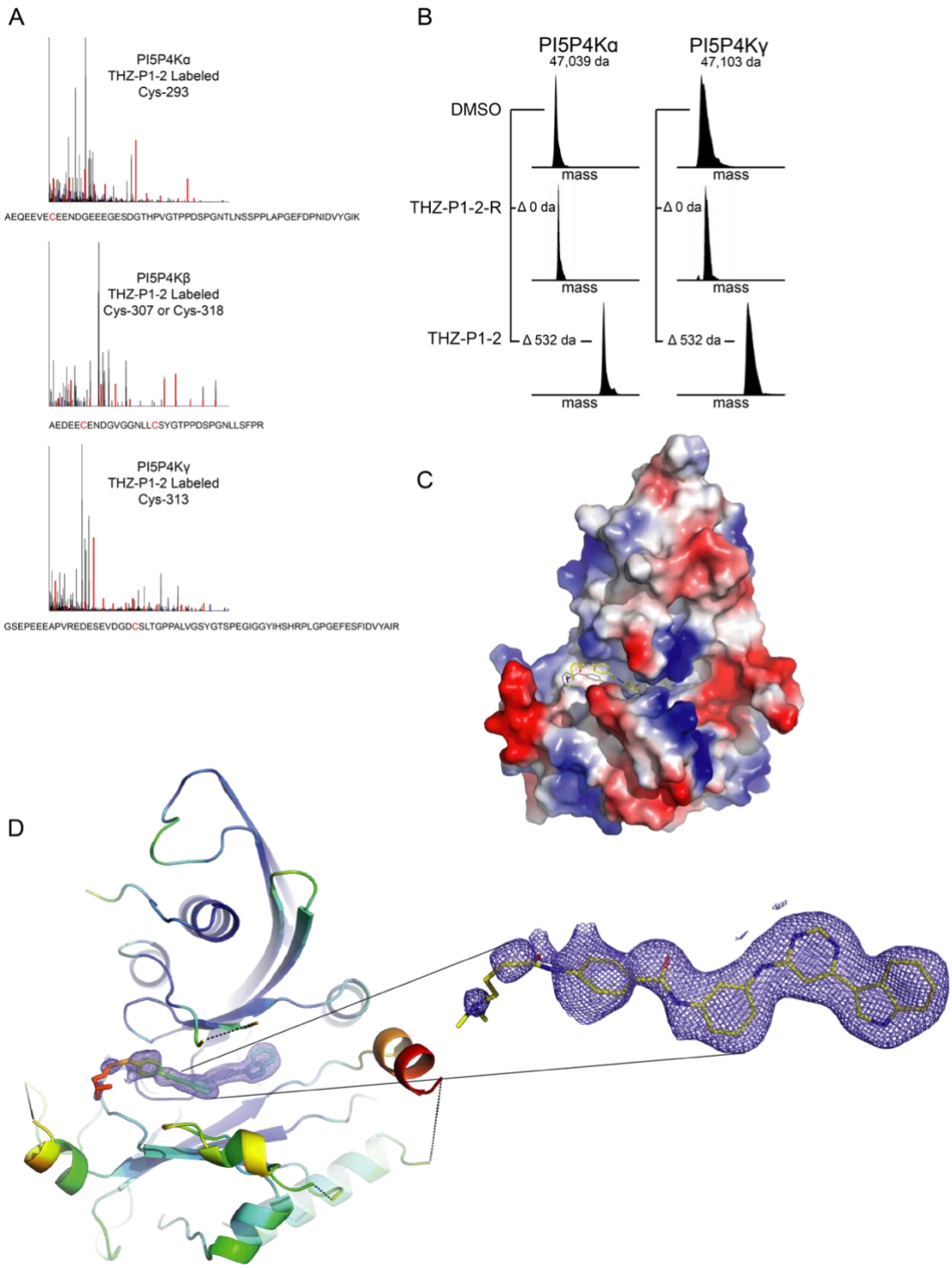

Figure S2. Supplemental mass spectrometry and structural data for THZ-P1-2 and THZ-P1-2-R. (A) Protease digestion and tandem mass spectrometry following intact mass labeling confirms that THZ-P1-2 covalently labels cysteine residues on all three PI5P4K isoforms. B) THZ-P1-2-R was found not to covalently label recombinant PI5P4Kα and γ when incubated with purified protein for 2 hours at 37°C. (C) Surface representation of co-crystal structure of PI5P4Kα in complex with THZ-P1-2. (D) Zoom-in of ligand electron density within the active site of PI5P4Kα. See Table S1 for diffraction data collection and refinement statistics.

Figure S3. Additional characterization data for THZ-P1-2. (A) THZ-P1-2-R and dtb-THZ-P1-2 were found to inhibit PI5P4Kα in an ADP-Glo assay, with a slight loss in potency with THZ-P1-2-R. Both compounds were incubated with PI5P4Kα for 15min before proceeding with a 1 hour reaction with ATP and development with ADP-Glo reagents. Plots are shown in comparison with THZ-P1-2 from Fig. 1B. (B) THZ-P1-2 engages PI5P4K isoforms at 2h and 4h timepoints, exhibiting prolonged engagement when a washout is performed. HEK293T cells were treated with DMSO or THZ-P1-2 at time, t=0 and cells were washed 2X with PBS at either 2 or 4h and harvested at the end of 6h. A streptavidin pulldown was then conducted in lysates after normalization of protein content with a BCA assay. (C) THZ-P1-2 inhibits the Type 1 PI4P5K kinases at a lower extent but shows potent inhibition on PIKfyve by ADP-Glo. *In vitro* kinase assays were performed by Carna Biosciences. (D) THZ-P1-2 causes vacuolar enlargement, characteristic of PIKfyve inhibition, at a concentration of 10 μM but not 1 μM, compared to PIKfyve inhibitor apilimod at 10 nM treatment. Vero cells were treated with DMSO or compound for 6h and imaged. (E) Incubation of Vero cells with 1 μM THZ-P1-2 was unable to impair the PIKfyve inhibitory phenotype of apilimod. Preincubation: Vero cells were incubated with DMSO/THZ-P1-2 for 1 or 6h, washed with PBS to completely remove compound, treated with DMSO/apilimod and imaged after 6h. Coincubation: Vero cells were incubated with DMSO/THZ-P1-2 for 1 or 6h, and then co-treated with DMSO/apilimod and imaged after 6h.

Figure S3 (Continued)

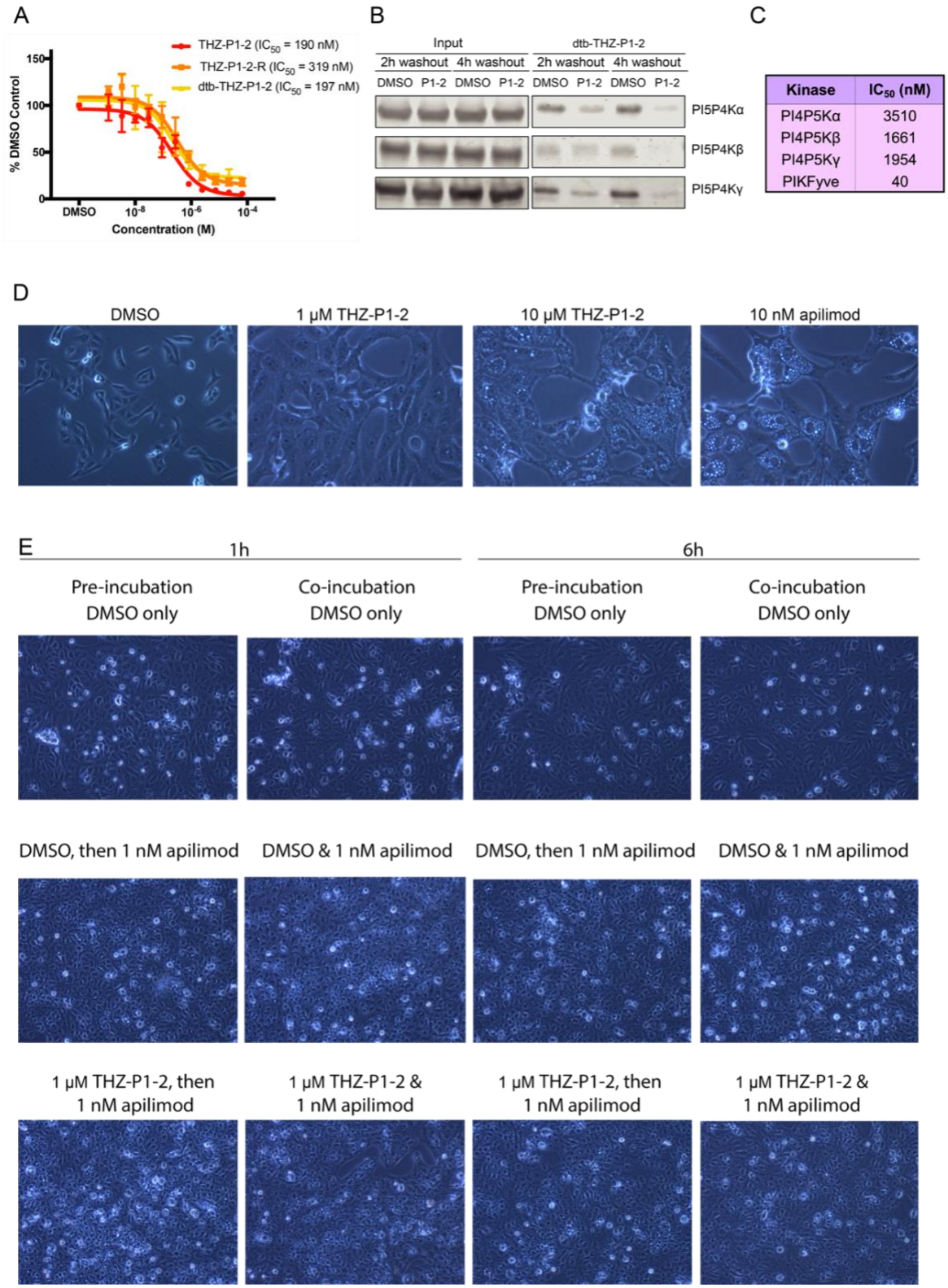

Figure S4. Selectivity profiling and autophagy follow-up characterization data for THZ-P1-2. (A) THZ-P1-2 inhibits off-target kinases identified in the DiscoverX KINOMEScan panel to varying degrees. *In vitro* kinase assays were performed by Invitrogen using the Adapta assay. (B) A streptavidin pulldown in HEK293T lysate shows little to no engagement of C-ABL and BRK by dtb-THZ-P1-2. (C) THZ-P1-2 shows mild antiproliferative activity on BCR-ABL addicted cell lines. Two cell lines containing BCR-ABL translocations, K562 and KU812F, were treated with THZ-P1-2 or known BCR-ABL inhibitors imatinib, nilotinib and dasatinib for 72h and assayed using Cell-Titer Glo. (D) THZ-P1-2 does not bind to and engage off-targets such as JNK, IRAK1, PKN3, CDK7 and CDK12 despite originating from the same core scaffold as inhibitors of these targets. Competitive streptavidin pulldowns in HEK293T cells were conducted with DMSO, 1 μM THZ-P1-2 and 1 μM of each target's corresponding inhibitor, followed by pulldown in lysate with 1 μM of the corresponding biotinylated or desthiobiotinylated inhibitor. (E) THZ-P1-2 causes a slight increase in LAMP1 and LC3B protein levels, as observed with positive control compounds bafilomycin A1 and chloroquine. HeLa cells were cultured for 24h in DMEM media supplemented with either 0.3% (serum-starved conditions) or 10% FBS. Cells were treated with DMSO, varying concentrations of THZ-P1-2 and single doses of bafilomycin A1 and chloroquine, harvested after 24h, and analyzed by Western blot.

Figure S4 (Continued)

A

Kinase	IC_{50} (nM)
ABL1	21.3
CSNK2A2	1340
KIT	>10000
PDGFRB	3050
RPS6KA4	>10000
TYK2	1600
BRK	313

B

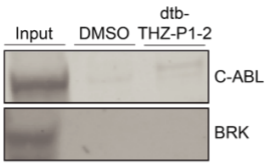

C

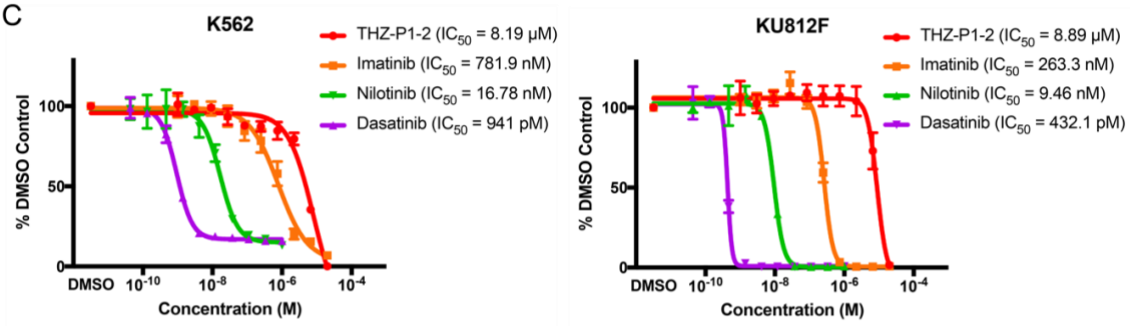

D

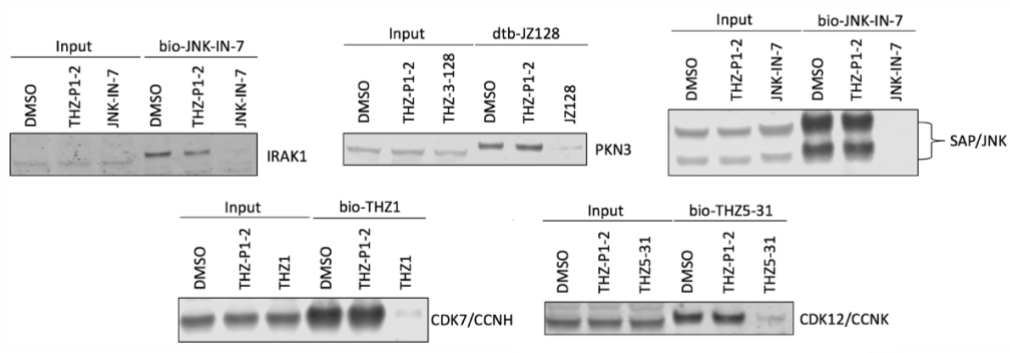

E

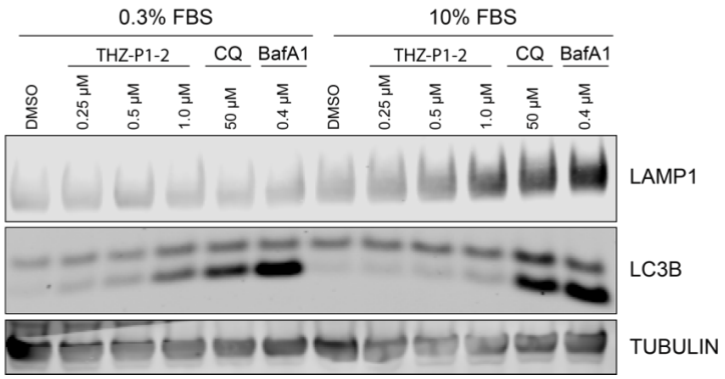

Figure S5. High-throughput screening supplemental data. (A) Plate image from Z'-factor test to verify dynamic range of assay. NIH55 (right - gift from NCATS/NIH) and THZ-P1-2 (middle) were used as strong and moderate positive controls respectively. (B) DMSO and NIH55 controls (red) are approximately equal across 15 screening plates, demonstrating assay stability. (C) Zoom-in of hits showing 90% inhibition. (D) Distribution of compound activities for library collection. (E) Less potent compounds among cherry-picked hits. (F) Counterscreen of cherry-picked hits.

Figure S5 (Continued)

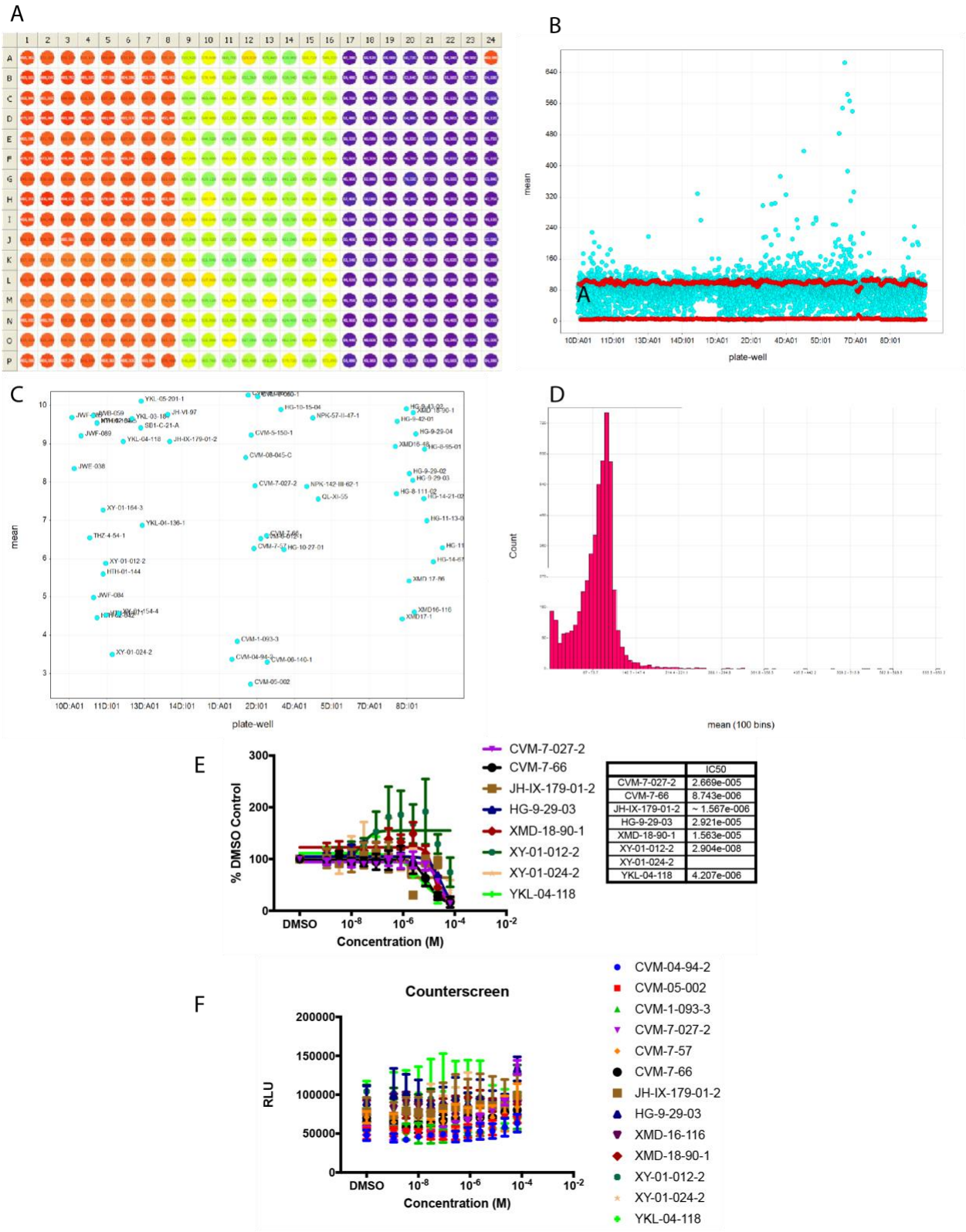

	IC50
CVM-7-027-2	2.669e-005
CVM-7-66	8.743e-006
JH-IX-179-01-2	~ 1.567e-006
HG-9-29-03	2.921e-005
XMD-18-90-1	1.563e-005
XY-01-012-2	2.904e-008
XY-01-024-2	
YKL-04-118	4.207e-006

Table S4. (Related to Figure 2.2C-D) Data collection and refinement statistics for co-crystal structure of complex PI5P4Kα with THZ-P1-2

PI5P4Kα/THZ-P1-2	
Wavelength	0.9792
Resolution range	44.1 - 2.21 (2.289 - 2.21)
Space group	P 1 21 1
Unit cell	44.19 98.68 105.12 90 93.66 90
Total reflections	166064 (16430)
Unique reflections	44717 (4416)
Multiplicity	3.7 (3.7)
Completeness (%)	99.17 (99.44)
Mean I/sigma(I)	13.44 (1.53)
Wilson B-factor	42.32
R-merge	0.06928 (0.8683)
R-meas	0.08115 (1.017)
R-pim	0.04193 (0.5246)
CC1/2	0.999 (0.647)
CC*	1 (0.886)
Reflections used in refinement	44706 (4414)
Reflections used for R-free	2319 (246)
R-work	0.1779 (0.3177)
R-free	0.2254 (0.3814)
CC(work)	0.968 (0.801)
CC(free)	0.951 (0.735)
Number of non-hydrogen atoms	5450
Macromolecules	5102
Ligands	92

Table S2. (Related to Figure 2.11) Data collection and refinement statistics for co-crystal structure of complex PI5P4Kα with CVM-05-002

PI5P4Kα/CVM-05-002	
Wavelength	0.9792
Resolution range	45.37 - 1.71 (1.771 - 1.71)
Space group	P 1 21 1
Unit cell	44.23 88.58 105.78 90 92.91 90
Total reflections	291561 (29776)
Unique reflections	85988 (8587)
Multiplicity	3.4 (3.5)
Completeness (%)	97.72 (97.59)
Mean I/sigma(I)	12.42 (1.34)
Wilson B-factor	32.73
R-merge	0.04003 (1.022)
R-meas	0.04773 (1.207)
R-pim	0.02566 (0.6364)
CC1/2	0.999 (0.754)
CC*	1 (0.927)
Reflections used in refinement	85916 (8579)
Reflections used for R-free	4198 (366)
R-work	0.1805 (0.3977)
R-free	0.2035 (0.4535)
CC(work)	0.967 (0.874)
CC(free)	0.949 (0.822)
Number of non-hydrogen atoms	5595
macromolecules	5211
ligands	50

Scheme 1. Synthetic route of THZ-P1-2, THZ-1-2-R, and dtb-THZ-P1-2.[a]

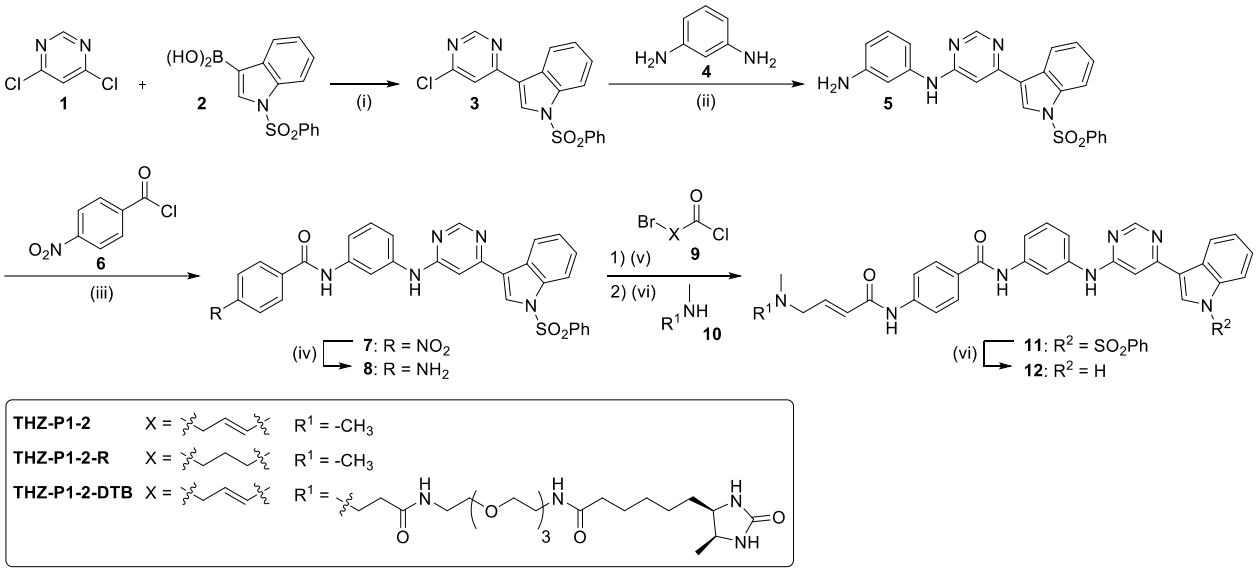

[a] Reagents and conditions: (i) $NaHCO_3$, $Pd(PPh_3)_2Cl_2$, ACN/H_2O (4:1, v/v), 90 °C, overnight, 61 % (ii) DIEA, NMP, 150 °C, overnight, 95 % (iii) pyridine, 80 °C, 3 h (iv) $SnCl_2 \cdot 2H_2O$, EtOAc/MeOH (5:2, v/v), 80 °C, overnight, 69 % over 2 steps (v) 1) DIEA, ACN, 0 °C, 5 min. 2) THF, rt, 2 h (vi) 1 m NaOH/1,4-dioxane (1:1, v/v), rt, 6 h, 7-73 % over 3 steps.

THZ-P1-2: MS m/z 532.24 $[M+H]^+$. ^1H NMR (400 MHz, DMSO-d_6) δ 11.73 (s, 1H), 10.50 (s, 1H), 10.19 (s, 1H), 9.55 (s, 1H), 8.63 (s, 1H), 8.27 (d, *J* = 7.2 Hz, 1H), 8.20 (s, 1H), 8.15 (d, *J* = 2.8 Hz, 1H), 8.00 (d, *J* = 8.7 Hz, 2H), 7.83 (d, *J* = 8.8 Hz, 2H), 7.59 – 7.44 (m, 2H), 7.37 (d, *J* = 8.3 Hz, 1H), 7.34 – 7.26 (m, 2H), 7.24 – 7.09 (m, 2H), 6.81 (dt, *J* = 15.4, 6.2 Hz, 1H), 6.40 (d, *J* = 15.4 Hz, 1H), 3.37 (d, *J* = 5.3 Hz, 2H), 2.39 (s, 6H).

THZ-P1-2-R: MS m/z 534.64 $[M+H]^+$. ^1H NMR (500 MHz, DMSO-d_6) δ 12.06 (s, 1H), 10.32 (s, 1H), 10.23 (s, 1H), 9.49 (s, 1H), 8.76 (s, 1H), 8.27 (d, *J* = 3.0 Hz, 1H), 8.24 (d, *J* = 2.1 Hz, 1H), 8.12 (d, *J* = 7.7 Hz, 1H), 7.97 (d, *J* = 8.6 Hz, 2H), 7.75 (d, *J* = 8.8 Hz, 2H), 7.56 (d, *J* = 7.7 Hz, 1H), 7.52 (d, *J* = 8.1 Hz, 1H), 7.43 (d, *J* = 8.2 Hz, 1H), 7.41 – 7.34 (m, 2H), 7.26 (p, *J* = 7.0 Hz, 2H), 3.16 – 3.04 (m, 2H), 2.81 (d, *J* = 4.6 Hz, 6H), 2.47 (d, *J* = 7.1 Hz, 2H), 2.02 – 1.90 (m, 2H).

Scheme 2. Synthetic route of CVM-05-002/TM-03-117 and TM-03-118.[a]

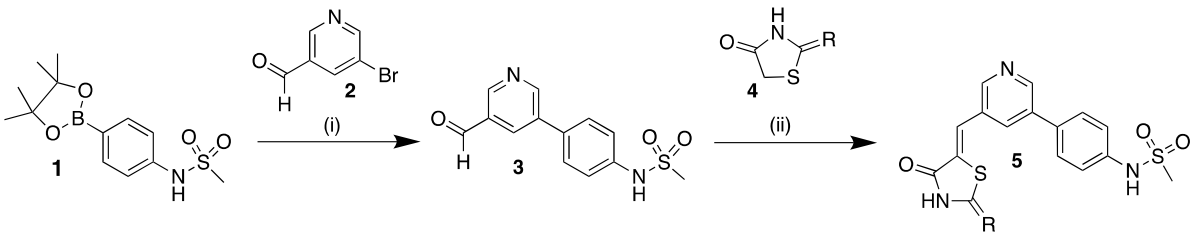

CVM-05-002/TM-03-117	R = NH
TM-03-118	R = O

[a] Reagents and conditions: (i) $NaHCO_3$, $Pd(PPh_3)_2Cl_2$, ACN/H_2O, 80 °C (ii) HOAc, 100 °C